Structural and Functional Characterisation of Magnesium Protoporphyrin IX Chelatase from *Thermosynechococcus elongatus*

Christopher J. Marklew

Ph.D. thesis

September 2012

Department of Molecular Biology
and Biotechnology

University of Sheffield

Structural and Functional Characterisation of Magnesium Protoporphyrin IX Chelatase from *Thermosynechococcus elongatus*

Christopher J. Marklew

Summary

The production of chemical energy from light energy is arguably the most important reaction known. Nearly all life depends on energy derived from light and it is by this process that the atmosphere of our planet was oxygenated. Chlorophyll is the pigment that absorbs light and donates an electron initiating the process of photosynthesis. This highly complex molecule is the result of many chemical reactions collectively known as chlorophyll biosynthesis. Chlorophyll is a modified tetrapyrrole and shares a common synthetic pathway to vitamin B_{12}, Siroheam and haem.

Photosynthetic organisms need both chlorophyll and haem, and the branch point they share, committing to the production of either is thought to be highly regulated. The common precursor to both pigments is protoporphyrin IX and the fate of the macrocycle depends on which divalent metal ion is inserted into the tetrapyrrole. The insertion of Fe^{2+} by ferrochelatase commits to the production of haem whereas the insertion of Mg^{2+} by magnesium chelatase commits to the production of chlorophyll.

The magnesium chelatase is comprised of three subunits that are all essential for activity and are known as ChlH (~150 kDa), ChlD (~75 kDa) and ChlI (~40 kDa). It is known that the H protein binds both the tetrapyrrole substrate and product of the reaction. The I and D subunits are thought to be the catalytic element of the enzyme and once a H•substrate complex is formed, this binds with an ID complex to initiate the reaction.

This work will focus on the structural and functional characteristics of a thermophilic magnesium chelatase (from *Thermosynechococcus elongatus*) which have never been previously studied.

Acknowledgements

My first and foremost thanks go to my supervisor Professor Neil Hunter FRS for his continued support, enthusiasm and patience throughout the four years I've been with the lab.

In relation to this work I would like to thank Drs: Jim Reid, for all things kinetic and for proofreading Chapter 5; Pu Qian, for EM analysis and structural models; Paul Davison and Amanda Brindley for general biochemical advice; Phil Jackson for mass spectrometry; Roman Sobotka, for *Synechocystis* strains and pull-down help; Dan Kenniffe for proofreading Chapter 4 and (soon to be Dr.) Nate Adams for technical help with kinetics.

Thanks go to E12 in its entirety for everyday things and being a great bunch of people to work with. In particular I would like to thank, Mo and Lizzy for simply everything (in equal measure), Dr. John Olson for always having a solution and Dr. Dan Kenniffe for great advice and help over the last four years. Special thanks also go the following for trying to keep me sane (in no particular order) Liz Bomb, Moses, Geezus 'H' Christ (and for giving me plenty of things to do on a Saturday morning), Puff Nuts, Cuddles/Fondles, Dr. R. von Leningrad, Sarah, Craig and Swordsman Dave.

Dr. Andy 'Disco Hands' O'Leary, Chad and Fry, thanks for heavy metal jaunts, superb banter and always having someone around to take my mind away from work. Well done Andy and good luck in your scientific career.

Thanks go to my Mum and Dad for their inexhaustible willingness to listen to me moan, for always been there and for having unwavering faith in me. I could not have done this without you. Also thanks to my brother Will for keeping a smile on my face and support throughout.

Last but never least, thanks to Nicki. You've have had the patience of a Saint over the last year and you've always believed in me. I would not be here if it wasn't for you. Five years have passed already and now we can look forward to our future. How exciting!

Contents

List of Figures

Chapter 1

Chapter 3

Chapter 4

Chapter 5

Chapter 6

Supplementary Figures

Abbreviations

λ	wavelength
2D	2 dimensional
3D	3 dimensional
Å	Angstrom
AAA$^+$	ATPases Associated with various cellular Activities
ADP	adenosine 5'-diphosphate
ALA	δ-aminolaevulinic acid
AMP	adenosine 5'-monophosphate
Amp^R	ampicillin resistant
ATP	adenosine 5'-triphosphate
AU	arbitrary units
BchD	D subunit from *Rhodobacter sphaeroides* or *Rhodobacter capsulatus* magnesium chelatase
BchH	H subunit from *Rhodobacter sphaeroides* or *Rhodobacter capsulatus* magnesium chelatase
BchI	I subunit from *Rhodobacter sphaeroides* or *Rhodobacter capsulatus* magnesium chelatase
BOG	n-Octyl-β-D-Glucoside
BSA	bovine serum albumin
C	centigrade
cDNA	complementary deoxyribonucleic acid
ChlD	D subunit of the magnesium chelatase from Chl producing organisms
ChlH	H subunit of the magnesium chelatase from Chl producing organisms
ChlI	I subunit of the magnesium chelatase from Chl producing organisms
CMC	critical micellar concentration
C-terminal	carboxy-terminal
D	D subunit of magnesium chelatase
DDM	n-dodecyl-β-D-maltopyranoside
D_{IX}	deuteroporphyrin IX
DNA	deoxyribonucleic acid

dNTP	2’-deoxynucleotide-5’-triphosphate (where N is any nucleotide)
DTT	dithiothreitol
DV	divinyl
E. coli	*Escherichia coli*
EDTA	ethylenediaminetetra-acetic acid
EM	electron microscopy
E.MgD$_{IX}$	enzyme bound metalloporphyrin complex
Ferrochelatase	protoporphyrin IX ferrochelatase
gun	genomes uncoupled
IPTG	isopropyl-β-D-thiogalactopyranoside
H	H subunit of magnesium chelatase
HEPES	4-(2-hydroxyethyl)-1-piperazineethanesulfonic acid
HPLC	high performance liquid chromatography
I	I subunit of magnesium chelatase
K_d	disassociation constant
kDa	kilo Daltons
LB	Luria Bertani
LHC	light harvesting complex
MgCH	magnesium protoporphyrin IX chelatase
MgD$_{IX}$	magnesium deuteroporphyrin IX
MgP$_{IX}$	magnesium protoporphyrin IX
m	meter
ml	10^{-6} litre
min	minutes
M	molar
MV	monovinyl
MOPS	3-[*N*-morpholino]propanesulphonic acid
NAD$^+$	nicotinamide adenine dinucleotide
NADP$^+$	nicotinamide adenine dinucleotide phosphate
NAD(P)H	nicotinamide adenine dinucleotide (phosphate) reduced form
nm	nanometer
Nm^R	neomycin resistant
NMR	nuclear magnetic resonance
N-terminal	amino terminal
P$_i$	inorganic phosphate

P_{IX}	protoporphyrin IX
PAGE	polyacrylamide gel electrophoresis
pchlide	protochlorophyllide
PCR	polymerase chain reaction
PDB	protein database
POR	light-dependent NADPH-protochlorophyllide oxidoreductase
PSI	photosystem I
PSII	photosystem II
R. capsulatus	*Rhodobacter capsulatus*
rpm	revolutions per minute
Rba. sphaeroides	*Rhodobacter sphaeroides*
Rba. capsulatus	*Rhodobacter capsulatus*
s	second
SAXS	small-angle X-ray scattering
SDS	sodium dodecyl sulphate
sp.	Species
T. elongatus	*Thermosynechococcus elongatus*
T_m	melting temperature
TAE	Tris-acetate-EDTA
TE	10 mM TrisHCl 1 mM EDTA pH 8.0
Tris	Tris(hydroxymethyl)methylamine
Tricine	N-tris(Hydroxymethyl)methylglycine
UV	ultra violet
Vis	visible

CHAPTER 1

Introduction

1.1.Photosynthesis

All life depends on photosynthesis either directly or indirectly, excluding only chemolithoautotrophs, making it the most important chemical reaction in nature mankind. Photosynthesis is the process of light-driven carbon fixation to form carbohydrates. Life is dependent on the energy stored from photosynthesis and it is likely that photosynthesis is responsible for the oxygen in Earth's atmosphere, allowing subsequent aerobic life to develop (Buick, 2008). Photosynthesis is used by plants, some bacteria and cyanobacteria to produce chemical energy from solar energy, through electrochemical energy, in the reaction:

$$2H_2A + CO_2 \xrightarrow{\text{Light}} (CH_2O)_n + H_2O + 2A \quad \text{(van Niel, 1962)}$$

Here CO_2 is reduced by H_2A to form carbohydrate and A is the oxidation product. Oxygenic photosynthesis is performed by plants and cyanobacteria to produce chemical energy with the reaction:

$$2H_2O + CO_2 \xrightarrow{\text{Light}} (CH_2O)_n + O_2 + H_2O$$

In this reaction water is used to provide the electrons that reduce carbon dioxide to a carbohydrate. This results in the release of O_2 as the oxidation product, hence the name oxygenic photosynthesis. In all other photosynthetic bacteria, photosynthesis occurs but water is not used as the electron donor. A number of reductants can be used examples being molecular hydrogen, succinate and hydrogen sulphide. This process results in oxidation products that differ from those for oxygenic photosynthesis and is thus termed anoxygenic.

Photosynthesis occurs in two separate stages known as the light-dependent and light-independent stages. In the light-dependent stages photons excite electrons in pigments

to a higher energy state. When the electron returns to its original energy state this energy is used to drive ATP and NAD(P)H production. The products of the light-dependent reaction power the fixation of carbon dioxide to carbohydrate in reactions similar to that of oxidative phosphorylation and in plants are known as the calvin cycle.

Energy capture is performed by pigments that absorb light at specific wavelengths. Chlorophyll (Chl) is the most abundant pigment on Earth and can be seen from outer space. Other pigments such as carotenoids and phycobilins also absorb light at specific wavelengths, which are often tuned by the proteins they associate with. Most wavelengths of light in the red and near-UV are collected by photosynthetic organisms. This is due to the high abundance of relatively low energy red light and the low abundance of relatively high energy near-UV light. The green reflected light of plants and cyanobacteria is in neither high enough abundance nor high enough energy to make it worthwhile to be utilised.

Photosynthesis is becoming an increasingly important topic of scientific debate. With the current global population growth and global energy demand soon to increase rapidly, current energy production may not supply demand. The concept of harvesting energy through sunlight using organisms is not new but increasingly interesting and within reach. At present cyanobacteria harvest just 0.2 - 0.3% of the solar energy available to Earth (Waterbury *et al*., 1979). This translates to around 25 times the current human consumption of energy and it is clear that if humans were able to tap into just a fraction of this energy efficiently it may provide sustainable green energy for our growing society.

1.2. Photosynthetic bacteria

Bacteria that can photosynthesise are usually found in either fresh water or marine environments. There are four major groups into which they can be categorised all utilising the environments that make up their distinct habitat. The four major groups are below: (Fig. 1, *A*)

1. Purple bacteria can be divided into two groups:
   a. Purple sulphur bacteria (*Chromatiales*) use hydrogen sulphide as an electron source for photosynthesis.
   b. Purple non-sulphur bacteria (*Rhodospirillaceae*) use organic compounds as an electron source for photosynthesis. The bacteria *Rhodobacter sphaeroides and Rhodobacter capsulatus* are classed within this group.
2. Green bacteria, which are subdivided into sulphur (*Chlorobiaceae*) and non-sulphur (*Chloroflexi*) bacteria. Green sulphur bacteria are non-motile obligate anaerobes that use sulphide as an electron source for photosynthesis. The green non-sulphur bacteria are facultative anaerobes and use reduced carbon compounds as a source of electrons in photosynthesis.
3. Cyanobacteria are oxygenic phototrophes and contain the species *Synechocystis*, *Thermosynechococcus elongates* and *Cyanothece.*
4. Heliobacteria, obligate anaerobes that utilise organic carbon compounds as electron donors.

Due to differing metabolic requirements photosynthetic bacteria are able to inhabit different niches. This results in each group developing specific optimum light harvesting signatures (Fig. 1, *B*).

1.3.*Synechocystis*

Cyanobacteria are also referred to as “blue-green algae” and comprise a group containing over 1500 species. *Synechocystis* sp. PCC6803 (from hereon Synechocystis) is a cyanobacterium capable of both phototrophic growth when grown in the light and heterotrophic growth when grown in the dark with a carbon source such as glucose. They are spherical, unicellular Gram-negative fresh water organisms that were first isolated in 1968 and it is widely accepted that cyanobacteria became chloroplasts in an endosymbiotic event as seen in Archaeplastida where the plastids are surrounded by just two membranes indicating they are the result of a primary endocytic event. In all other groups the plastids contain three or more membranes (Adl *et al.,* 2005).

Some cyanobacteria have the ability to fix nitrogen but due to the oxygenic nature of photosynthesis the two processes cannot coincide. Nitrogenase activity is strongly inhibited even in microaerobic environments and in oxygenic phototrophs the two should not be able to operate together. The circadian clock is a cellular ability to monitor time over a ~24 hour period. This gives the ability to monitor and adapt to temporal changes in the environment, for example temperature or light, and circadian clocks were thought to exist in eukaryotic cells only. Traditionally the circadian clock was thought to only exist in cells with a doubling time that is longer than that of the clock itself. Kondo *et al*., (1997) were the first to provide evidence of a circadean clock in *Synechococcus,* a cyanobacterium with a doubling time of just 8 hours. It has been postulated that the circadian clock in cyanobacteria gives rise to the ability to both photosynthesise and fix nitrogen due to the expression of photosynthetic genes during daylight and nitrogen fixing activity limited to night time (Johnson *et al.,* 1999; Kucho *et al.,* 2005).

A

Photosynthetic Bacteria					
Purple		Green		Cyanobacteria	Heliobacteria
Sulphur	Non-sulphur	Sulphur	Non-sulphur		
Thiospirillum	*Rhodobacter*	*Chlorobaculum*	*Chloroflexus*	*Synechocystis*	*Helicobacter*
Chromatium	*Rhodospirillum*	*Prosthecochloris*		*Synechococcus*	*Heliobacillus*
Thiocapsa	*Rhodopseudomonas*	*Pelodictyon*		*Cyanothece*	*Heliophilum*
Amoebacter	*Rhodocyclus*	*Chlorochromatium*		*Phormidium*	*Heliorestis*
Thiopedia	*Rhodomicrobium*	*Pelochromatium*		*Plectonema*	

B

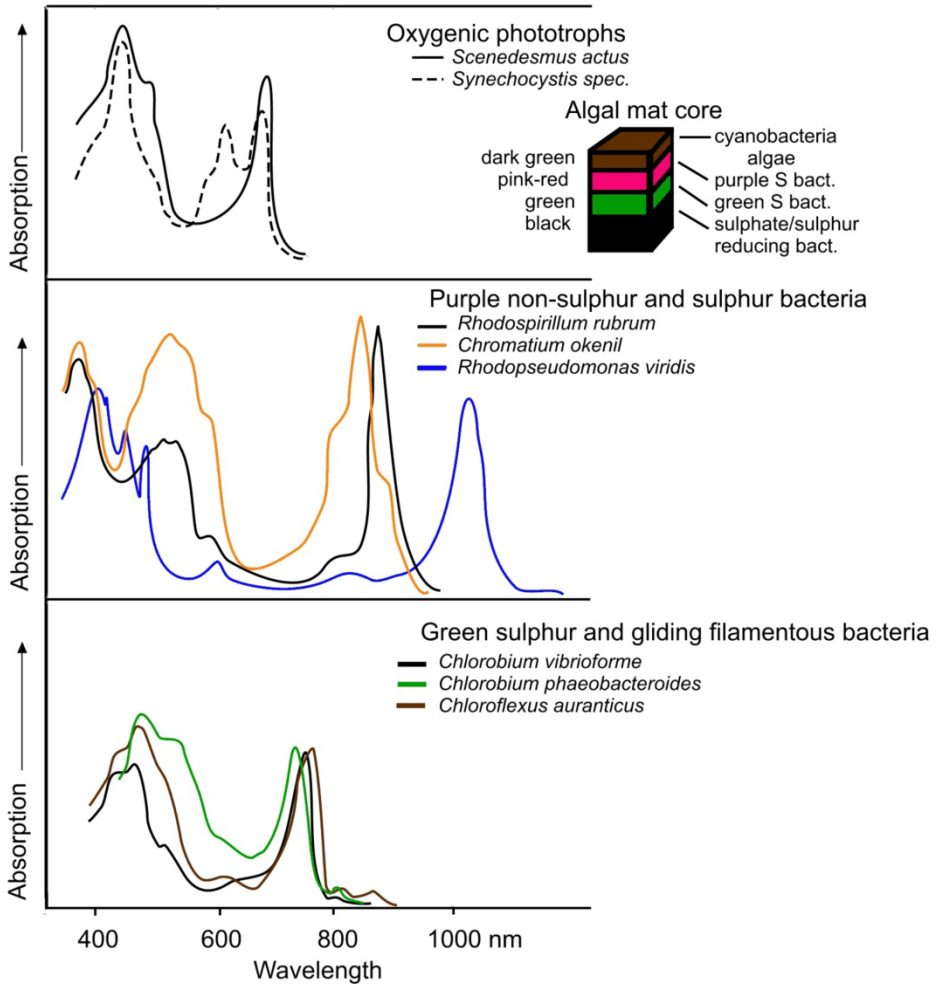

Figure 1 - Taxonomy and absorption spectra of photosynthetic bacteria

A) Taxonomy of phototrophic bacteria.

B) Absorption spectra of living photosynthetic organisms.

Synechocystis has been studied intensively as a model organism for photosynthesis. In general, cyanobacteria are suitable as model organisms for the study of plant plastids because of the highly similar organisation of their photosynthetic apparatus to that of plants and unlike other photosynthetic bacteria they perform oxygenic photosynthesis. The genome of *Synechocystis* was one of the first to be sequenced and it was the first phototrophic organism to be mapped (Kaneko and Tabata, 1997). The simplified prokaryotic genetic material is also a benefit to study this organism as opposed to plants.

1.4.*Thermosynechococcus elongatus*

Thermosynechococcus elongatus BP-1 (from here on *T. elongatus*) is a cyanobacterium capable of both phototrophic and heterotrophic growth. It was isolated from a hot spring near Beppu, a northern city on the most southern of Japan's main islands. It is a unicellular rod-shaped cyanobacterium with an optimum growth temperature of 55 °C and the genome has been sequenced (Nakamura *et al.,* 2002). *T. elongatus* has long been used as a model organism for photosynthesis, mostly for the same reasons as *Synechocystis* but also due to thermostable nature of the organism and the advantages in structural studies with regard to the increased stability of proteins during purification. Using gene products from this organism successful attempts to obtain X-ray structural information of proteins and protein complexes have been documented (Zouni *et al.*, 2001; Jordan *et al.*, 2001; Ferreira *et al*., 2004; Davison *et al.*, 2005).

1.5.Structure of chlorophylls and bacteriochlorophylls

Tetrapyrroles function in energy capture and comprise an extensive group of compounds. They are composed of four pyrrole subunits (C_4H_4NH) connected by methine bridges, excluding corrins which have only three connecting methine bridges. Porphyrins are cyclic arrangements of the pyrrole groups and form the macrocycle of Chls and haems, although pyrroles can also be arranged linearly in phycobilins and bilanes.

Chlorins are a discrete group of pigments to which Chls belong. They are modified tetrapyrroles identifiable by the presence of a fifth isocyclic ring E, and a long-chain esterifying alcohol at position C17. The most abundant chlorins are Chl *a* (Fig. 2) and Chl *b* but there are many other derivatives of Chl all with a Mg^{2+} ion coordinated through pyrrole-derived nitrogens, with differing functional side-chain groups. Both *Synechocystis* and *T. elongatus* use only Chl *a* for energy transfer.

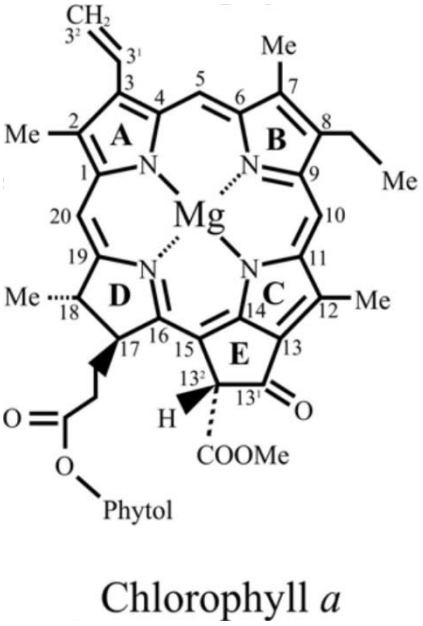

Figure 2 - Structure of the most common chlorophyll

The IUPAC numbering system for the carbon skeleton is shown on the structure of chlorophyll a.

The formation of δ-aminolaevulinic acid is the first committed step in the synthesis of tetrapyrroles. Haem and Chl follow the same biosynthetic pathway up until the chelation of the metal ion. This branch point determines the path of the macrocycle to the formation of either haem or Chl and it is likely that this branch point has a role in regulation.

1.6. Tetrapyrrole biosynthesis

1.6.1. Formation of δ-aminolaevulinic acid

The formation of δ-aminolaevulinic acid (ALA) is the first committed step of tetrapyrrole biosynthesis and ALA is the first specific precursor. There are two pathways known that make ALA, the C_4 or Shemin pathway and the C_5 pathway. The Shemin pathway is found in animals, fungi, protozoa and the α-proteobacteria group of bacteria. ALA is made from the condensation of glycine with succinyl-coenzyme A by the enzyme ALA synthase **(**Gibson et al., 1958; Kikuchi et al., 1958**)**.

In the C_5 pathway ALA is formed through a three-step mechanism starting with the activation of glutamate with ATP and Mg^{2+} performed by the enzyme glutamyl-tRNA synthetase (GluRS). NADPH or NADH reduces glutamate to glutamate-1-semialdehyde (GSA) by the glutamyl-tRNA reductase (GluRT) and finally a transamination reaction by the glutamate-1-semialdehyde aminotransferase (GSAT) forms ALA from GSA. It was discovered that ALA was synthesised in *E. coli* via the C_5 pathway and this allowed a major foothold to allow the elucidation of the processes more easily (Li et al., 1989);(O'Neill et al., 1989). Bacteria that use the C_5 pathway lack an α-ketoglutarate-dehydrogenase that enables the formation of succinyl-coenzyme A. This may indicate that the C_5 pathway may be older that the Shemin pathway and this supports the proposed origin of chloroplasts because cyanobacteria and plants both utilise this pathway.

GluRS performs the first reaction in the formation of ALA in the C_5 pathway. It was first discovered when activity was abolished in cell free extracts by the pre-incubation of RNAase A. Activity could be reconstituted upon the addition of a ribonuclease inhibitor and tRNA (Kannangara *et al*., 1988; Huang and Wang, 1986a). Glutamate is activated by ligation with $tRNA^{Glu}$ in the presence of Mg^{2+} and ATP. This glutamyl-$tRNA^{Glu}$ complex is the substrate for the following reaction (Kannangara *et al*., 1988; Huang *et al*., 1984). The UUC anticodon for glutamate and the 3`-terminal CCA sequence are found in both the $tRNA^{Glu}$ involved in ALA synthesis and in protein translation and this has led to the suggestion that $tRNA^{Glu}$ performs the same job in both roles (Schön *et al*., 1986). Many GluRS have been isolated and it has been suggested that they may associate as homodimers in nature (Beale, 1999).

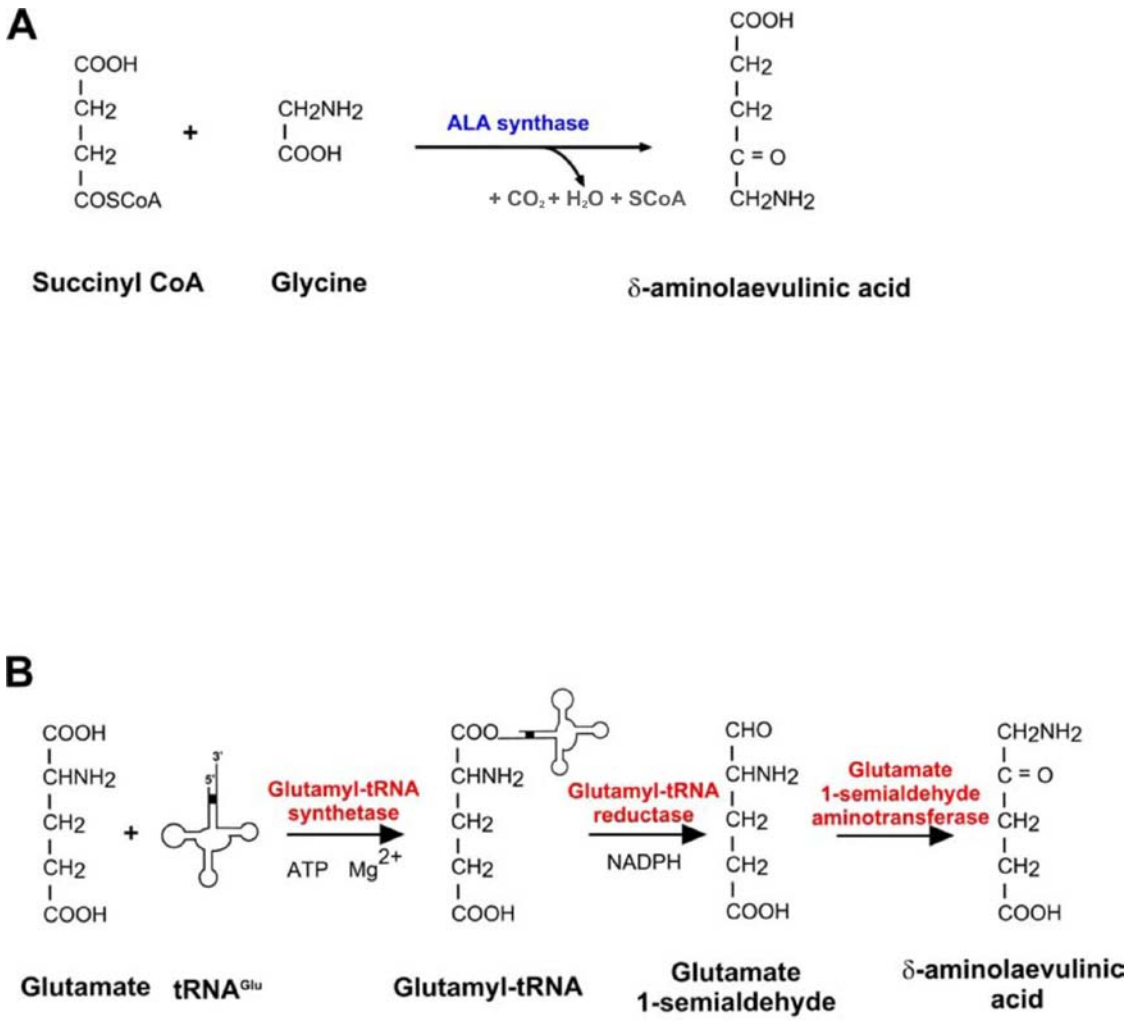

Figure 3 - The Shemin and C5 pathways

A) The Shemin pathway, showing the formation of ALA by the condensation of glycine and succinyl coenzyme A, catalysed by ALA synthase.

B) The C5 pathway, showing the formation of ALA from glutamate.

The reaction catalysed by GluTR is the NADPH-dependent reduction of glutamyl-$tRNA^{Glu}$ to form GSA and is the second committed step of ALA synthesis. Using an ALA auxotroph in *E. coli*, *hemA*, GluTR activity was abolished leading to suggestions that *hemA* encodes GluTR (Avissar and Beale, 1989a). In a study by Chen *et al*., (1994) the *hemA* gene product is overexpressed and is able to complement the auxotrophic phenotype of *hemA*. When cell-free extracts of the overexpressed cultures were applied to a gel filtration column, the eluted fractions were assayed for GluTR activity, and a fraction with an estimated MW of 126 kDa exhibited activity. In addition the cell free cultures were analysed using native PAGE and a band at 117 kDa was observed. When both the gel filtration GluTR active eluate and the 117 kDa band from native PAGE were analysed using denaturing PAGE a band of 46 kDa was observed. It was proposed that the high MW expressed products are homo-oligomers or as proposed previously by Jahn (1992) a complex formed with GluRS and $tRNA^{Glu}$ (Chen *et al*., 1996). GluTR has been purified as homo-oligomers of eight 39 kDa subunits from *Synechocystis* (Rieble and Beale, 1991) and five 54 kDa subunits from barley (Pontoppidan and Kannangara, 1994). An X-ray structure of GluTR as a homodimer is available showing a V-shaped arrangement (Moser *et al*., 2001).

The third reaction in the formation of ALA, the transamination of GSA, can occur spontaneously at physiological pH providing GSA is in a high enough concentration (Beale *et al*., 1990) and the initial committed step of ALA synthesis is performed by the same enzyme in protein synthesis. This strongly implies that it is the GluTR step that is regulated and it has been proposed by de Armas-Ricard *et al*. (2011) that haem regulates the GluTR enzyme. These authors also show that haem binds only to the dimeric form of GluTR in a ratio of 1:1 haem:GluTR dimer suggesting the dimer is the active form of the enzyme. Both the GluRS and the GluTR need a divalent metal ion to be functional. GluRS requires Mg^{2+} or Mn^{2+} and the GluTR needs either of these or Ca^{2+}. The GluTR is inhibited by Zn^{2+} even at micromolar levels (Mayer *et al*., 1994).

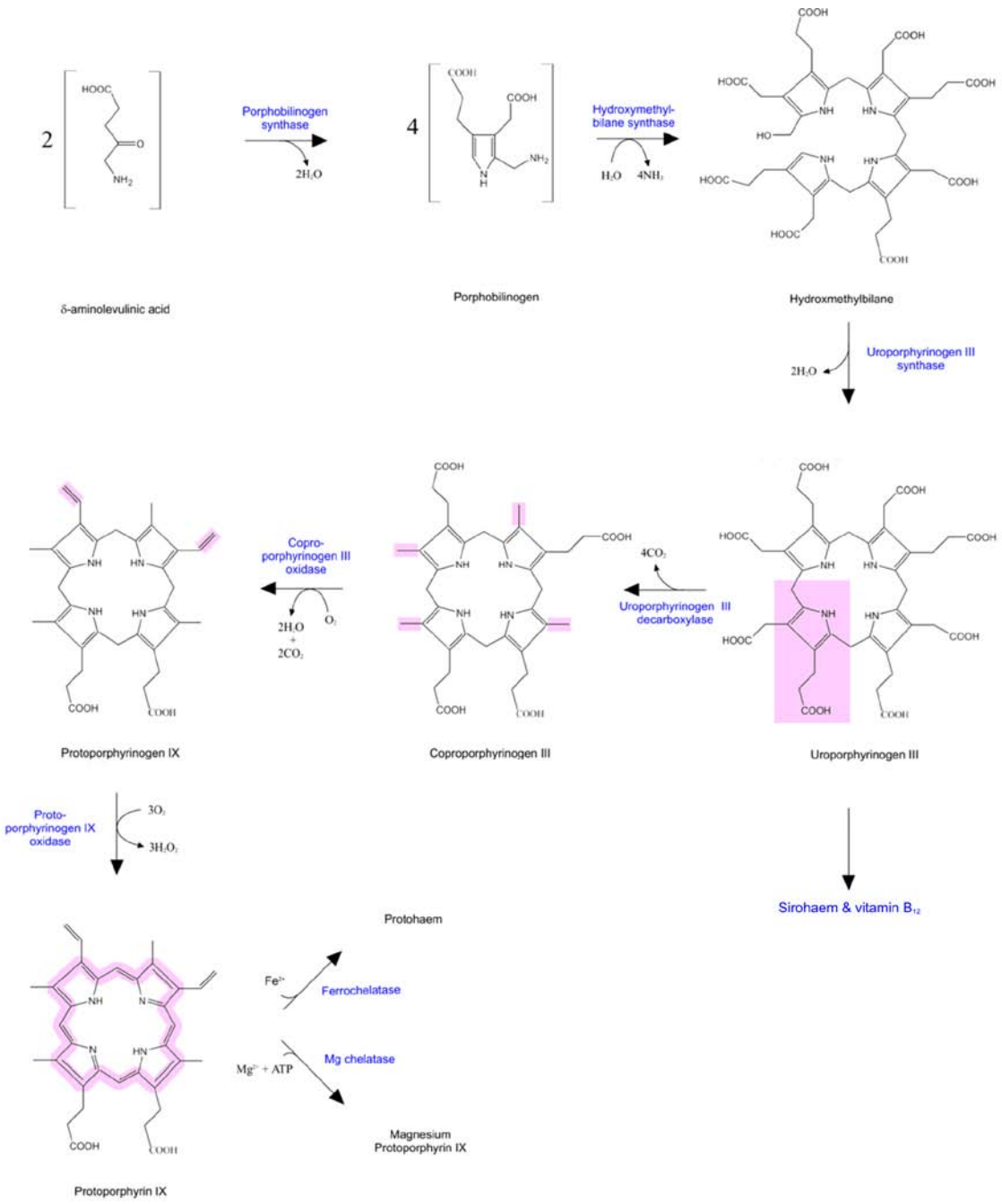

Figure 4 - The common tetrapyrrole pathway from δ-aminolaevulinic acid to protoporphyrin IX

The enzymes catalysing each step are shown in blue. Magenta shading indicates the groups modified at each stage.

The GSAT has been purified to give a molecular weight between 60-100 kDa. Many of the plant and bacterial enzymes show high homology when compared to the aspartate aminotransferase family (Elliot *et al*., 1990; Mehta and Christen, 1994). Avissar and Beale (1989) showed that the aminotransferase from the species *Chlorella vulgaris* is dependent on a cofactor for its function. Pyrixodal phosphate (PLP) was discovered as a possible cofactor when activity of the enzyme was inhibited with the addition of PLP inhibitors aminooxyacetate and gabaculine (Hoober *et al*., 1988; Soper and Manning, 1982). Avissar and Beale purified the aminotransferase and excluded PLP from the buffers and demonstrated the dependence of the enzyme on PLP. The structure of the aminotransferase from the *Synechococcus* was solved by Hennig *et al*., (1997).

1.6.2. δ-aminolaevulinic acid to porphobilinogen

The next reaction is a condensation reaction where two ALA molecules form porphobilinogen (PBG), the first step common to all known tetrapyrrole biosynthetic pathways. PBG is the first pyrrole molecule in the pathway and forms the building blocks for the formation of the remainder of the tetrapyrrole. The reaction is catalysed by ALA dehydratase (ALAD), also known as porphobilinogen synthase, a highly conserved protein of ~35 kDa (Jaffe, 2004). The gene that encodes ALAD is *hemB*. ALADs have a requirement for divalent metal ions and can be categorised into two main groups; those that are dependent on Zn^{2+}; and those that are dependent on Mg^{2+} to function (Senior *et al*., 1996). X-ray structural information is available for the yeast and *E. coli* ALADs showing a barrel like homo-octamer holoenzyme made up of four homo-dimers (Erskine *et al*., 1999a; Erskine *et al*., 1999b).

The ALADs that are dependent on Zn^{2+} comprise the mammalian, yeast and *E. coli* enzymes. ALAD from bovine liver functions as a homo-octamer, each subunit having one active site with two conserved lysine residues, and one zinc ion bound per subunit through the thiol side group of three conserved cysteines (Erskine *et al*., 1999; Tsukamoto *et al*., 1979). Loss of this coordinated zinc resulted in significant but not complete loss of activity (Tsukamoto *et al*., 1979). All ALADs that are zinc-dependent appear to have varied optimum pH ranging from 6.3 to 9.8 (Senior *et al*., 1996). They are extremely sensitive to oxidation and have thiol groups that are involved in zinc coordination. Mg^{2+}-dependent ALADs include higher plants and have pH optima of

between 8.0 - 8.5. These also appear to be functional as homo-octomers and are less sensitive to oxidation than the Zn^{2+} dependent ALADs but they are more dependent on the coordinated metal ion resulting in complete loss of activity in their absence. The cysteine residues and therefore thiol groups are not involved in the metal ion coordination of Mg^{2+}-dependent ALADs and this may explain their reduced sensitivity to oxidation (Senior *et al*., 1996).

1.6.3. Porphobilinogen to hydroxymethylbilane

The *hemC* encodes porphobilinogen deaminase (PBGD), that catalyses the third committed step of tetrapyrrole biosynthesis. PBGDs are monomeric and have molecular mass between 34 – 44 kDa (Witty *et al*., 1993). The formation of hydroxymethylbilane (HMB) proceeds through four deamination reactions of porphobilinogen to form a linear tetrapyrrole. PBGDs utilise a cofactor, dipyrromethane, which binds to PBGD through a cysteine-242 that is conserved across many divergent species (Warren and Jordan, 1988; Hart *et al*., 1988; Witty *et al*., 1993). The dipyrromethane functions as a primer to which PBG can attach and after four serial reactions a hexapyrrole intermediate is formed (Jordan and Warren, 1987; Miller *et al*., 1988). The second function of the dipyrromethane appears to be a mechanism to limit the total number of ligated PBG miolecules to six thus limiting the product of the reaction to a tetrapyrrole. The next PBG to bind stimulates hydrolytic cleavage and the release of hydroxymethylbilane (Battersby *et al*., 1983). The protein-cofactor complex is permanent and the cofactor is required for the protein stability. The structure of PBGD from *E. coli* has been determined to a resolution of 1.76 Å (Louie *et al*., 1992). It has been shown that only one active site exists in the protein due to the absence of structural repeats that would indicate several catalytic sites of similar function. In a mutagenic study Asp84 replaced with Glu abolished activity by 99% and replacement with a non-acidic residue completely abolished activity (Louie *et al*., 1996). Steady-state levels of *hemC* mRNA have been shown to be linked to enzymatic activity of the PBGD and light has a strong effect on the induction of the gene (Witty *et al*., 1993).

HMB is extremely unstable as a molecule and if the subsequent enzyme in the pathway, uroporphyrinogen III synthase, is inactive or absent the molecule will spontaneously cyclise to form uroporphrinogen III (Battersby *et al*., 1979a). In patients

with congenital porphyria (patients deficient in uroporphyrinogen III synthase) the oxidation product of Urogen I, Uro I, is found in urine samples (Rimington and Miles, 1951). When uroporphyrinogen III synthase is active HMB is converted to uroporphyrinogen III (Battersby *et al.*, 1979b).

1.6.4. Hydroxymethylbilane to uroporphyrinogen III

The formation of urogen III from HMB is catalysed by the urogen III synthase. The reaction performed is the spontaneous cyclisation by inversion of the ring D with the formation of an intermediate spiro-pyrrolenine product (Leeper *et al.*, 1994). The product of the reaction, urogen III, is the first cyclic macrocycle biosynthetic precursor for all tetrapyrroles.

It has been postulated that urogen III and PBGD may form a complex *in vivo* and the ability to shuttle the molecule from one enzyme directly to the next would be highly beneficial to the system due to the instability of the product/substrate (Higuchi and Bogorad, 1975). Battersby *et al*., (1979a) have also shown that the K_m of urogen III synthase for PGB is altered upon the incubation with PGBD.

The structure of urogen III synthase has been solved to 1.85 Å and shows a bi-lobed structure where domains 1 and 2 are connected by two anti-parallel β-sheets and each lobe has parallel β-sheets with α-helices between them (Shoolingin-Jordan, 1995). The structure has been solved with substrate bound (Schubert et al., 2008) but mutational studies have yet to identify any residues that are vital for activity (Mathews *et al.*, 2001) The .

1.6.5. Uroporphyrinogen III to coproporphyrinogen III

The fourth step of tetrapyrrole biosynthesis is the first branchpoint determining the fate of the macrocycle into several final products. Decarboxylation of urogen III by urogen III decarboxylase commits metabolism to the formation of Chl, Bchl or protohaem, shown in Fig. 4. In the other branch sirohaem synthase catalyses the formation of sirohaem (Murphy and Sigel, 1973) and a third branch, through further modifications of urogen III, vitamin B_{12} is formed (Battersby, 1994). Decarboxylation of all four of

the acetate groups of urogen III by urogen III decarboxylase starts on the D ring and continues clockwise until all the groups are decarboxylated (Luo and Lim, 1993) to form coproporphyrinogen III (Coprogen III). In plants urogen III decarboxylase is located in the plastids and as a result the plant decarboxylase sequence have an N-terminal translocation sequence to direct transport to the plastids. The first structural information of urogen III decarboxylase by X-ray diffraction was for the human enzyme and showed that it has one active site and is assembled as a dimer, which may be important for catalysis (Whitby *et al.,* 1998). Phillips *et al.,* (2003) solved the urogen III decarboxylase structure with the substrate bound and showed the importance of Asp86 in binding the substrate to the active site through hydrogen bonds between the NH groups in the pirrole and a carboxylate oxygen atom. A point mutation of Asp86 to Asn results in near complete inhibition of wild type activity and the structure of this mutant showed an empty active site cleft. A mutation exchanging Asp86 for Glycine significantly reduced activity to below 5% of the WT level but still bound substrate; Asp86 to Glu retained up to 10% activity (Philips *et al.,* 2003). The X-ray structural data produced by Martins *et al.,* (2001) for the plant enzyme confirms that previously solved for human urogen III decarboxylase.

Urogen III, like other tetrapyrrole intermediates, is highly sensitive to light and if it is not stabilised by a protein chaperone can lead to the formation of reactive oxygen species which can be highly detrimental to the cell. Accumulation of urogen III in plants either due to a carboxylase mutation or due to problems with expression has been shown to result in the formation of necrotic lesions in leaves (Hu *et al*., 1998; Mock and Grimm, 1997; Mock *et al*., 1998).

1.6.6. Coproporphyrinogen III to protoporphyrinogen IX

Protoporphyrinogen IX (Protogen) is formed from Coprogen III by oxidative decarboxylation to form vinyl groups from the propionate groups of rings A and B. The enzyme that catalyses this reaction is Coprogen III oxidase and in plants it is found solely in the plastids (Smith *et al.,* 1993). Unlike expression of other enzymes in the pathway the expression of Coprogen III oxidase is not linked to light levels or circadian rhythms, but is determined by a number of factors such as the stage of differentiation (Kruse *at al*., 1995a; Papenbrock *et al*., 1999). In tobacco transformation with an antisense Copragen III oxiades gene led to accumulation of the

enzyme substrate, resulting in leaf necrosis that was dependent on light intensity (Kruse *et al.,* 1995b). In Coprogen III oxidase-deficient plants several responses against reactive oxygen species (ROS) were observed but failed to prevent cell death due to a reduction in antioxidants when compared to wild type (Kruse *et al.,* 1995b; Mock *et al*., 1998). This was shown in the *Arabidopsis* mutant *lin2* which necrotic lesions due to a defective Coprogen III oxidase gene (Ishikawa *et al.,* 2001).

1.6.7. Protoporphyrinogen IX to protoporphyrin IX

Protogen oxidase (PPO) is the last enzyme that is common to both haem and Chl biosynthesis and it catalyses the flavin-dependent conversion of protoporphyrinogen IX (Protogen) to protoporphyrin IX (Proto). The reaction involves the six-electron oxidation of the macrocycle. In plants the reaction can be catalysed by two different gene products, PPOI and PPOII that show relatively low similarity to one another in the same species, typically with an amino acid identity of around 28%. When the enzyme isoforms are compared with other organisms, each isofrom shares around 70% identity (Lermontova *et al.,* 1997; Watanabe *et al.,* 2001). PPO is the first enzyme involved in tetrapyrrole metabolism to be located in two different subcellular locations, the mitochondria and plastids, but only one isoform is found in each cell (Jacobs and Jacobs, 1981; Smith *et al*., 1993). In bacteria the reaction is catalysed by an oxygen-dependent enzyme encoded by the gene *hemY*; and an oxygen-independent enzyme encoded by the gene *hemG* (Kato *et al*., 2010).

PPO has been shown to be important in the function of some herbicides. The chemical compound Phthalimide was shown to cause the accumulation of protoporphyrin IX (Proto), a Chl precursor with high photolability (Scalla *et al*., 1990; Duke *et al*., 1991). Exposure of Proto to high light results in the formation of singlet oxygen that often results in lipid peroxidation and finally cell death (Matringe and Scalla, 1988). It was shown that PPO was inhibited and accumulation of Proto, the substrate of PPO, was in fact due to the initial accumulation of Protogen which is oxidised by peroxidases bound to plasma membranes to form Proto. Protogen is an intermediate of haem, which is negative feedback regulator of its own synthesis. The absence of haem results in the upregulation of tetrapyrrole synthesis and the blocking at the PPO step results in the accumulation of Protogen and therefore Proto.

Recently a third PPO gene named *hemJ* has been found in the cyanobacterium *Synechocystis*, whichs lack both *hemY and hemG*. The predicted sequences of *hemY* and *hemG* show no similarity to *hemJ* and structural predictions indicate that the encoded protein may have transmembrane helices and may not be flavin-dependent (Boynton *et al.*, 2011; Kato *et al*., 2010). Another gene essential for tetrapyrrole synthesis has been discovered in Gram-positive bacteria. A proposed peroxidase gene *hemQ* found adjacent to genes encoding PPO has also been shown to be essential for PPO activity. The role of the enzyme has been attributed to the need for the breakdown of toxic hydrogen peroxide produced by the reaction (Dailey *et al.*, 2010).

The crystal structure of mitochondrial PPO from tobacco is available and shows a dimeric arrangement. The structure also suggests that PPO can shuttle Proto to ferrochelatase limiting the exposure to light (Koch *et al*., 2004).

1.6.8. The branch point of tetrapyrrole biosynthesis

After the formation of Proto the next step involves the chelation of two possible divalent metal ions. The path which produces protohaem or haem B is catalysed by ferrochelatase inserting an Fe^{2+} ion into the macrocycle. This is the last reaction and the product can be utilised in cytochromes or for a protein in the peroxidase family. The ferrochelatase does not have a requirement for energy and although the reaction is energetically favourable it cannot spontaneously occur. The result of the second possible metal insertion event is the production of chlorophyll, initially committed by the chelation of a magnesium ion into the tetrapyrrole. Magnesium chelatase is a complex three-subunit enzyme with an absolute requirement for ATP due to the unfavourable nature of the reaction. It has been proposed that this is due to the high energy requirements of removing the hydration shell form the magnesium ion to allow chelation (Reid and Hunter, 2004).

In photosynthetic cells both protohaem and chlorophyll are essential but in different quantities depending on the time of year and organism. It is of paramount importance for each cell to regulate the shuttling of Proto down the required pathway with absolute precision. As mentioned earlier ferrochelatase is involved in the regulation of the haem pathway and it is obvious that the magnesium chelatase will too have a role in the regulation of the branch point.

1.6.9. Ferrochelatase

Ferrochelatase (FeCH) performs the ATP-independent chelation of Fe^{2+} into Proto forming haem (haem B). The gene product of *hemH*, FeCH is a membrane-associated protein of ~55 kDa and is found as either a monomer or homo dimer. The X-ray structure of a FeCH was first elucidated in 1997 by Al-Karadaghi *et al.*, from *Bacillus subtilis* (*B. subtilis*) and was followed by the human FeCH structure (Wu *et al.*, 2001). Soon after a model proposing a mechanism for porphyrin binding was proposed for *B. subtilis* FeCH highlighting the distortion of the porphyrin ring of N-methylmesoporphyrin IX (an FeCH inhibitor) giving a tilt of around 5° to pyrrole rings B, C and D and and a 36° tilt to ring A. It was suggested that this larger tilt of ring A was associated with ferrous iron chelation (Lecerof *et al.*, 2000). This was however disputed by Medlock *et al*., (2007) where, in the human FeCH structure, they showed porphyrin binding with a 100° rotation relative to that previously published and the macrocycle was buried an additional 4.5 Å deeper within the enzyme. A further publication by the Al-Karadaghi group showed that their work describing porphyrin binding in *B.* subtilis was indeed correct (Karlberg *et* al., 2008). This suggests that although porphyrin binding differs in a physical manner between (at least) these two species the same method of chelation appears to be shared. The chelation reaction appears to mainly conserved between bacterial and human FeCH but the solubility, size and isolation as either a monomer or homodimer differ between species and the presence of a [2Fe-2S] cluster appears to be involved in dimer stability (Dailey *et al*, 2000). The activity of plant FeCH was first demonstrated in both the mitochondria and in plastids (Porra and Lascelles, 1968). The insertion of Fe^{2+} into Proto has been described as a two-step process. Firstly, fast porphyrin binding step takes place and the reaction is completed with a, slow, irreversible chelation step (Hoggins *et al*, 2007).

It has been proposed that there are two types of FeCH in plants, type-I and type-II, which differ in gene sequence and in expression characteristics. It was shown that type-I was localized in both the mitochondria and chloroplast whereas type-II was solely imported into chloroplasts (Chow *at al*., 1997, 1998; Suzuki *et al*., 2000, 2002). Chow *et al*., (1998) proposed that the type-I was a mitochondrial FeCH and type-II was chloroplastic. Supporting work showed that a homologous type-I FeCH, found in cucumber, was expressed in a light-independent manner in non-photosynthetic tissues and was not found in cotyledons (Suzuki *et al*., 2002). The expression of type-II FeCH

in cucumber was shown to be strongly linked to illumination. It was also reported that type-I FeCH could be translocated into mitochondrion and the type-II FeCH was mainly translocated into thylakoid membranes and to a limited extent into the envelope (Suzuki *et al*., 2000, 2002). The two types of FeCH are reported to be involved in haem biosynthesis for different cellular requirements. In the case of type-I FeCH, photoprotective molecules and cytochromes are formed in non-photosynthetic tissues. Photosynthetic tissues with the type-II FeCH have to balance the formation of haem and Chl (Singh *et al*., 2002; Suzuki *et al*., 2002).

Roper and Smith (1997) described the localisation of FeCH to both the envelope and thylakoid membranes in pea chloroplasts indicating that regulation between the ion chelating branch in tertapyrrole biosynthesis is not by sublocalisation of enzymes. Papenbrock *et al*., (2001), however, reduced type-II FeCH activity through the use of antisense RNA expression, which did not reduce type-I FeCH activity but neither was it able to compensate for the loss of activity in plastids. The excess Proto destined for haem biosynthesis was not channeled into Chl production. Sobotka *et al*., (2005) have shown that the C-terminal extension of FeCH found exclusively in oxygenic phototrophs is involved in Chl binding and regulation of Chl biosynthesis. This C-terminal extension is also essential for FeCH activity and analysis of the role of this C-terminal domain suggests a role for FeCH in Proto regulation (Sobotka *et al*., 2008; 2011), consistent with the proposal that haem availability decreases tetrapyrrole synthesis (Beck and Grimm, 2006) possibly due to downregulation of GluTR activity (Srivastava and Beale, 2005).

1.6.10. Magnesium chelation into protoporphyrin IX

The next step is the chelation of a divalent metal ion into the macrocycle. This commits to the formation of either haem or Chl depending on which ion is inserted. Fe^{2+} by ferrochelatase commits to haem synthesis and is energetically favourable, so the reaction is ATP-independent. The weter shell that exists around Mg^{2+} makes the reaction energetically unfavourable and so studies into the enzyme that catalyses this reaction show there to be a requirement for ATP (Gibson *et al*., 1995; Jensen *et al*., 1996a).

Three genes *bchI*, *bchD* and *bchH* in of *Rba. capsulatus* and *Rba. sphaeroides* were discovered to be essential for MgCH activity as mutation in these genes resulted in abolition of MgProto synthesis (Coomber *et al*., 1990; Suzuki *et al*., 1997; Naylor *et al.*, 1999) and accumulation of Proto (Bollivar *et al*., 1994a). Gibson *et al*., (1995) overexpressed the genes in *E. coli* and *in vitro* assays demonstrated that BchI, BchD and BchH were the essential subunits of active MgCH. The homologous genes ChlI, ChlD and ChlH were also discovered to be the essential MgCH genes in *Synechocystis* using the same technique (Jensen *et al*., 1996a). These studies provided the first direct evidence that three different protein subunits were required for Mg chelation, and showed that the enzyme was well conserved between purple bacteria and cyanobacteria.

Using purified subunits from *Rba*. *sphaeroides* and *Synechocystis* stoichiometries of 36BchH:4BchI:1BchD and 4ChlH:2ChlI:1ChlD respectively, were found to be optimum for *in vitro* steady-state assays (Gibson *et al*., 1999; Jensen *et al*., 1999a). Studies have been performed using enzyme from tobacco (Papenbrock *et al*., 1997) and recently rice (Zhou *et al*., 2012).

The Mg chelatase subunits, Chl/BchH, Chl/BchI and Chl/BchD, have predicted molecular masses of 120-155 kDa, 37-46 kDa and 60-87 kDa, respectively. Walker and Willows (1997) have shown that across various species the protein sequence identity vary from 38-86% for the H subunit, 50-90% for the I subunit and 28-58% for the D subunit. The N-terminus of the D subunit shares around 40 % identity to BchI and ChlI. This has led to the proposal that through the process of evolution there was a duplication of the I subunit and a gene fusion forming D (Jensen *et al*., 1996a).

With the overexpression and purification of active MgCH subunits it has been possible to assign roles to each protein despite the actual mechanism of chelation remaining unknown. The H subunit has been shown to bind both the substrate and product of the MgCH reaction (Karger *et al*., 2001) but does not exhibit ATPase activity (Sirijovski *et al*., 2006). The I and D subunits were first shown to form a complex dependent on the presence of ATP and Mg^{2+} by Gibson *et al*., (1999). This was quickly followed by evidence to show that the I subunit has ATPase activity, is a member of the ATPases Associated with carious cellular Activities (AAA^{+}) family of proteins (Jensen *et al*., 1999; Neuwald *et al*., 1999) and formed complexes with an estimated MW of 290 kDa

in the presence of ATP (Jensen *et al*., 1998). The D subunit has a Metal Ion Dependent Adhesion Site (MIDAS) that has been proposed to be associated with divalent metal ion binding (Jensen et al., 1996; Axelsson *et al*., 2006). I and D preincubation in the absence of ChlH was able to reduce the lag phase in the MgCH reaction that has been observed (Jensen *et al*., 1998; Reid *et al*., 2003). The I subunit has also been shown to be capabale of binding Mg^{2+} and ATP hydrolysis only occurs on the binding of a second magnesium. The I•D subunit has significantly reduced ATP hydrolysis when compared to the full MgCH complex or the I subunit alone. Most kinetic analyses of MgCH show a cooperative response to Mg^{2+} (Jensen *et al*., 1998; Gibson *et al*., 1999). Reid *et al*., (2003) have shown that the I subunit will isomerise upon binding to nucleotide changing its affitity for Mg^{2+}. 15 MgATP molecules are hydrolysed for each MgCH reaction turnover and Mg^{2+} bound enzyme is more effective as a catalyst confirming the notion of Mg^{2+} positive cooperativity.

AAA^{+} proteins form oligomeric complexes and Reid *et al*., (2003) have shown that the I subunit from *Synechocystis* forms a heptameric complex and hexamers have been seen in BchI complexes (Fodje *et al*., 2001; Willows *et al*., 2004). The structure of BchI has been solved to 2.1 Å (Fodje *et al*., 2001). Karger *et al*. (2001) observed red shifts in both porphyrin fluorescence excitation and emission when BchH bound tetrapyrrole, which is consistent with non-planar distortion of the macrocycle. This suggests a conformational change occurs in H when binding tetrapyrrole. The only structural information available for the H subunit is a negative stain EM 3D single particle reconstruction from *Rba. capsulatus*. The model confirms a conformational change in the H subunit upon the binding of Proto shown in Fig. 5 (Sirijovski *et al*., 2008).

Sawicki and Willows (2008) show that when the BchH•proto complex is formed it will bind tightly, with no evidence of chelation. Pre-incubation of BchD and BchI appear to form a complex, expected to be double hexamer. This complex appears to interact with BchH in a transient fashion whereby BchH undergoes a conformational change, perhaps distorting the protoporphyrin in a similar fashion to that of ferrochelatase described by Al-Karadaghi *et al*., (2006). Al-Karadaghi *et al*., (2006) infer that this distortion of the porphyrin macromolecule is to specify which metal is to be chelated into the ring structure, and so it can be assumed that the degree of distortion enables this specificity. Although no mechanistic evidence has been published, models have

been proposed for the interaction between the MgCH subunits. As well as D having N-terminal homology to I (which may catagorise D in the AAA^+ family) it also contains an integrin I domain at the C-terminus. H and I have also been proposed to contain integrin I binding motifs which could indicate sites of interaction (Fodje *et al*., 2001). Sawicki and Willows (2008) have devised a scheme whereby BchH undergoes a conformational change to $BchH^*$ in the presence of the BchI•BchD complex. Here it is possible to predict a bend in the porphyrin, consequent chelation of a metal ion and disassociation of the BchI•BchD complex and BchH. An additional transient interaction between the BchI•BchD complex and BchH exchanges Mg-protoporphyrin IX for Proto (if available) and the cycle continues (Fig. 6).

It appears that the rate limiting step in this reaction is the interaction and binding of BchH and Proto, the hydrolysis of ATP by BchI•BchD is ~40 fold greater. It must also be noted that post chelation, ATP hydrolysis does not stop, even in the absence of Proto. This indicates that *in vivo* there must be some interaction with another protein or molecule that inhibits ATPase activity. A possible suggested inhibitor could be the next enzyme in the pathway, Mg-protoporphyrin methyltransferase (ChlM/BchM) due to their previous observed interaction (Pontier *et al.*, 2007; Shepherd, McLean and Hunter, 2005).

In addition to being the MgCH Proto binding protein ChlH has also been associated with other functions. The plant hormone abscisic acid (ABA) has been shown to be bound by ChlH (Zhang *et al.*, 2002; Shen *et al.*, 2006) but Müller and Hansson (2009) questioned these results as they were unable to observe binding in barley ChlH. ChlH has also be postulated to have a role in sugar catabolism by regulating the anti-sigma factor, SigE (Osanai *et al.*, 2009).

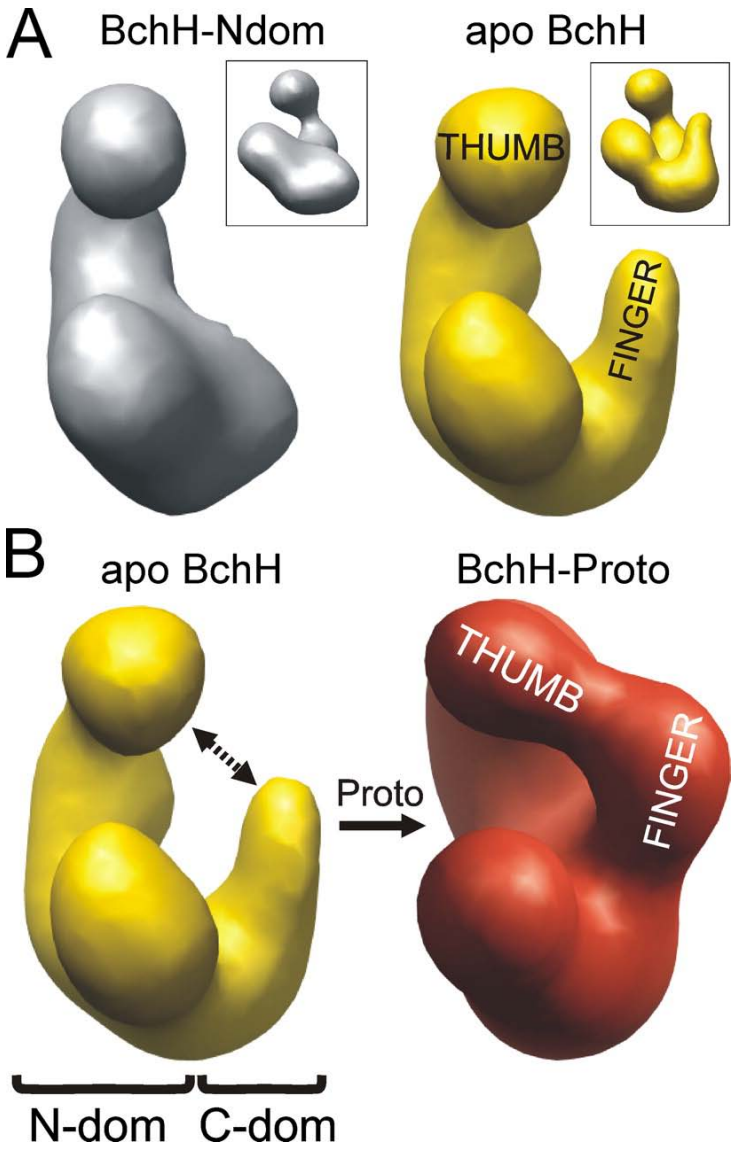

Figure 5 - Electron microscopy negative stain single particle 3D reconstruction of BchH

Grey represents the N terminal domain of BchH. Yellow show apo BchH and red indicates BchH•Proto complex. The N- and C-terminal domains fuse upon substrate binding of the substrate (Sirijovski et al., 2008).

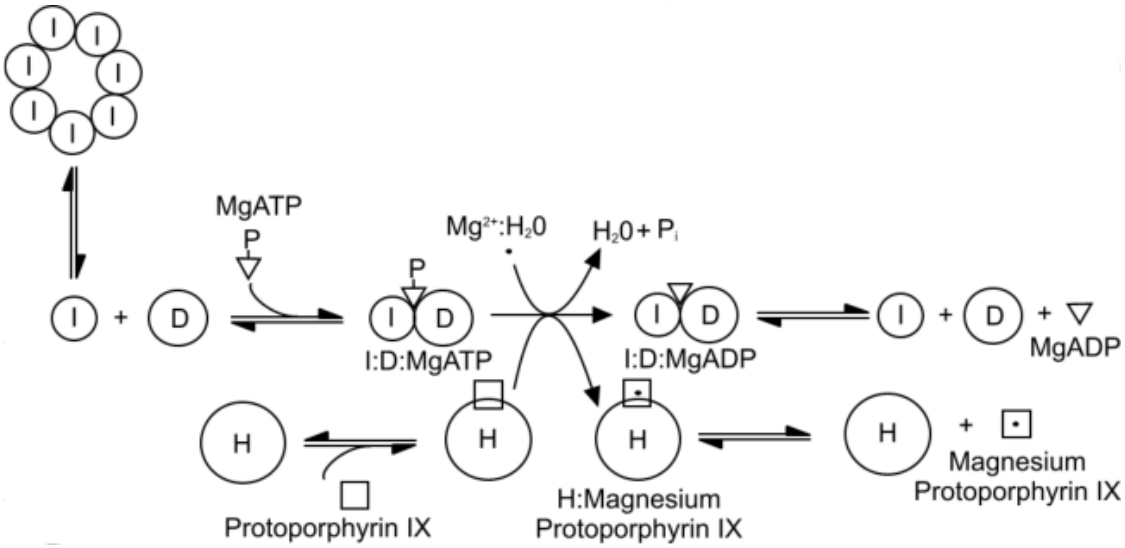

Figure 6 – A mechanism explaining one possible scenario of Mg^{2+} chelation of protoporphyrin IX by MgCH

A proposed method for the MgCH reaction based on current understanding of the enzyme. H binds Proto preventing photooxidation and the creation of singlet oxygen radicals. Energy is probably used to remove the hydration shell from Mg^{2+} (Heyes and Hunter, 2009).

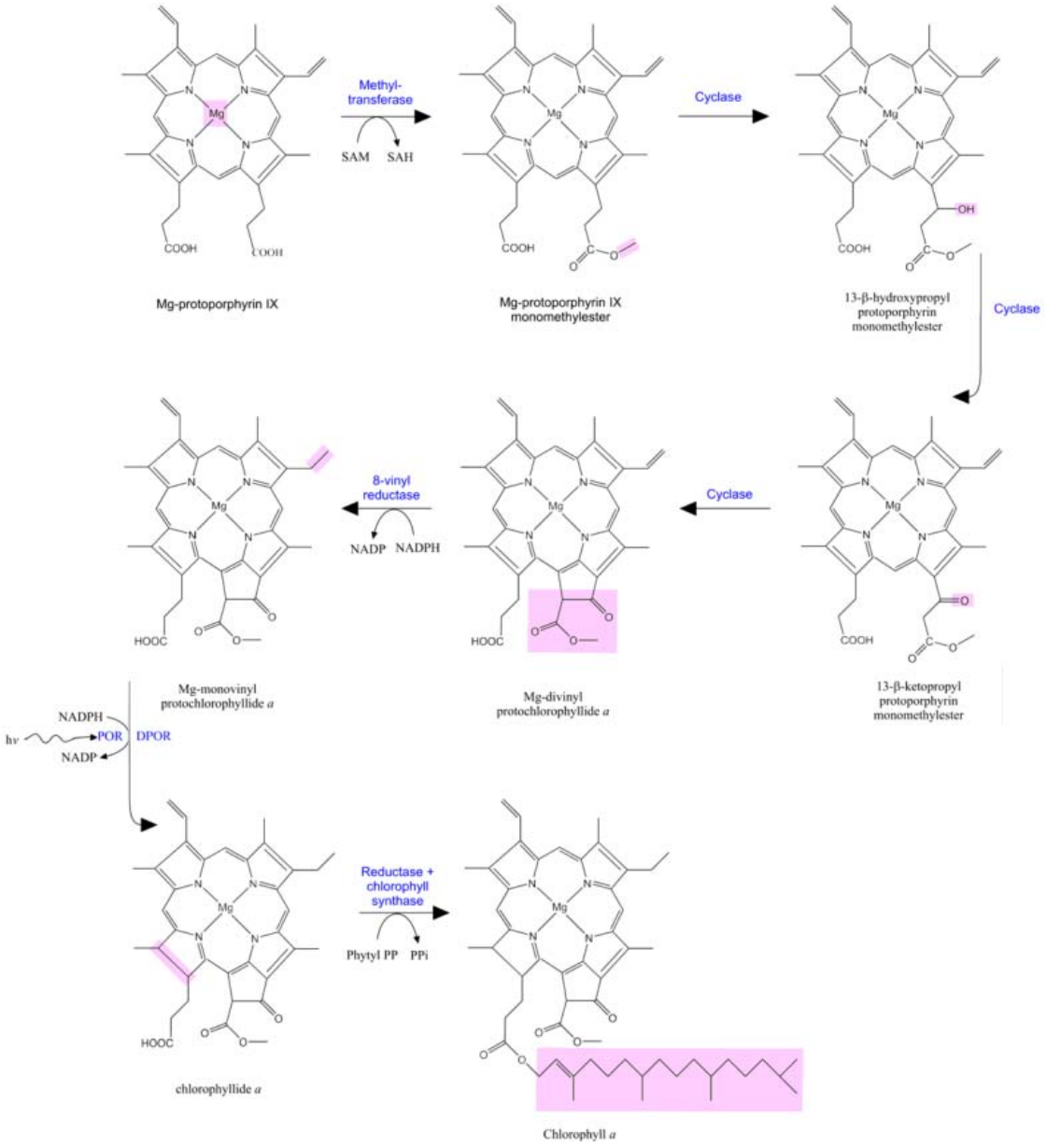

Figure 7 - Magnesium protoporphyrin IX to chlorophyll a

The enzymes catalysing each step are shown in blue. Magenta shading indicates the groups modified at each stage.

1.6.11. Gun4

Signalling between the plastid and nucleus allows the regulation of genes expressing proteins with photosynthetic function. It was discovered that tetrapyrroles are involved in signalling with the identification of *gun* (*g*enome *un*coupled) mutants in *Arabidopsis* found to have derepressed levels of *Lhcb* transcripts (Mochizuki *et al*., 2001). These mutants had the expression of nuclear encoded genes uncoupled from the physiological state of the plastid. Of the *gun* genes that were identified, *gun2* encoded haem oxygenase, *gun3* encoded phytochromobilin synthase and *gun5* was identified as encoding the H subunit of Mg-chelatase (Mochizuki *et al*., 2001). Due to the *gun* mutants effect on tetrapyrrole biosynthesis the amount of MgP_{IX} in tetrapyrrole biosynthesis was lowered. To check for a change in the expression of ChlH, ChlI mutants were used but had no effect. Through binding of the substrate and/or product of the MgCH reaction ChlH has been proposed to regulate synthesis of both haem and Chl (Gibson *et al*., 1996). The change in nuclear gene expression indicated that ChlH signalling had been uncoupled from the nucleus.

When the *gun5* gene was cloned from *Arabidopsis* a substitution mutation of A990V in a region conserved throughout H homologues was discovered (Mochizuki *et al*., 2001) and this mutation reduced Chl levels by around 25 % of WT (Strand *et al*., 2003). Another *gun* mutant *Gun4* was shown to be necessary for Chl accumulation but not its synthesis. When Gun4 was analysed by gel filtration a soluble protein of 22 kDa was isolated and co-purified with ChlH (Larkin *et al*., 2003). In light of this, a *gun4gun5* double mutant was produced which showed severe Chl deficiency (Mochizuki *et al*., 2001).

Gun4 has been shown to be non essential to the MgCH chelation reaction both *in vivo* and *in vitro*. It does however dramatically increase the rate at which the enzyme can work. Gun4 also binds MgP_{IX} more tightly than ChlH suggesting a role of chaperoning Chl intermediates to the next enzyme in the pathway or sequestering the product until needed (Larkin *et al*., 2003). Davison *et al*. (2005) performed more detailed kinetic analysis of the effect of Gun4 on MgCH activity and noted the lowered concentration of Mg^{2+} required for activity. The cooperativity for Mg^{2+} shown by MgCH means that in the dark when magnesium levels in the chloroplast are low (~0.5 mM) MgCH is

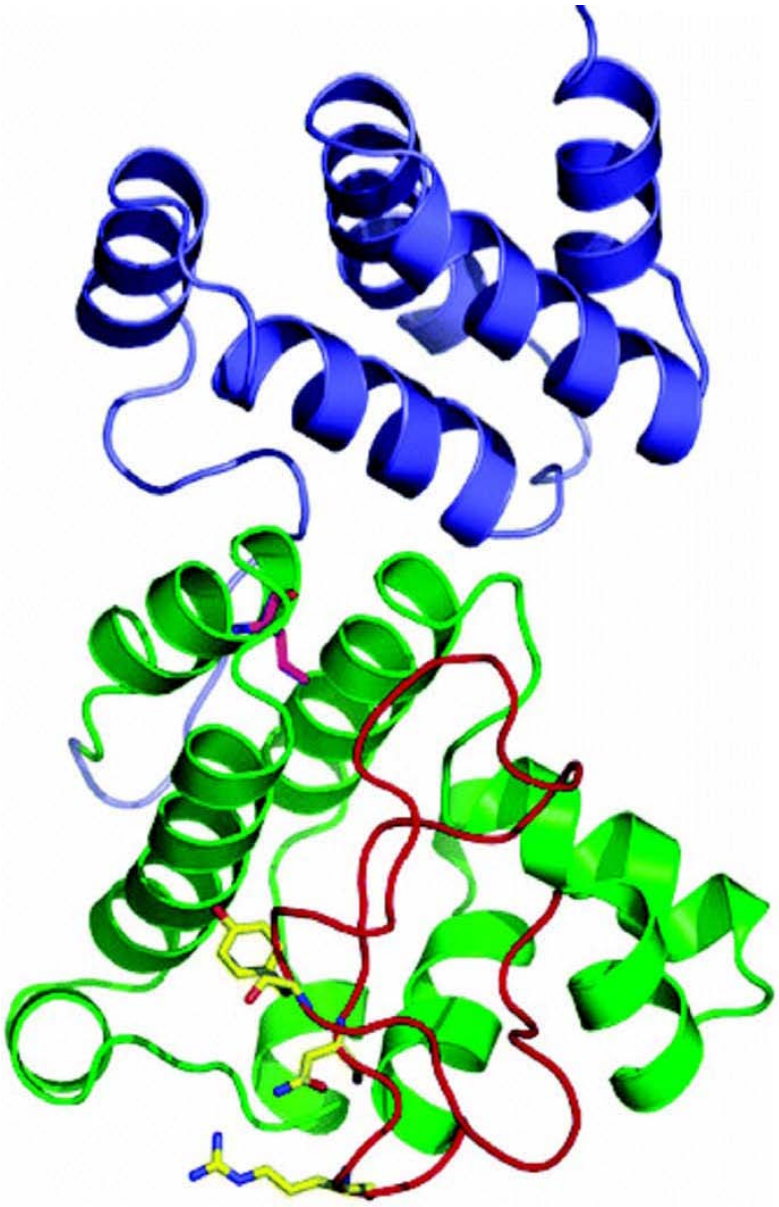

Figure 8 - The structure of Gun4 from T. elongatus

1.5 Å structure of the Thermosynechococcus elongatus Gun4. The Green domain is the Gun4 domain which is conserved between T. elongatus and Arabidopsis and the blue domain is unconserved. The red loop contains many invariant residues and is thought to have a role in ligand binding (Davison et al., 2005).

inactive. During the day the [Mg^{2+}] rises (~6 mM) and so the MgCH is active and it would appear that the role of Gun4 is to act as a switch to allow Chl synthesis in lowered Mg^{2+} or P_{IX} conditions (Reid and Hunter, 2004; Davison *et al*., 2005). Recent studies have shown that Gun4 also has the capacity to revive the *cch* and *gun*5 mutants in *Synechocystis* to WT levels (Davison and Hunter, 2011). Structures of both the *Synechocystis* and *T. elongatus* Gun4 (Fig. 8) proteins have been solved showing a two-domain, highly helical protein with invariant residues clustered in a patch on the surface providing the proposed porphyrin binding region within a small hydrophobic cleft (Verdecia *et al* 2005; Davison *et al*., 2005).

1.6.12. Magnesium protoporphyrin IX to magnesium protoporphyrin IX monomethyl ester

ChlM/BchM is the succeeding enzyme in the pathway after the chlorophyll/haem branch. ChlM/BchM is a methyltransferase and methylates Mg-protoporphyrin to Mg-protoporphyrin monomethylester (MgPME), using S-adenosyl-L-methionine (SAM) as a co-factor and methyl group donor (Jensen *et al.*, 1999). Pontier *et al*., (2007) show that ChlM/BchM is absolutely essential in chlorophyll metabolism and chloroplast assembly. In ChlM/BchM absent mutants there is evidence to show an accumulation of Mg-protoporphyrin that cannot progress through the following steps of the pathway.

(Bacterio)chlorophyll metabolism is a highly regulated process, with key steps managing the flux of intermediates down the pathway (Masuda, 2008). Pontier *et al.*, (2007) describe a ChlM/BchM deficient mutant where, as a result, the light harvesting chlorophyll-binding protein (LHCB) mRNA concentration is greatly reduced. This indicates that the substrate, Mg-protoporphyrin, acts as a negative effector and its accumulation reduces the translation of genes of the photosynthetic machinery. Conversely, Mg-protoporphyrin monomethylester may act as a positive effector and its absence in the cell prevents the correct signals reaching the nucleus through retrograde signalling (Pesaresi *et al.*, 2006; Pontier *et al.*, 2007).

Furthermore it appears that ChlM/BchM has activity involving the formation of cytochrome b6f which has a role in the formation of charge separation through the electron transport chain (Pontier *et al.*, 2007).

1.6.13. Formation of the isocyclic ring

The Mg-protoporphyrin monomethylester cyclase (MgCy) is an enzymatic complex that is involved in the conversion of Mg-protoporphyrin monomethylester to 3,8-divinyl protochlorophyllide (Pchlide). This occurs through the incorporation of oxygen in position 13 of the 13-methyl propionic acid side chain forming a keto group and the isocyclic ring (ring E) that makes up the fifth ring of chlorophyll. The keto group is functionally essential for active chlorophyll; there is currently no evidence of a functional chlorophyll molecule without this group located at position 13 (Rudiger, 1997). The MgCy in higher plants and *Synechocystis* has been shown to have both soluble and membrane bound components whereas the *C. reinhardtii* MgCy appears to be found exclusively in the thylakoids (Beale, 1999; Bollivar and Beale, 1996). Cyanobacteria and purple bacteria have both oxygen dependent and independent forms of the MgCy (Minamizaki *et al*., 2007; Peter *et al*., 2009).

The MgCy has never been successfully purified despite attempts for over 50 years and consequently is the least understood enzyme of the chlorophyll biosynthesis pathway. Despite the absence of any hard evidence, a number of theoretical assumptions have developed since pioneering experimentation by Granick. In 1969, Ellsworth and Aronoff identified intermediates of cyclic ring formation that correlated with Granick's suggestion that the formation followed a similar fashion to the β-oxidation of fatty acids. These oxygen independent intermediates have been described as acrylate, β-hydroxy and β-keto, the oxygen dependent pathways do not appear to involve the acrylate intermediate.

Walker *et al*., (1989) studied the MgCy in higher plants investigating the origin of the incorporated oxygen in the isocyclic ring. Through their studies, using $^{18}O_2$ labelling, strong evidence suggests that oxygen is derived from the atmosphere, through identification using mass spectrometry. A number of additional studies confirm these observations in higher plants and in green algae (Spiller *et al.*, 1982; Chereskin *et al.*, 1983; Bollivar and Beale, 1995). However, in purple bacteria, a similar experiment was performed using $^{18}O_2$ in either the atmosphere or in water ($H_2{}^{18}O$). Their results showed that oxygen for the isocyclic ring was derived exclusively from water (Porra *et al*., 1996).

Because *Synechocystis* and higher plants have both a soluble and membrane requirement to the function of MgCy it is evident there are at least two subunits that are essential. It has been suggested that the membrane fraction may incorporate a heavy element, whereas the soluble component has a mass >30 kDa and may have interaction with porphyrins. Bollivar and Beale (1996) showed that NADPH and non-heme Fe are both important for the reaction, as the inclusion of Fe chelators inhibited the cyclase reaction. *bchE* from *R. capsulatus* (Bollivar *et al*., 1994) and *R. sphaeroides* (Naylor *et al*., 1999) and *acsF* from *R. gelatinosus* (Pinta *et al*., 2002) and *Synechocystis* (Minamizaki *et al*., 2007) with newly discovered *ycf54* (Hollingshead *et al*., 2012) remain the only genes to be identified. In these studies, a knockout of either gene resulted in the accumulation of Mg-protoporphyrin monomethylester, resulting in a blockage in the pathway. *bchE* encodes a protein with a predicted molecular weight of ~66kDa. In a proposed mechanism for the anaerobic reaction *bchE* uses a cobalamin co-factor, where adenosylcobalamin uses an adenosyl radical which results in a 13_1-radical of MgPME and a subsequent 13_1-cation. 13_1-hydroxy intermediate of MgPME results from reaction with a hydroxyl ion and Pchlide is formed from the loss of 3 hydrogen atoms (Bollivar *et al*., 1994)

.

This reaction is ultimately what changes the colour of the tetrapyrrole from red to green and consequently give plants and algae their characteristic colour.

1.6.14. Reduction of the 8-vinyl group

The 8-vinyl group of the B ring is reduced at some point in the biosynthesis and is an essential step for the formation of chlorophyll. It is however not currently known at which specific stage it is reduced. There is evidence for a number of specific intermediates, but they appear to be influenced by environmental conditions and the species of organism. It has been further proposed that there may be several enzymes capable of following several pathways and even one enzyme that have a broad degree of substrate specificity for the many intermediates (Shioi and Takamiya, 1992); (Rebeiz et al., 1994);(Tripathy and Rebeiz, 1986); (Tripathy and Rebeiz, 1988).

1.6.15. Reduction of protochlorophyllide to chlorophyllide

1.6.15.1. POR

After the reduction of the 8-vinyl group of ring B, Pchlide is reduced via the addition of a hydrogen atom across the C17-C18 double bond of the D ring. This results in the formation of chlorophyllide, or Chlide. There are two separate enzymes that can catalyse this reaction, one is dependent on light and the other is not. NADPH-Pchlide oxidoreductase is the light-dependent enzyme and is found in all chlorophyll producing organisms, whereas the light independent Pchlide oxidoreductase ((dark) DPOR) appears to be absent in angiosperms but present in all other photosynthetic organisms. Bacteriochlorophyll producing organisms appear to only have the light independent enzymes (Suzuki and Bauer, 1995).

The light dependent enzyme POR shares its dependency for light with only one other enzyme, DNA photolyase. The reaction mechanism works through the use of NADPH as a co-factor, where in the dark a ternary complex of Pchlide-POR-NADPH forms. On illumination of the photoreceptor complex, the hydride molecule is transferred quickly to the Pchlide molecule forming Chlide (Heyes and Hunter, 2005).

Using 4R and 4S ^{3}H-labelled isomers detailed information has been obtained determining the essential processes. The *pro-S* hydride from the nicotinamide ring found in NADPH is transferred to the C17 in Pchlide. It is thought that a lysine (Lys193, in *Synechocystis*) enables a tyrosine residue (Tyr 189 in *Synechocystis*) to become de-protonated, by lowering the pKa and therefore able to donate a proton in much the same way as a general acid, to C18 (Heyes and Hunter, 2005; Wilks and Timko, 1995). The Tyr and Lys residues appear to be highly conserved across all species The photoreductive process that they enable is very important and inherent to the assembly of the photosynthetic machinery.

Recent studies show that it is essential for POR to be pre-bound to NADPH to allow substrate binding. The binding of NADPH to POR is itself intricate with three probable kinetic phases. These phases are characterised with structural changes in the protein to

allow correct docking and this seems to be further consistent with the continuation of structural changes in POR. It is therefore not surprising that the initial formation of the ternary complex is the rate limiting process of the formation of Chlide from Pchlide (Heyes *et al.*, 2008).

1.6.15.2. DPOR

Three genes have been identified that are essential to the light independent reduction of Pchlide. They are known as *bchL, bchN* and *bchB* in *R. capsulatus* and the homologous genes in cyanobacteria and a variety of other species including some of the red and green algae and liverwort known as *chlL, chlN* and *chlB.* These prove to be extremely similar in peptide sequence to the nitrogenase subunits NifH, NifD and NifK. Between the NifH and BchL/ChlL, four Cys residue are highly conserved and in the NifH subunit these are located in an ATP-binding domain and would suggest the likely possibility of an ATP dependent electron transfer role in DPOR (Nomata *et al*., 2006). Fujita and Bauer (2000) observed co-purification of the BchN and BchB subunits, suggesting a tight complex formation between the two. Recently active BchL and BchN/BchB complex have been purified in *E. coli* and potentially promise the further elucidation of crystal structures and kinetic information (Yamamoto, Nomata and Fuita, 2008).

In all bacteriochlorophyll and most chlorophyll containing organisms, both the POR and DPOR systems are available for the reduction of Pchlide to Chlide. Only angiosperms remain totally dependent on light for the production of chlorophyll. This raises questions as to why both mechanisms, that appear to be independently regulated, evolved in parallel. It has been observed in *Plectonema boryanum* that in high light intensities POR contribution to the reduction of Pchlide is greater (Yamazaki et al., 2006). It could be that in the higher light intensities it is preferential to convert more of the chlorophyll intermediates to the more stable chlorophyll to prevent and reduce the extent of photooxidative damage.

1.6.16. Esterification of (bacterio)chlorophyllide to (bacterio)chlorophyll

The last reaction is the addition of a phytol tail to Chlide to produce Chl. After esterfication, numerous hydrogenation reactions follow. The ring D is esterified with phytol by the product of the *bchG*/*chlG* genes, Chl synthase, origionally found in *Rba. sphaeroides* by Bollivar *et al*., 1994. As a result of this, hololologues were found in *Synechocystis* (Kaneko *et al*., 1995), *Rba. sphaeroides* (Naylor *et al*., 1999) and *Arabidopsis* (Gaubier *et al*., 1995). BchG/ChlG is a membrane bound protein, likly to have nine trans-membrane helices, explaining failed attempts topurify soluble active protein (Rüdiger *et al*., 1980; Schmid *et al*., 2001). *Geranylgeranyl*-Chlide is formed form the addition of geranylgeranyl phosphate to Chlide.

The increased hydrophobicity by the esterfication significantly helps the assembly of the light-harvesting complexes. The tails are also involved in the orientation of the transition dipoles of the tetrapyrrole rings that allows rapid energy transfer (Freer *et al*., 1996).

Active recombinant *Synechocystis* ChlG, purified from *E. coli*, was able to esterify Chlide but not bChlide, and *Rba capsulatus* BchG was able to perform the converse (Oster *et al*., 1997).

Geranylgeraniol-Chl reductase encoded by the gene *chlP* and its homologous counterpart *bchP*, engages in a three step reduction to form a phytyl group form the geranylgerany group (Addlesee and Hunter, 1999; Warren and Smith, 2009). Unlike BchG/ChlG, a *Rba sphaeroides* non-active *bchP* mutant could be complemented with a *Synechocystis chlP* gene, the result was BChls esterified with phytol. All the steps in the pathway after the chelation of Mg into protoporphyrin are shown in Fig. 7.

1.7. Photosystem II

Oxygenic photosynthesis occurs through two photosystems knows as photosystem I (PSI) and photosystem II (PSII). Energy flow through this system typically travels from PSII to PSI via an electron transport pathway. The electrons are derived from the splitting of water generating O_2 as a by product. The reduction of $NADP^+$ to NADPH and the formation of ATP from the proton gradient formed through this process allows the Calvin cycle to reduce CO_2 to carbohydrates.

The D1 and D2 proteins in PSII bind the cofactors involved in energy transfer like the L and M proteins do in the in the bacterial reaction centre. Absorption of light by the "special pair" of electrons in PSII (a pair of chlorophyll molecules that behave as a dimer), referred to as P680 due to the wavelength of light they absorb, transfer an electron to a nearby pheophytin. Pheophytin, a chlorophyll molecule without a Mg^{2+} ion and with two H^+ ions instead, in turn donate an electron to plastoquinone at site Q_A. This electron is then transferred to plastoquinone site Q_B and with the uptake of two protons from the stromal side of the thylakoid membrane results in the species known as QH_2.

The PSII special pair left is a strong oxidant ($P680^+$) from the loss of the electron. This electron is replaced by the splitting of water at the oxygen-evolving complex, consisting of four manganese ions, a calcium ion, a chloride ion and a tyrosine residue. mitThe manganese cluster, of the oxygen-evolving complex, is stripped of an electron by $P680^+$ leaving it reduced. Manganese, with its ability to form strong bonds with oxygen, is able to oxidise two molecules of water in this reduced state, forming O_2, the four resulting H^+ remain in the thylakoid lumen creating a proton gradient. (Bricker, 1990; Metz *et al*., 1989; Barber *et al*., 1997).

Zouni *et al*. (2001) solved the PSII structure from *T. elongatus* to 3.8 Å (figure 9). It clearly shows that PSII is a homodimer and accounts for most of the polypeptides and cofactors including the Mn_4 cluster.

The reduced plastoquinol made from the excitation of P680 and the splitting of water is transferred to oxidised plastocyanin, reducing it, via the Fe-S protein of the

cytochrome *bf* complex. The oxidation of plastoquinol initiates the release of the protons, initially taken up from the chloroplast stroma, into the thylakoid lumen further adding to the proton gradient generated from the splitting of water.

1.8. Photosystem I

The special pair of chlorophylls in PSI, known as P700 for the same reason as for P680, absorb light and transfer an electron to a 4Fe-4S cluster via a quinone. This electron goes on to reduce ferredoxin. The oxidised $P700^{+}$ gains an electron from the reduced plastocyanin from the reactions of PSII.

Two reduced ferredoxin proteins have their electrons removed by the enzyme ferredoxin-$NADP^{+}$ reductase. The sequential uptake of the electrons by ferredoxin-$NADP^{+}$ reductase reduces the enzyme which then drives the transfer of H^{-} to $NADP^{+}$ forming NADPH that goes on to be used in the Calvin cycle. The uptake of a proton in the formation of NADPH further increases the proton gradient. The proton gradient that is formed drives the enzyme ATP synthase, found in the thylakoid membrane between the proton gradient, and forms the ATP needed for the Calvin cycle.

Photosynthesis relies on the absorption of photons by pigment molecules. For efficient transduction of energy it is essential that the pigment is in close proximity with a quinone molecule and thus the electron can be transferred. This would however result in photon energy located outside the photosystem reaction centres to be lost. Structural arrays of light capturing pigments have evolved to surround reaction centres energy is then transferred to reaction centres often via a number of intermediate pigments. Chlorophyll absorbs at wavelength spectra of ~440 and ~680nm (Shen e*t al.,* 1993) and exhibits initial limitations to any energy outside of these two specific wavelengths. Cyanobacteria have evolved a method to circumvent this limitation in the formation of phycobilisomes, protein complexes of phycobiliproteins connected together through linker polypeptides. Phycobilisomes range in their structure and can absorb light in a vast range, 500–650 nm, which is transferred to photosystem II. It has been suggested (Liu *et al.,* 2005) that the specific tuning of these specific absorbance wavelengths are perhaps due to the combination of phycobiliproteins and their associated linker peptides.

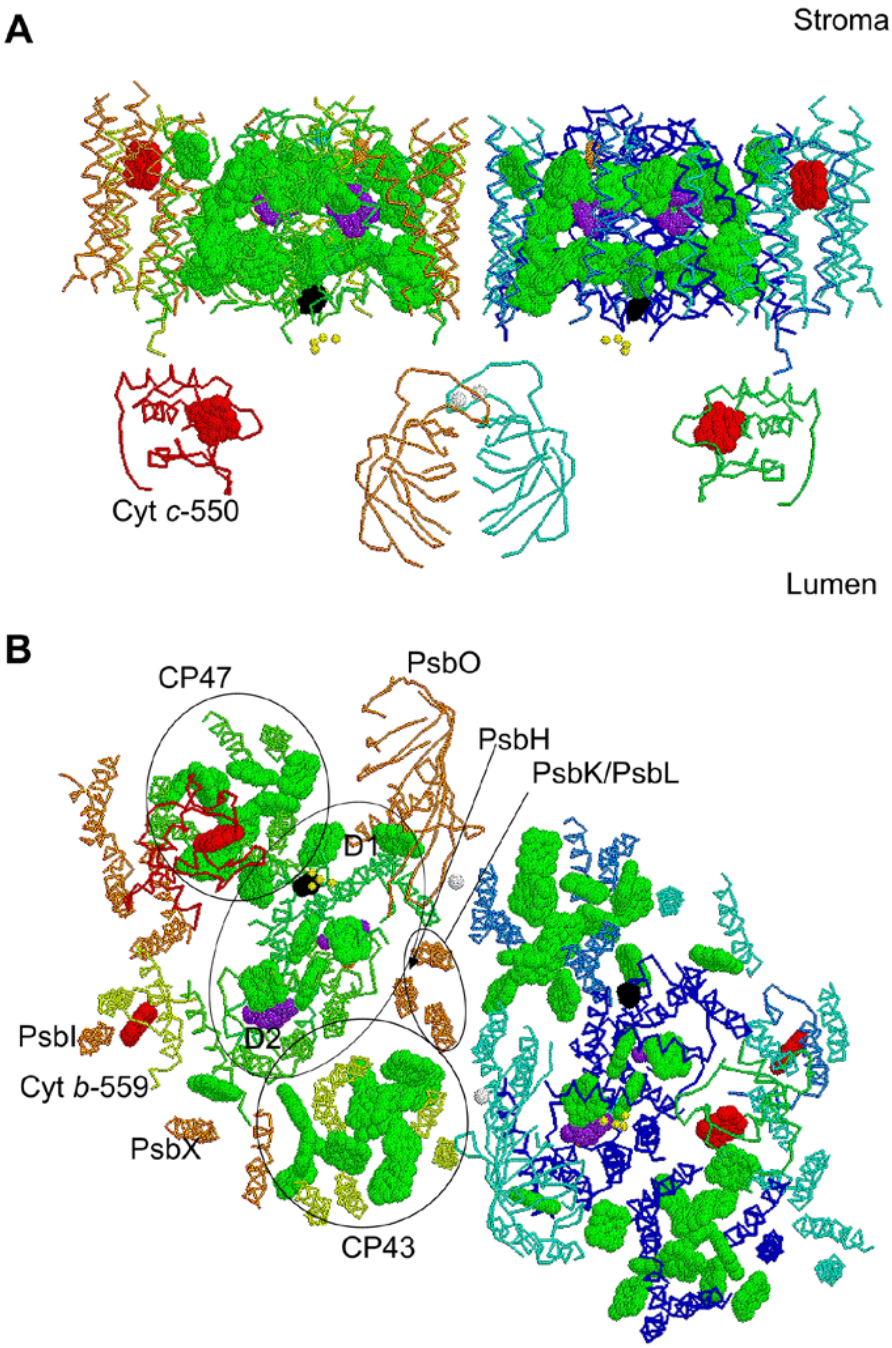

Figure 9 - The structure of the PSII dimer from Thermosynechococcus elongatus

A) Side view along the plane of the membrane

B) View from the lumenal face. D1 and D2 refer to the RC subunits and the circles labelled CP43/CP47 refer to the core antenna. CP43/CP47 on the other half of the dimer have been omitted. The following cofactors are shown with their colours in brackets: Chlorophyll a (green), haem (red), manganese cluster (yellow), non-haem iron (cyan) phaeophytin (purple), plastoquinone (orange) Tyr2 (black) (adapted from Zouni et al., 2001).

1.9.Project Aims

1. Devise a protocol for the purification of *T. elongatus* ChlH that is of a high enough quality for structural studies. Devise a method that allows the observation that ChlH is either bound or unbound to the substrate D_{IX}.

2. Collect single particle images of highly pure apo and substrate bound ChlH using electron microscopy. Using the single particles collected; create a 3D model of the protein in both states with collaboration with Dr. Pu Qian.

3. Investigate any interesting characteristics of the ChlH structure for functional properties.

4. Characterise the kinetic parameters of the thermophilic MgCH from *T. elongatus.*

5. Try to obtain any evidence for the interaction of MgCH *in vivo* using FLAG-tagged MgCH subunits in *Synechocystis*.

CHAPTER 2

Materials and Methods

3.1.Materials

Unless otherwise stated, chemicals were obtained from Sigma Chemical Co. and were of analytical grade. Glutathione, benzamidine, chelating, anion exchange and size exclusion Sepharose was purchased from GE Healthcare. All porphyrins were purchased from Frontier Scientific Porphyrin Products. All chemicals for acrylamide electrophoresis were purchased from Novagen.

3.2.Standard Buffers, Reagents and Media

All buffers and culture media were prepared as described in Sambrook *et al*. (1989), unless otherwise stated. Growth media were prepared using deionised water. Buffers and solutions for DNA work were prepared using distilled water, which was further purified by passage through a Milli-Q system (Millipore) (QH_2O). Analytical-grade reagents were used for DNA work. Growth media, buffers and solutions used for DNA work were sterilised by autoclaving at 15 p.s.i. for 20 min, or by filtration through 0.2 μm filters. Heat-labile solutions, such as antibiotics, were only added to culture media once they had cooled to below 50°C.

3.3.*Escherichia coli* strains and plasmids

All *E. coli* strains and plasmids used in this work are listed at the end of this chapter. Strains were routinely grown in Luria-Bertani (LB) medium, and when grown in liquid were agitated at 300 rpm. When antibiotic selection was required, the following concentrations were used; 30 μg ml^{-1} neomycin, 150 μg ml^{-1} ampicillin, 8.5 μg ml^{-1},

chloramphenicol. Stocks of *E. coli* strains were stored at -80°C in 50:50 LB medium:glycerol (v/v).

3.4.*Synechocystis* strains

All strains of *Synechocystis* sp. PCC 6803 described in this thesis, detailed in Chapter 4, were derived from the WT strain of Prof. Wim Vermaas (Arizona State University), donated by Dr. Roman Sobotka (Institute of Microbiology, Třeboň, Czech Republic). Strains were routinely grown in BG-11 medium (Rippka *et al*, 1979), and when grown in liquid were agitated at 150 rpm. Stocks of *Synechocystis* strains were stored at -80°C in 3:1 BG-11 medium:40% DMSO (v/v).

3.5.Production of competent *E. coli* cells

3.5.1. Chemically competent *E.coli* cells

All *E. coli* strains were treated as described by Hanahan (1985). *E. coli* cells were grown in 50 ml LB medium at 37°C until the OD_{600} of the cultures had reached between 0.4 and 0.5. The cells were pelleted by centrifugation, resuspended in 67 ml RF1 (0.1 M RbCl, 50 mM $MnCl_2$, 30 mM potassium acetate, 10 mM $CaCl_2$, 15% (v/v) glycerol, pH 5.8) and incubated on ice for 15 min. The cells were then centrifuged again and the pellet resuspended in 17 ml of RF2 (10 mM RbCl, 75 mM $CaCl_2$, 10 mM MOPS, 15% (v/v) glycerol, pH 6.8). The competent cells were stored as 100 µl aliquots at -80°C. Transformation efficiencies were routinely between 10^6 and 10^7 colony forming units per µg of DNA.

3.5.2. Electrocompetent *E. coli* cells

All *E. coli* strains were treated as described by Ausubel *et al.*, (1987). *E. coli* cells were grown in 500 ml LB medium at 37°C until the OD_{600} of the cultures had reached between 0.5 and 0.7 and incubated on ice for 25 min. The cells were pelleted by centrifugation and resuspended in 500 ml 10% (v/v) glycerol pH 7.0. Further centrifugation and resuspension steps were carried out using 250 ml, 50 ml and 1 ml

10% (v/v) glycerol pH 7.0 respectively. The cells were frozen in liquid nitrogen and stored as 50 µl aliquots at -80°C. Transformation efficiencies were routinely between 10^9 and 10^{11} colony forming units per µg of DNA.

3.6. Genetic transformation of cells

3.6.1. Chemical transformation of *E. coli*

An aliquot of chemically competent *E. coli* cells (prepared as in section 2.5.1) was thawed on ice. 10-50 ng of plasmid DNA in QH_2O was added to 100 µl of the cell suspension in a 1.5 ml microcentrifuge tube. After incubation on ice for 30 min, the cells were heat-shocked at 42°C for 45 s and incubated on ice for 5 min. 1 ml of LB medium was then added to the suspension. The cells were incubated at 37°C for 1 h, harvested by centrifugation, resuspended in 50 µl LB medium and spread on an LB agar plate with the appropriate selection. Colonies were allowed to grow overnight at 37°C.

3.6.2. Electroporation of *E. coli*

Electroporation was carried out as described by Miller and Nickoloff (1995). An aliquot of electrocompetent *E. coli* cells (prepared as in section 2.5.2) was thawed on ice. A precipitated ligation reaction (see section 2.7.1), dissolved in 10 µl QH_2O was added to 50 µl of the cell suspension in a 1.5 ml microcentrifuge tube. After incubation on ice for 2 min, the cells were transferred to an electroporation cuvette. An electric current was applied to the cuvette, 1 ml SOC medium was immediately added and the cells transferred to a 1.5 ml microcentrifuge tube. The cells were incubated at 37°C for 1 h, harvested by centrifugation, resuspended in 50 µl LB medium and spread on an LB agar plate with the appropriate selection. Colonies were allowed to grow overnight at 37°C.

3.7.Nucleic acid manipulation

3.7.1. Precipitation of DNA

Removal of chemical contaminants from DNA solutions was achieved by adding $1/10^{th}$ volume 70% glycogen or 3 M sodium acetate pH 5.2 followed by 2 volumes 96% ethanol. The DNA was then precipitated at -80°C for 2 h. The precipitated DNA was pelleted by centrifugation, washed in 200 µl 70% ethanol and repelleted. The DNA was then dissolved in a desired volume of QH_2O.

3.7.2. Small-scale preparation of plasmid DNA (mini-prep)

Small quantities of plasmid DNA were prepared using the FastPlasmid Miniprep DNA purification system (Eppendorf), according to the manufacturer's instructions, a copy of which can be downloaded from www.eppendorf.com. Transformed *E. coli* cultures were grown overnight in sterile plastic 7 ml universals containing 3 ml of LB medium with the appropriate antibiotic selection at 37°C in an orbital shaker (300 rpm). The DNA pellets were resuspended in 50 µl of QH_2O and stored at -20°C. The yield was typically about 5 µg of plasmid DNA per mini-prep.

3.7.3. Larger-scale preparation of plasmid DNA (midi-prep)

Larger quantities of plasmid DNA were prepared using the Hi-Speed Plasmid Midi Kit (Qiagen), according to the manufacturer's instructions, a copy of which can be downloaded from www.qiagen.com. Transformed *E. coli* cultures were grown overnight in 250 ml conical flasks containing 50 ml of LB medium with the appropriate antibiotic selection at 37°C in an orbital shaker (300 rpm). The DNA pellets were resuspended in 500 µl of QH_2O and stored at -20°C. The yield was typically about 50 µg of plasmid DNA per midi-prep.

3.7.4. Polymerase chain reaction (PCR)

Reactions were performed in a total volume of 50 µl containing 25 µl of 2x reaction mix (2.5 units of ACCUZYME, 2 mM dNTPs, 4 mM $MgCl_2$) (Bioline) 125 ng of each primer (table 2.4), and 100 ng of template DNA. Primers were produced by Sigma and resuspended in QH_2O to 125 ng μl^{-1}. Reactions were carried out using conditions appropriate to the T_m of the primers and the length of the fragment to be amplified, as specified in the Accuzyme instruction manual, a copy of which can be downloaded from www.bioline.com. Primers were denatured for 3 min at 95°C followed by 30 cycles of amplification using a touchdown PCR method where the annealing temperature was reduced by 2 °C every two cycles starting initially at 80 °C and finishing at 45 °C (e.g. 96°C, 1 min; 60°C, 45 s; 72°C, 2 min kb^{-1}) with a final extension for 10 min at 72°C in a PHC-3 Thermal Cycler (Techne). Following amplification, PCR reactions were cleaned up via gel purification (2.7.9.).

3.7.5. Restriction enzyme digestions

Restriction enzymes were purchased from Promega, and the suppliers' instructions followed with regard to reaction buffers and incubation temperatures. The DNA was then gel-purified (2.7.9).

3.7.6. Dephosphorylation of DNA

The 5'-phosphate groups were removed from the ends of DNA fragments, where necessary, by the addition of 1 unit of calf intestinal phosphatase (Boehringer Mannheim) to a restriction digest at the end of the digestion period. Incubation was continued for a further 30 min at 37°C. The reaction was then incubated at 65°C for 10 min prior to DNA gel purification (2.7.9).

3.7.7. Filling in recessed 3' ends of DNA fragments

Recessed 3' ends of DNA fragments were made blunt using the Klenow fragment of *E. coli* DNA polymerase I (Boehringer Mannheim). This was added to restriction enzyme digests after the reactions were complete, or to purified DNA fragments. $MgCl_2$ was added to purified fragments to a final concentration of 5 mM prior to the addition of Klenow fragment and dNTPs. Typically 1 unit of Klenow was added per μg of DNA and each dNTP was added to a final concentration of 0.1 mM. Reactions were incubated for 15 min at room temperature and then stopped by incubation at 65°C for 10 min.

3.7.8. Agarose gel electrophoresis of DNA

Restriction enzyme digests, PCR reaction products and purified DNA fragments were routinely analysed by electrophoresis through 0.8% agarose gels in 1 x TAE (40 mM Tris-acetate, 1 mM EDTA) running buffer containing 0.5 μg ml^{-1} ethidium bromide (Sambrook *et al*., 1989). 6x gel loading buffer (0.03% bromophenol blue, 0.03% xylene cyanol, 60% glycerol, 60 mM EDTA in 10 mM Tris-HCl, pH 7.6) was added to DNA samples, and 10-500 ng of DNA were typically loaded per lane; 200 ng of 1kb DNA ladder (Fermentas) was run as a marker alongside the samples in order to estimate the sizes of DNA fragments. DNA was visualised by exposure to a source of 254 nm ultraviolet light.

3.7.9. Recovery of DNA from agarose gels

DNA fragments requiring purification were electrophoresed through low-melting-point agarose gels in 1x TAE. The desired fragment was excised from the gel and the gel slice incubated at 65°C for 5-10 min. The DNA was extracted from the melted agarose using the QiaQuick Gel Extraction Kit (Qiagen), according to the manufacturer's instructions, a copy of which can be downloaded from www.qiagen.com.

3.7.10. Ligation of DNA fragments

In-Fusion® Advantage PCR Cloning was performed as according to the user manual available from (www.clontech.com) and then transformed into electrocompetent *E. coli* DH5α cells as described in 2.6.2.

3.7.11. DNA sequencing

A sample of plasmid DNA prepared by midi-prep (2.7.3) was diluted to give 15 µl at a concentration of 100 ng μl^{-1}. Samples were sent to Lark Technologies Inc. for sequencing. Results were returned by email and sequences analysed using the DNA Star software programme.

3.8. Protein expression

3.8.1. Protein overexpression in *E. coli*

Genes which had been cloned into expression vectors were transformed into *E. coli* strain BL21 (DE3). The resulting transformants were grown at 37°C in 500 ml LB medium containing the relevant antibiotic until the OD_{600} of the cultures had reached 0.3. The temperature was then decreased to 25°C until the cultures reached an OD_{600} of between 0.6 and 0.8. Protein synthesis was induced by the addition of IPTG to a final concentration of 0.4 mM and the cells were grown for a further 16 h at 20°C before harvesting by centrifugation at 4000 x *g* for 20 min. The synthesis of proteins in *E. coli* was monitored by removing 1 ml samples prior to and after IPTG induction, with analysis by SDS-PAGE. Harvested cells were stored at -80°C.

3.8.2. Protein expression in *Synechocystis*

Synechocystis mutants were grown photoautotrophically in 1.25 L BG-11 medium at 30°C. Protein synthesis was induced by growth under high light conditions (50 µmol photons m^{-2} s^{-1}). Cultures were grown until they reached an OD_{730} of 1.0 before being

harvested by centrifugation at 10,000 x *g* for 20 min. Harvested cells were stored at -80°C.

3.9. Protein analysis

3.9.1. Determination of protein concentration

Protein concentrations were determined by applying the following equation to absorbance readings at 280nm in a suitable resuspension buffer:

$$A_{280}\ (1\text{mg ml}^{-1}) = (5960n_{Trp} + 1280n_{Tyr} + 120n_{Cys}) / Mr$$

where n_{Trp}, n_{Tyr} and n_{Cys} are the numbers of tryptophan, tyrosine and cysteine residues respectively, and Mr is the predicted molecular mass of the protein (Gill and von Hippel, 1989). Protein concentrations were also determined using the Bradford protein assay (Biorad), according to the manufacturer's instructions, which are available to download from www.bio-rad.com. Bovine serum albumin (BSA) was used to obtain a standard curve.

3.9.2. SDS-polyacrylamide gel electrophoresis (SDS-PAGE)

Protein samples were separated by SDS-polyacrylamide gel electrophoresis using the buffer system of Laemmli (1970), and the protocol of Sambrook *et al*. (1989). A 5% stacking gel and a 12%, 10% or 8% separating gel were used in all cases. All samples were boiled for 5 min prior to loading; 10-20µl were loaded per well. Protein bands were visualised by staining gels with Coomassie Brilliant Blue R250. Kaleidoscope or Precision Plus Prestained Standards (Biorad) were used as a molecular weight marker.

3.9.3. Western analysis of proteins

Western analysis of SDS-PAGE gels was essentially performed as described by Sambrook *et al*. (1989). Following electrophoresis the gels were equilibrated for approximately 15 min in transfer buffer (10 mM $NaHCO_3$, 3 mM Na_2CO_3, 10% methanol). Under complete saturation of transfer buffer, a sandwich consisting of the

gel, two porous pads, sheets of Whatman 3 mm paper and nitrocellulose or polyvinylidene difluoride (PVDF) transfer membrane was constructed. The layers were pressed together within a transfer cassette, such that the transfer membrane was in direct contact with the gel. This was placed in the blotting apparatus (Biorad) at 40 mA overnight, with the blotting membrane placed between the gel and the anode of the blotting tank. Upon completion of transfer the membrane was removed from the cassette and stored in TBS buffer (50 mM Tris/HCl pH 7.6, 150 mM NaCl).

3.9.4. Immunodetection

Following Western blotting, the nitrocellulose membrane was blocked for 60 min at room temperature in 30 ml blocking buffer (0.2% Tween 20 in TBS) with shaking. The membrane was then incubated with a 1/2500-1/4000 dilution of the relevant primary antibody, raised in rabbit, in 30 ml antibody buffer (0.05% Tween 20 in TBS) for 4 h at room temperature with shaking. The membrane was washed with antibody buffer for 3 x 5 min and then incubated with a 1/10,000 dilution of peroxidase-conjugated goat anti-rabbit IgG secondary antiserum in 30 ml antibody buffer for 60 min at room temperature with shaking. Finally, the membrane was washed for 3 x 5 min in antibody buffer before the immunoreactive bands were detected with Amersham ECL Western blotting luminol and enhancer solutions (GE Healthcare) as described by Sambrook *et al.* (1989).

3.9.5. Native-polyacrylamide gel electrophoresis (Clear Native-PAGE)

Protein samples were separated by native-polyacrylamide gel electrophoresis using the buffer system of Laemmli (1970) based on the Clear Native Polyacrylamide Gel Electrophoresis technique, developed by Schägger (1994), using precast 3-8 % *NativePAGE NOVEX* (Invitrogen). Gels were set up as detailed by the manufacturers' instructions (available from www.invitrogen.com), using Tris-Glycine buffer in both upper and lower chambers of the of the system. 20 µl of protein sample were prepared with an equal volume of 2x sample buffer and loaded onto the gel alongside 10 µl of NativeMark unstained native protein marker (Invitrogen). The gels were run at 150

mV for 120 min at 4 °C and protein bands were visualised using Coomassie brilliant blue G250.

3.10. Protein purification

3.10.1. Purification of His_6-tagged proteins

Protein synthesis was induced by IPTG in 500 ml cultures of *E. coli* BL21 (DE3) cells containing pET9a derivatives, as described in section 2.8.1. The cells were harvested by centrifugation and pellets from 1-3 l of culture were resuspended in 20ml chilled binding buffer (50 mM sodium phosphate pH 7.4, 300 mM NaCl, 10 mM imidazole) containing protease inhibitor. The cells were disrupted by sonication for 6 x 20 s and the cell debris removed by centrifugation at 48,000 x *g* for 20 min at 4°C. The supernatant was passed through a 0.2 µm filter and loaded onto a 10 ml pre-equilibrated Chelating Sepherose™ Fast Flow column pre-charged with one column volume of 100 mM nickel sulphate and allowed to bind under gravity flow. The column was washed with 50 ml wash buffer (50 mM sodium phosphate pH7.4, 300 mM NaCl, 50 mM imidazole), repeated three times with a final 10 ml wash with buffer containing 100 mM imidazole. $A_{280/260}$ spectra was taken to ensure all unbound protein and any DNA had been washed from the column. His_6-tagged proteins were eluted from the column with 20 ml elution buffer (50 mM sodium phosphate pH7.4, 300 mM NaCl, 300 mM imidazole). Imidazole was removed from the sample by diafiltration using an ultrafiltration concentrator.

3.10.2. Purification of GST-tagged proteins

Protein synthesis was induced by IPTG in 500 ml cultures of *E. coli* BL21 (DE3) cells containing pGEX-4T-1, as described in section 2.8.1. The cells were harvested by centrifugation and pellets from 1-3 l of culture were resuspended in 20 ml chilled PBS buffer pH 7.3 (140 mM NaCl, 2.7 mM KCl, 10 mM Na_2HPO_4, 1.8 mM KH_2PO_4) containing protease inhibitor. The cells were disrupted by sonication for 6 x 20 s and the cell debris removed by centrifugation at 48,000 x *g* for 20 min at 4°C. The supernatant was passed through a 0.2 µm filter and loaded onto a pre-equilibrated 1 ml Glutathione Sepharose column. The column was washed with 10 column volumes of

PBS buffer. The GST-tag was cleaved by loading 1 ml of PBS containing 80 units of thrombin onto the column and incubating for 16 h at 20°C. Cleaved proteins were eluted from the column with 3ml PBS. Thrombin was removed from the sample by loading onto a pre-equilibrated 1ml Benzamidine Sepharose column. The column was washed with 10 column volumes of low salt buffer (15.5 mM Na_2HPO4, 4.5 mM NaH_2PO4, 150 mM NaCl). Proteins were eluted with 10 column volumes of high salt buffer (15.5 mM Na_2HPO4, 4.5 mM NaH_2PO4, 1 M NaCl). Salt was removed from the sample by diafiltration using an ultrafiltration concentrator, and the sample was dispersed in PBS buffer pH 7.3.

3.10.3. Further purification of proteins

3.10.3.1. Ion exchnage

After initial purification procedures proteins would be purified further using ion exchange chromatography. Protein was buffer exchanged into 90:10, buffer A:B and loaded onto a ResourceQ anion exchange column (GE Healthcare) pre-equilibrated with 90:10, buffer A:B (Buffer A, 50 mM Tricine pH 7.9, 0.3 M glycerol, 1 mM dithiothreitol (DTT); Buffer B is buffer A with 1 M NaCl). The column was washed with 5 column wolumes of 90:10, buffer A:B and then eluted with a NaCl linear gradient of 10% - 35 % buffer B.

3.10.3.2. Gel Filtration

Size exclusion chromatography was performed either preparatively on an FPLC (ÄKTA - FPLC, GE Healthcare) using a HiLoad 16/60 Superdex 200 PG column (GE Healthcare) or analytically on an HPLC (Agilent 1200) using a BioSeph-Sec-4000 column (Phenomenex). Gel filtration buffer was 50 mM Tricine, 0.3 M NaCl, 0.3 M glycerol, 1 mM DTT. Protein elution was detected by monitoring the UV absorbance at 280 nm except when DDM or ATP was used in the buffer / sample and tryptophan fluorescence was measured with an excitation wavelength of 290 nm and an emission wavelength of 350 nm.

3.10.4. Purification of FLAG-tagged proteins

Protein synthesis was induced by growing 1.25 L cultures of *Synechocystis* strains under high light conditions as described in section 2.8.2. The cells were harvested by centrifugation and pellets from 3-5 L of culture were resuspended in 10 ml thylakoid buffer containing protease inhibitor. The cells were disrupted by bead beating for 9 x 1 min. The soluble and thylakoid fractions were separated by centrifugation at 48,000 x *g* for 20 min at 4°C. Proteins contained in the thylakoid fraction were solubilised by rotation for 1 h at 4°C in 10 ml thylakoid buffer containing n-Dodecyl β-D-maltoside (β-DDM) at a final concentration of 2% (w/v). The solubilised and insoluble fractions were separated by centrifugation at 48,000 x *g* for 20 min at 4°C. Depending on the localisation of the FLAG-tagged protein of interest, either the soluble or solubilised thylakoid fraction was passed through a 0.2 µm filter and loaded onto a pre-equilibrated 1 ml Anti-FLAG M2 Affinity gel column. The column was washed with 15 column volumes of thylakoid buffer containing 0.04% DDM (w/v). FLAG-tagged proteins were eluted by adding 100 µg pure FLAG peptide dissolved in 1 ml thylakoid buffer containing 0.04% DDM (w/v) to the plugged column, transferring the suspended resin to a cryovial and rotating for 1 h at 20°C. The protein was separated from the resin by centrifugation at 1500 x *g* for 5 min in a Costar Spin-X centrifuge tube containing a cellulose acetate membrane with 0.22 µm pores.

3.11. Buffer exchange of aggregated protein

Aggregated protein was diluted into the desired buffer incubated in a sonication water bath at room temperature for 3 min and concentrated using an ultrafiltration concentrator.

3.12. Substrate preparation

3.12.1. Porphyrin preparation

Approximately 5 mg of porphyrin was dissolved in chelatase buffer (50 mM MOPS/KOH pH 7.7, 0.3 M glycerol, 1 mM DTT). The solution was centrifuged to remove any insoluble porphyrin and transferred to a sterile black microcentrifuge tube.

Pigment concentrations were determined in 0.1 M HCl using extinction coefficient (ε_{399} = 433000 $M^{-1}cm^{-1}$) from Falk (1964).

3.12.2. ATP preparation

Approximately 250 mg of adenosine 5'-triphosphate disodium salt (ATP) or 5'-O-(3-thiotri-phosphate) tetralithium salt (ATPγS) were dissolved in 1 ml of QH_2O with adjustment of pH to 7 using KOH. The concentrations were determined in water using the extinction coefficient (ε_{259} = 15400 $M^{-1}cm^{-1}$) from Dawson (1969).

3.13. Fluorescence and absorbance spectroscopy

Fluorescence spectra were recorded on a Jobin Yvon spectrofluorimeter fitted with a temperature-controlled cuvette holder set to 34°C at a scan speed of 2 nm s^{-1}. All samples (1ml) were in 50 mM MOPS/KOH pH 7.7, 0.3 M glycerol, 1 mM DTT and were incubated for at least 5 minutes at 34°C before transfer to a clean 1 ml quartz cuvette. Protein fluorescence was monitored using an excitation wavelength of 295 nm and an emission wavelength of 340 nm. Excitation and emission slit widths corresponding to 4.5 nm and 18 nm, respectively were used for excitation scans. For emission scans both slits were set at 4.5 nm. Spectra were corrected by subtraction of buffer-only samples. Absorbance spectra were recorded on a Cary50 UV-Vis spectrophotometer (Varian) at room temperature. The buffers used were the same as for fluorescence spectroscopy.

3.14. Steady-state assays of magnesium chelatase

Reactions were carried out in 50 mM MOPS/ KOH pH 7.7, 0.3 M glycerol, 1 mM DTT at the specified temperature and fixed ionic strength I = 0.1, in a total volume of 100 µl. A Bio-Tek F2 microplate reader with excitation through a 420 ± 25 nm filter and emission observed through a 590 ± 17.5 nm filter was used to detect MgD_{IX} evolution over a period of one hour. Protein concentrations were 0.1 µM ChlD, 0.2 µM ChlI, 1 µM ChlH (except where stated) and substrate concentrations were 5 mM $MgATP^{2-}$, 10 mM Mg^{2+} and 5 µM D_{IX} (except where stated). The maximum rate during an assay was taken as the steady-state rate and generally occurred after 12

minute lag phase. Known concentrations of MgD_{IX} were analysed in the same way to produce a standard curve.

Steady-state rates were calculated from chelatase progress curves using the instrument software, fitting to a linear slope after the initial lag. All V_{ss} values were plotted against substrate concentration or subunit concentration and these data were fitted to equations as detailed through the chapters using unweighted nonlinear regression (Sigmaplot 8, SPSS.).

3.15. Nanogold labelling of His_6 tagged protein

Protein was buffer exchanged into nanogold binding buffer (20 mM Tris, 300 mM NaCl, 0.2% Tween 20, 5 mM imidazole). Protein was then added to nickel-nitrilotriacetic acid-Nanogold (Nanoprobes, Inc.) to give equimolar concentrations and was incubated at room temperature for 5 min. The solution was applied to an EM grid and imaged as described previously.

3.16. Circular Dichroism Spectroscopy

CD spectra of proteins (2-10 μM) were recorded on a Jasco J-810 spectropolarimeter at room temperature for 5 min. The machine was flushed with nitrogen at 3 L min^{-1} for 30 min, prior to turning the lamp on. All samples were in 50 mM Tricine/NaOH pH 7.9, 1mM DTT. Buffer-only measurements showed that this buffer did not mask the protein signal, with no absorption in the region of interest.

Table 1 - *Escherichia coli* strains

Strain	Properties	Source/Reference
DH5α	*supE44* Δ*lacU169* (Φ*80lacZ*Δ*M15*) *hsdR17 recA1 endA1 gyrA96 thi-1 relA1*	Hanahan, 1985
BL21 (DE3)	(F^- *ompT* r_B^- m_B^-) + bacteriophage DE3	Studier and Moffat, 1986
BL21 (DE3) pLysS	F^- *ompT hsdS*$_B$ (r_B^- m_B^-) *dcm gal* λ(DE3) pLysS (Cm^R)	Novagen

Table 2 – Comercial Plasmids

Plasmid	Properties	Source/Reference
pET9a	pBR322-based expression vector with the T7 promoter and terminator, Nm^R	Novagen
pET9aHis	pET9a derivative containing the *Xba*I-*Nde*I DNA fragment of pET14b containing the ribosome binding site and His_6-tag encoding region, Nm^R	Jensen *et al*., 1996a
pGEX-4T-1	pBR322-based expression vector with the T7 promoter and terminator, N-terminally encoded GST-tag and thrombin cleavage site, Nm^R	Fermentas
pBluescript II KS	pUC-based cloning vector containing a *lacI* promoter, Amp^R	Fermentas

Table 3 – Plasmids encoding genes described in this thesis

Plasmid[gene]	**Protein**	**Organism**
pET9a-His_6[*TchlH*]	ChlH	*T. elongatus*
pET9a-His_6[*ΔN160H*]	ΔN-terminal160 ChlH	*T. elongatus*
pET9a-His_6[*TchlI*]	ChlI	*T. elongatus*
pET9a-His_6[*TchlD*]	ChlD	*T. elongatus*
pGEX[*TchlD*]	ChlD	*T. elongatus*

Table 4 – Primers

Plasmid	**Forward primer**	**Reverse primer**
pET9a-His_6[TchlD]	5`-CGCGGCAGCCATATGACGC TCGCGATCGCCCCCTTTCCC-3`	5`-TTAGCAGCCGGATCCCTAA AATTGCAGGGCGTTCTGGG-3`
pGEX[TchlD]	5`-GATCCCCAGGAATTCATGACG CTCGCGATCGCCCCCTTTCCC-3`	5`-TCACGATGCGGCCGCCTAA AATTGCAGGGCGTTCTGGG-3`

CHAPTER 3

The structural characterisation of the ChlH subunit of the enzyme magnesium chelatase from *Thermosynechococcus elongatus*

4.1.Summary

Magnesium protoporphyrin IX chelatase (Mg-chelatase) catalyses the insertion of a Mg^{2+} ion into protoporphyrin IX (Proto). The H subunit of the multi-subunit enzyme has been identified as the porphyrin-binding subunit as it binds Proto as well as the product Mg-protoporphyrin IX (MgProto) in the absence of the other Mg-chelatase subunits (Karger *et al*., 2001). Recently a low resolution structure has become available for the *Rba. capsulatus* BchH (Sirijovski *et al*., 2008). It was shown that BchH undergoes a conformational change upon the binding of Proto and it appears that two lobes of the tri-lobed protein come together perhaps forming a more enclosed environment for the binding of Proto. Because the similarity of the H subunit between oxygenic photosynthetic organisms is high it would be interesting to map the structure of a cyanobacterial or plant protein. This chapter documents the purification of ChlH from *T. elongatus* and presents a basic characterisation of the protein as the porphyrin-binding subunit of magnesium chelatase. A low resolution EM-3D reconstruction of the protein is shown with ChlH in both apo and bound states. The protein appears to have a multi-lobed structure with a large body, and a small head region with an estimated MW of 15.7 kDa. The 3D reconstruction is similar to the small angle X-ray scattering (SAXS) structure for ChlH from *Synechocystis* (Qian et al., 2012). Finally the N-terminal domain of the *T. elongatus* protein is identified using Ni^{2+}-nitrilotriacetic acid (NTA)-nanogold particles bound to the N-terminal His_6 tag on the protein and subsequent EM imaging of negatively stained ChlH particles. Future possibilities for obtaining structural information for a complex between ChlH and the magnesium chelatase enhancer protein Gun4 is discussed following the possible isolation of a ChlH•Gun4 complex.

4.2. Introduction

Haems and chlorophylls share the same common biosynthetic pathway from the formation of aminolaevulinic acid through to protoporphyrin. The next enzymatic step involves the chelation of a divalent metal ion into the macrocycle. The chelation of iron commits to the production of haem, which is vital for cyto/phytochromes and haemoglobin and this step is catalysed by a 38 - 51 kDa ATP-independent ferrochelatase (Hunter *et al*., 2011). The alternative branch is the insertion of magnesium into Proto committing to the biosynthesis of chlorophyll. This ATP-driven process is catalysed by magnesium chelatase (MgCH), a far more complex enzyme when compared to ferrochelatase. MgCH consists of three essential subunits designated ChlH/BchH, ChlI/BchI and ChlD/BchD depending on whether the subunits are from oxygenic or non-oxygenic organisms, respectively. A fourth gene, *gun4* (*g*enome *un*coupled), encodes an additional protein that acts as an enhancer to the enzyme (Larkin *et al*., 2003 and Davison *et al*., 2005). The chelation reaction requires Mg^{2+} and Proto with energy from ATP (Gibson et al 1995; Jensen et al., 1996).

The I subunit is a ~40 kDa ATPase (Jensen *et al*., 1998) from the AAA^{+} (*A*TPases *A*ssociated with diverse cellular *A*ctivities) family and the structure from *Rba. capsulatus* has been solved to 2.1 Å resolution (Fodje *et al*., 2001). AAA^{+} proteins often form oligomeric rings (Fodje *et al*., 2001; Hansson *et al*., 2002) and Willows *et al*., (2004) show evidence that BchI can form hexameric complexes in the presence of ATP. Heptameric complexes have also been observed from *Synechocystis* ChlI (Reid *et al*., 2003).

The D subunit has a molecular weight of ~70 kDa and its N-terminal half has homology to the I subunit and also contains a MIDAS motif that is suggested to be associated with metal ion binding (Jensen et al., 1996; Axelsson *et al*., 2006). The I and D subunits can form a complex in the presence of Mg^{2+} and ATP (Gibson *et al*., 1999; Jensen *et al*., 1999a). Lundqvist *et al*., (2010) have published a cryo-EM 3D reconstruction of the BchI•BchD complex as a hexameric double ring. Because D can form oligomeric complexes independent of ATP or magnesium (Axelsson *et al*., 2006) it has been proposed that the D ring assembles to form a scaffold on which I can then

associate. It may be that D binds magnesium and then assembles with I and this complex interacts with the rest of the enzyme to enable activity.

The H subunit is the largest subunit of MgCH and has a molecular weight of ~140 kDa. H has been shown to be the tetrapyrrole binding subunit and it binds both the substrate and product of the reaction (Karger *et al*., 2001). The dissociation constant, K_d, of H for D_{IX} was calculated to be 1.22 ± 0.42 μM for ChlH and 0.53 ± 0.12 μM for BchH. The K_d for MgD_{IX} was calculated to be 2.43 ± 0.46 μM for ChlH and 0.22 ± 0.038 μM for BchH (Karger *et al*., 2001). H appears to be catalytically inactive and it has been suggested that it has a role in distorting the porphyrin ring and enabling the insertion of magnesium (Al-Karadaghi *et al*., 2006).

ChlH is a multifunctional protein and it is apparently involved in a variety of other processes not associated with chlorophyll biosynthesis. SigE, an anti-sigma factor, regulates sugar catabolism and ChlH has been shown to repress SigE posttranslationally by binding it to prevent transcription (Osanai *et al.*, 2009). Interestingly sugar catabolism is regulated in what appears to be a light/dark sensitive manner and H regulates SigE through magnesium fluctuations during light/dark cycles (Osanai *et al.*, 2009). Abscisic acid (ABA) is a plant hormone that regulates many processes under stressful conditions. In broad bean a ~45 kDa protein was shown to be a mediator in abscisic acid binding and thus signaling. This protein was found to be a 770 amino acid C-terminal fragment of ChlH and in *Arabidopsis* full size ChlH was shown to bind ABA (Zhang *et al.*, 2002; Shen *et al.*, 2006). Further work indicated that in *Arabidopsis* the ChlH C-terminal domain was important in ABA binding whereas the N-terminal domain appears not to be, supporting previous work (Wu *et al.*, 2009). These results conflict with other work in barley (Müller and Hansson, 2009; Tsuzuki *et al*., 2011). There is no detailed structural information for any Mg chelatase H subunit and when bioinformatic searches are used there are no structures available for any H-like protein. There is a low resolution structure for BchH obtained from negative stain electron microscopy 3D reconstruction (Sirijovski *et al.*, 2008). This structure reveals a three-lobed protein with lobe I containing the “thumb” and lobe III sporting a “finger”. Upon binding of substrate there is a conformational change whereby the finger and thumb come together perhaps providing a hydrophobic environment for the hydrophobic Proto to reside to enable catalysis. It may also be that in this more

hydrophobic environment the hydration shell is removed from the hydrated magnesium to form the divalent cation.

Table 1 shows the similarity between various H subunits from different species and the large subunit of the cobalt chelatase, a three-subunit enzyme performing the insertion of cobalt into hydrogenobyrinic acid *a*,*c*-diamide, in a reaction similar to that of MgCH (Brindley *et al*., 2003). The sequence homologies of H proteins are high, particularly between Chl-producing organisms. It is clear that there is a large drop in similarity between ChlH and BchH proteins and inspection of Fig. 1 shows a sequence (cyan bar) that is present in oxygenic photosynthetic organisms but absent from anaerobic photosynthetic organisms.

Table 1 - Percentage sequence identities among Mg-chelatase H subunits from a selection of plants, cyanobacteria and photosynthetic bacteria. Abbreviations explained below:

HV.H, Hordeum vulgare ChlH; AT.H, Arabidopsis thaliana ChlH; CR.H, Chlamydomonas reinhardtii ChlH; SYN.H, Synechocystis ChlH; TE.H, Thermosynechococcus elongatus ChlH; PM.H, Prochlorococcus marinus ChlH; RC.H, Rhodobacter capsulatus BchH; PV.H, Prosthecochloris vibrioformis BchH; COBN, Pseudomonas denitrificans cobaltochelatase subunit N.

	HV. ChlH	AT. ChlH	CR. ChlH	SYN. ChlH	TE. ChlH	PM. ChlH	RC. BchH	PV. BchH	COBN
HV. ChlH	100	82	67	67	67	64	38	33	28
AT. ChlH		100	68	66	66	65	38	32	28
CR. ChlH			100	66	66	64	39	33	29
SYN. ChlH				100	78	71	38	33	29
TE. ChlH					100	69	38	34	34
PM. ChlH						100	38	35	33
RC. BchH							100	34	34
PV. BchH								100	26
COBN									100

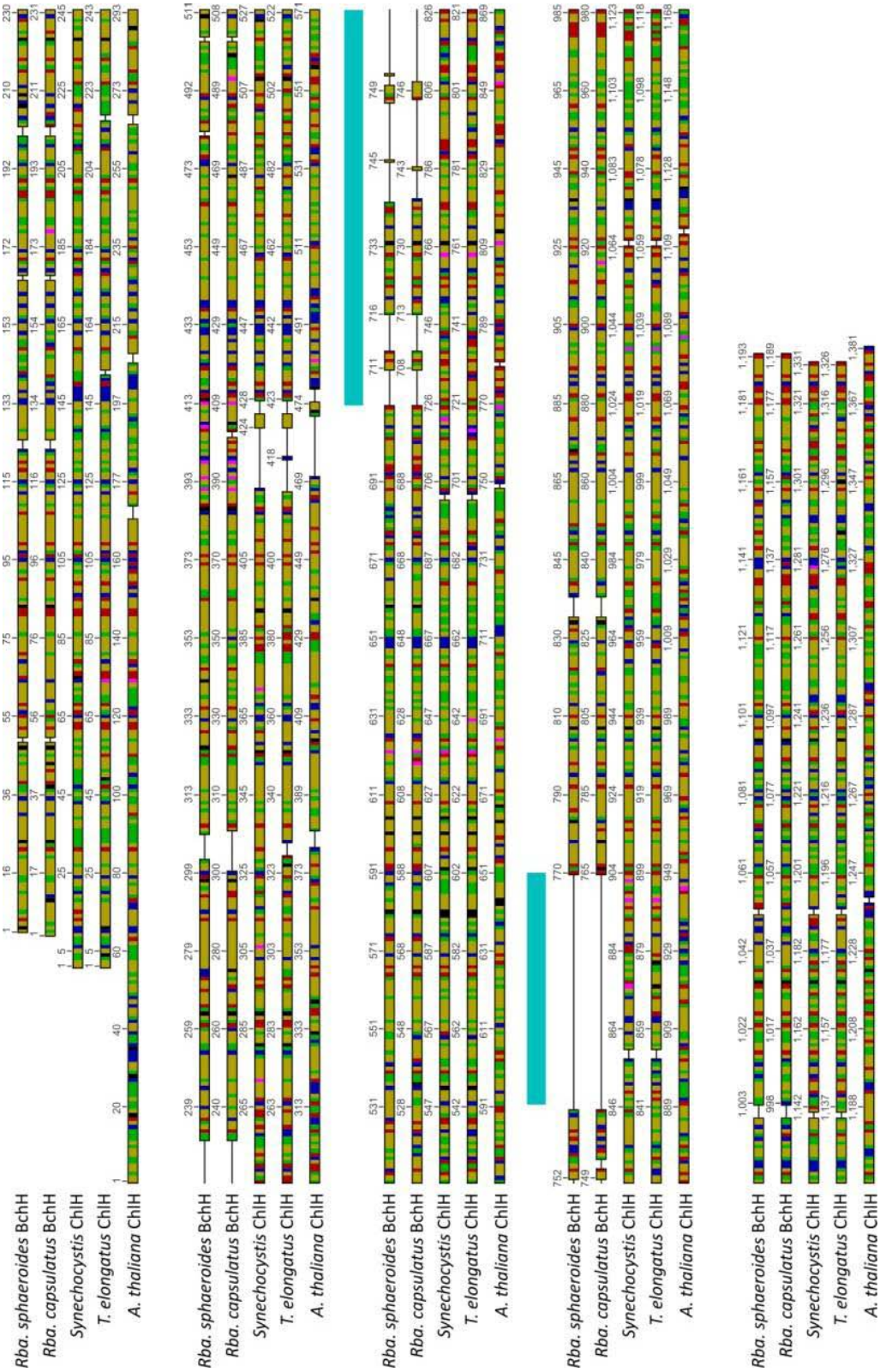

Figure 1 - Alignment of Mg-chelatase porphyrin binding subunits from selected purple bacteria, cyanobacteria and a higher plant

According to the characteristics of the amino acid side chains. Color annotation: black, histidine; blue, positively charged; green, polar; magenta, cysteine; red, negatively charged; yellow, non-polar. Compiled using Geneious software (Drummond et al., 2010). The cyan bar indicates a region of ChlH proteins found in oxygenic phototrophs but not in purple photosynthetic bacteria.

4.3.Results

4.3.1. Purification and functional analysis of the ChlH protein

The pET9a-His_6 plasmid containing the *chlH* gene was a kind gift from Dr. Paul Davison. *E. coli* BL21 (DE3) cells were transformed with the construct containing the ChlH gene and the cells were induced overnight with 0.4 mM IPTG. ChlH, ChlI and ChlD were purified as in section 2.10 and a typical purification of *T. elongatus* ChlH can be seen in the inset in Fig. 2, *A* shows HPLC gel filtration traces of apo-ChlH (top trace) and ChlH that has been incubated with 10 μM $D_{IX,}$ a water-soluble substitute for protoporphyrin (bottom trace). The apo-ChlH trace shows that recombinant ChlH does not significantly co-purify with endogenous Proto from *E. coli,* as shown by the large protein absorbance at 280 nm but the negligible tetrapyrrole peak (398 nm). The preincubated ChlH•D_{IX} shows large peaks for both the protein and tetrapyrrole. This confirms that the apo-ChlH sample was free of porphyrin and that in the preincubated samples, the substrate was indeed bound. The retention time of 38 minutes correlated with an estimated molecular weight of 150 kDa. Fig. 2, *B* shows magnesium chelatase assays of *Synechocystis* ChlH and *T. elongatus* ChlH incubated with ChlI, ChlD, magnesium, ATP and D_{IX}. The negative control without ChlH shows that it is essential for the MgCH activity and that that the suspected *T.* elongatus *chlH* gene does indeed encode the large subunit of magnesium chelatase. As perhaps expected a lower activity is seen when compared to that of *Synechocystis* ChlH due to possible incompatibilities between the proteins from different species.

4.3.2. Porphyrin binding studies

Having performed the functional analysis of *T. elongatus* ChlH, the detection of both apo-ChlH sample and a ChlH•D_{IX} sample was possible but the percentage of substrate bound in the ChlH•D_{IX} sample was not determined. Estimation of the dissociation constant (K_d) between *T. elongatus* ChlH and D_{IX} would guide the incubations needed (10x K_d) to ensure that the majority of proteins imaged would indeed be bound to tetrapyrrole.

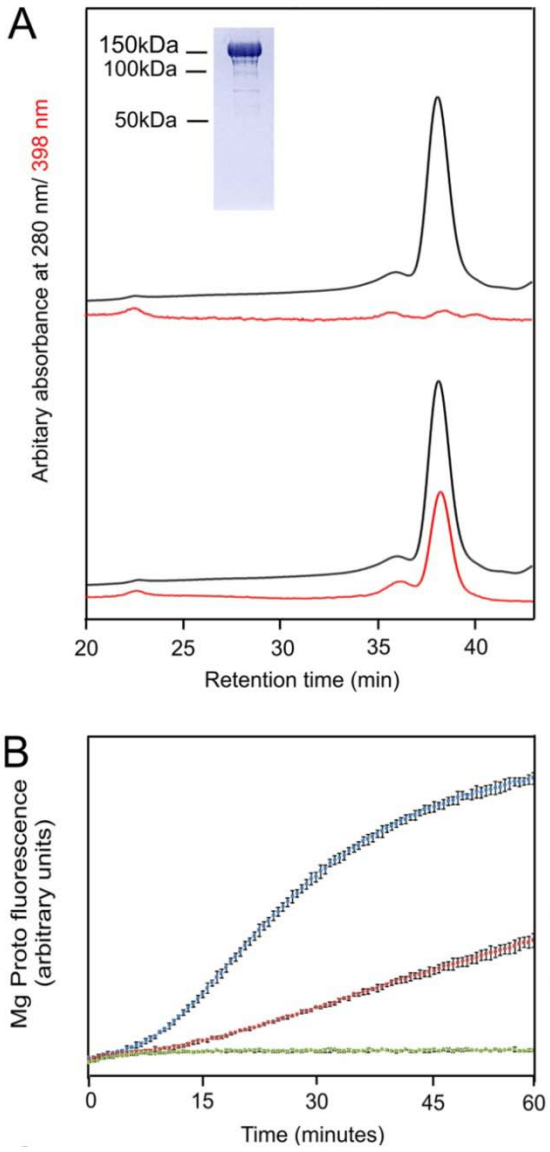

Figure 2 - Proto binding and enzyme activity of the magnesium chelatase ChlH subunit from T. elongates

A, the purity of the apo-ChlH subunit is indicated by the elution trace from the HPLC gel filtration column (black line, detection of absorption at 280 nm; red line, detection at 398 nm), and the SDS-PAGE analysis (inset). The two lower traces show the analysis of the sample where ChlH and D_{IX} were premixed prior to gel filtration. B, plot of ChlH fluorescence at 350 nm in arbitrary units (A.U.) as a function of D_{IX} concentration. B, Mg chelatase assays run in duplicate with H, I, and D subunits from Synechocystis as a positive control (blue), and I and D subunits alone as a negative control (green). The data in red show the progress of a Mg chelatase reaction with the T. elongatus ChlH subunit mixed with the Synechocystis ChlI and ChlD subunits.

The disassociation constants for ChlH and D_{IX}/MgD_{IX} were determined using the methodology described in 2.13 (Karger *et al*., 2001). Fig. 3 displays plots of integrated ChlH fluorescence as a function of tetrapyrrole concentration. In each case the binding titration data were fitted to equation 1, in which a single type of binding site is assumed (Karger *et al*., 2001).

$$F_{obs} = F_0 + F_{max} \frac{[L]_T + [E]_T + K_d - \sqrt{\left([L]_T + [E]_T + K_d\right)^2 - 4[L]_T[E]_T}}{2[E]_T}$$

(Equation 1)

F_{obs} is the observed fluorescence, F_0 is initial fluorescence, F_{max} is the maximum amplitude of fluorescence quenching, $[L]_T$ is the total ligand concentration, $[E]_T$ is the total concentration of protein and K_d is the disassociation constant.

The calculated K_d of *T. elongatus* ChlH for D_{IX} and MgD_{IX} were 1.48 ± 0.3 μM and 2.12 ± 0.2 μM respectively. The data prented are from single titrations and the errors reflect the error in the K_d obtained using the equation. These calculations are in good agreement with the previously published K_d values for *Synechocystis* ChlH for D_{IX} and MgD_{IX} of 1.22 ± 0.42 μM and 2.43 ± 0.46 μM.

4.3.3. Electron microscopy and 3D reconstruction of negatively stained apo-ChlH and ChlH-D_{IX} particle

Purified proteins were adsorbed onto freshly glow-discharged carbon-coated copper grids that were subsequently negatively stained. Fig. 4, *A* and *D*, shows the electron micrographs of apo-ChlH and ChlH•D_{IX} samples, respectively. Under such conditions, about 70 particles with a clear background could be picked from a single 1K × 1K micrograph. Fig. 4, B and E, show representative boxed images of single molecules of apo-ChlH and ChlH•D_{IX} samples, respectively, with the presence of several domains within ChlH already evident from these images. Initial reference-free classifications were run on the data sets that contained 15930 particles of apo-ChlH and 12310 particles of the ChlH•D_{IX} complex. The top rows of Fig. 4, *C* and F, show six selected averaged two-dimensional classes. Below are the 3D reconstructions viewed at the corresponding Euler angles, and the bottom rows show the corresponding reprojections from the 3D models, which are consistent with the averaged classes in each top row.

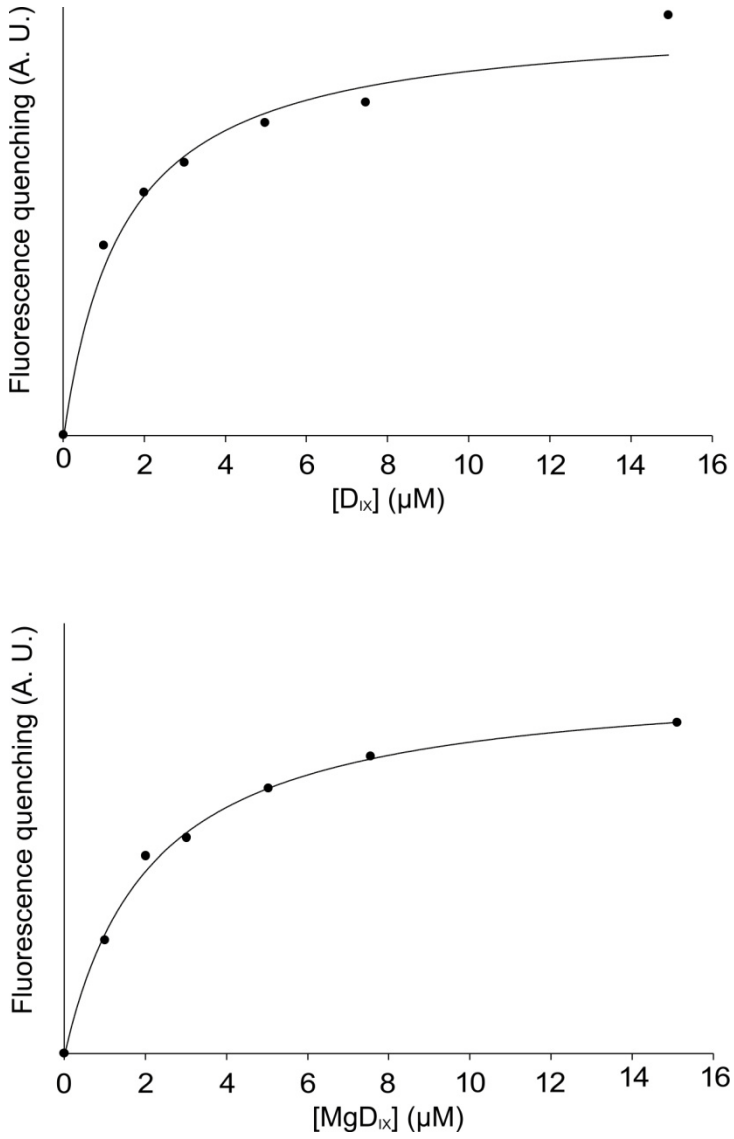

Figure 3 - ChlH fluorescence change upon binding of tetrapyrrole

Fluorescence quenching data for ChlH with reference to its substrate and product. The curve fits the experimental data to a single substrate binding model.

The resolution of the apo-ChlH and ChlH•D_{IX} structures was calculated as 27Å and 28 Å, respectively. The final 3D structural models are shown in Fig. 5, *A* and *B*, rotated successively by 90° about the *z* axis, and both filtered to 30 Å resolution for comparison. Apo-ChlH (Figure Fig. 5 *A, cyan*) shows a hollow structure with an internal cavity of ~100 nm^3 and a small globular domain connected to the rest of the protein by a narrow neck. Comparison with the ChlH•D_{IX} complex (Fig. 5 *B, red*) shows that there is little observable effect of substrate binding at this resolution. Fig. 5 also compares the 3D models of ChlH with the apo- and porphyrin-bound structures of BchH (*C* and *D*, respectively), taken from the earlier work of Sirijovsky *et al.* (2008). The larger size of ChlH is apparent, mainly attributable to the region of ~100 residues indicated by the *cyan bar* in Fig. 1. The length of the body and head domain of ChlH appears to be around 12 nm in total.

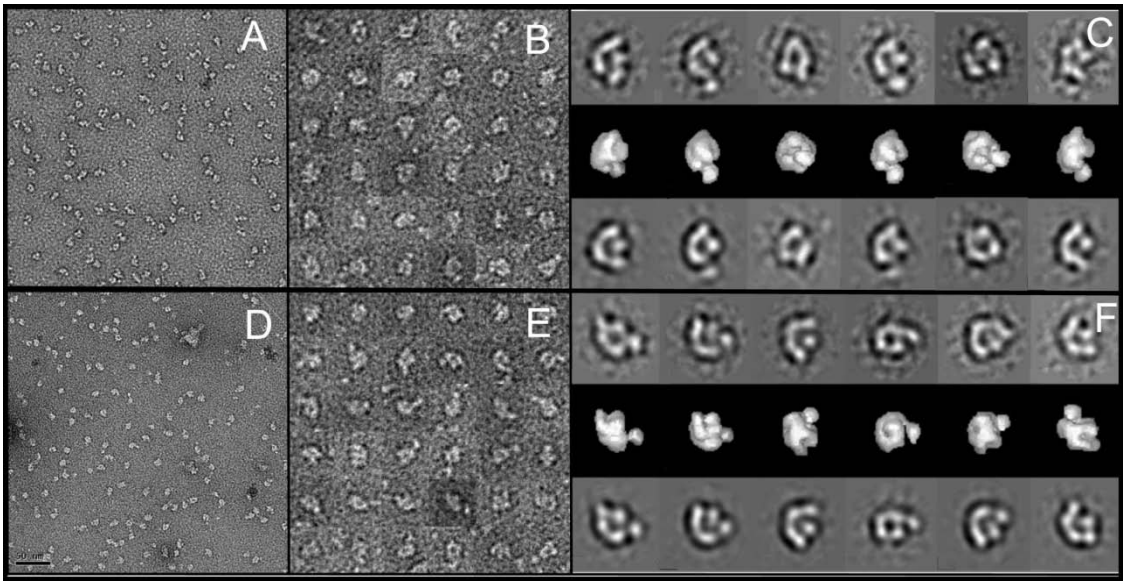

Figure 4 - Electron microscopy and 3D reconstruction of negatively stained apo-ChlH and ChlH-D_{IX} particles

A and D, electron micrographs of apo-ChlH and ChlH-D_{IX} samples, respectively. Scale bar = 100 nm (A and D). B and E, 36 boxed single molecules of apo-ChlH and ChlH•D_{IX} samples, respectively. The box size is 25 nm × 25 nm. C, reconstruction of apo-ChlH. Top row, six selected averaged 2D classes; centre row, 3D reconstructions viewed at Euler angles corresponding to those assigned to the class averages above; bottom row, corresponding reprojections from the 3D models. F, reconstruction of apo-ChlH with details as for C.

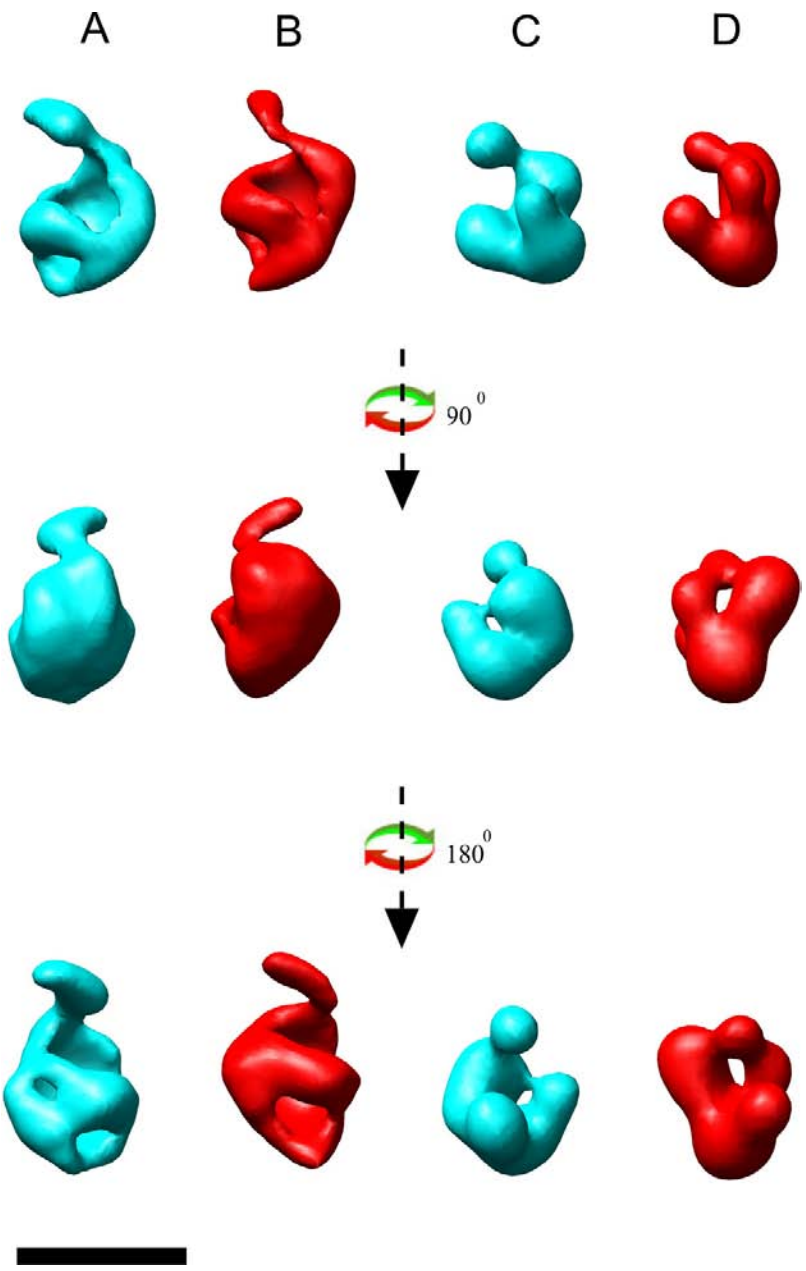

Figure 5 - A and B, 3D models of apo-ChlH (cyan) and the ChlH-DIX complex (red), calculated at a cutoff resolution of 30 Å

The threshold value of each model was adjusted to correspond to the molecular mass of ChlH. In the centre and bottom rows, the molecules are rotated successively by 90° about the z axis. The handedness for each of the apo-ChlH and ChlH•D_{IX} models that gave the best fit to the SAXS model in Figs. 5 and 6 was chosen. C and D, 3D models of BchH taken from Sirijovski et al. (2008). The apo-BchH structure is in cyan (C), and the porphyrin complex is in red (D). In the centre and bottom rows, the molecules are rotated successively by 90° about the z axis. Scale bar 10 nm. The 3D models were generated using Chimera (Pettersen et al., 2004).

4.3.4. Identification of the N-terminal of ChlH

To identify the N-terminal domain in these reconstructions, we exploited the availability of the N-terminal His_6 tag and used 5 nm-diameter NTA-nanogold particles as a labelling reagent. Fig. 6 shows a gallery of labelled apo-ChlH proteins, with the electron-dense nanogold particles clearly visible in each case. In each image, ChlH appears to be joined to the nanogold by the globular head region, so it is suggested that this is the N-terminal domain.

4.3.5. Extraction and visualisation of ChlH direct from native PAGE

Protein complexes that arise from loose associations are difficult to isolate especially if they are able to form a series of complexes of variable stoichiometry. ChlH associates with the enhancer Gun4 (Larkin *et al*., 2003; Davison and Hunter, 2011)) and structural information to elucidate the nature of association between the two would be of significant interest. Knispel *et al.* (2012) have shown that it is possible to isolate protein complexes on to pre-glow discharged copper EM grids direct from native PAGE protein bands. Because it is now possible to identify ChlH using EM it is possible to evaluate the efficiency of the method demonstrated by Knispel *et al.* (2012) for protein and therefore complex isolation.

T. elongatus ChlH was run on native PAGE and a unstained gel slice with the same migration size as that of the stained band was excised and placed onto an EM grid. ChlH successfully diffused from the gel and adsorbed onto the grid (Fig. 7)

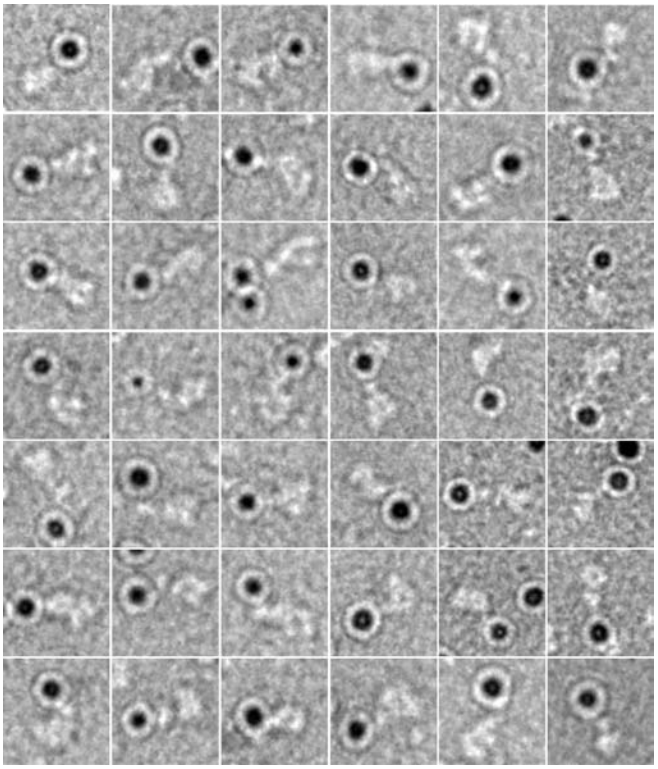

Figure 6 - Nanogold labeling of purified magnesium chelatase H-subunit

The box size in the gallery is 30 × 30 nm. Gold particles are in black because of heavy scattering against electron beam, and magnesium chelatase H-subunits are in white.

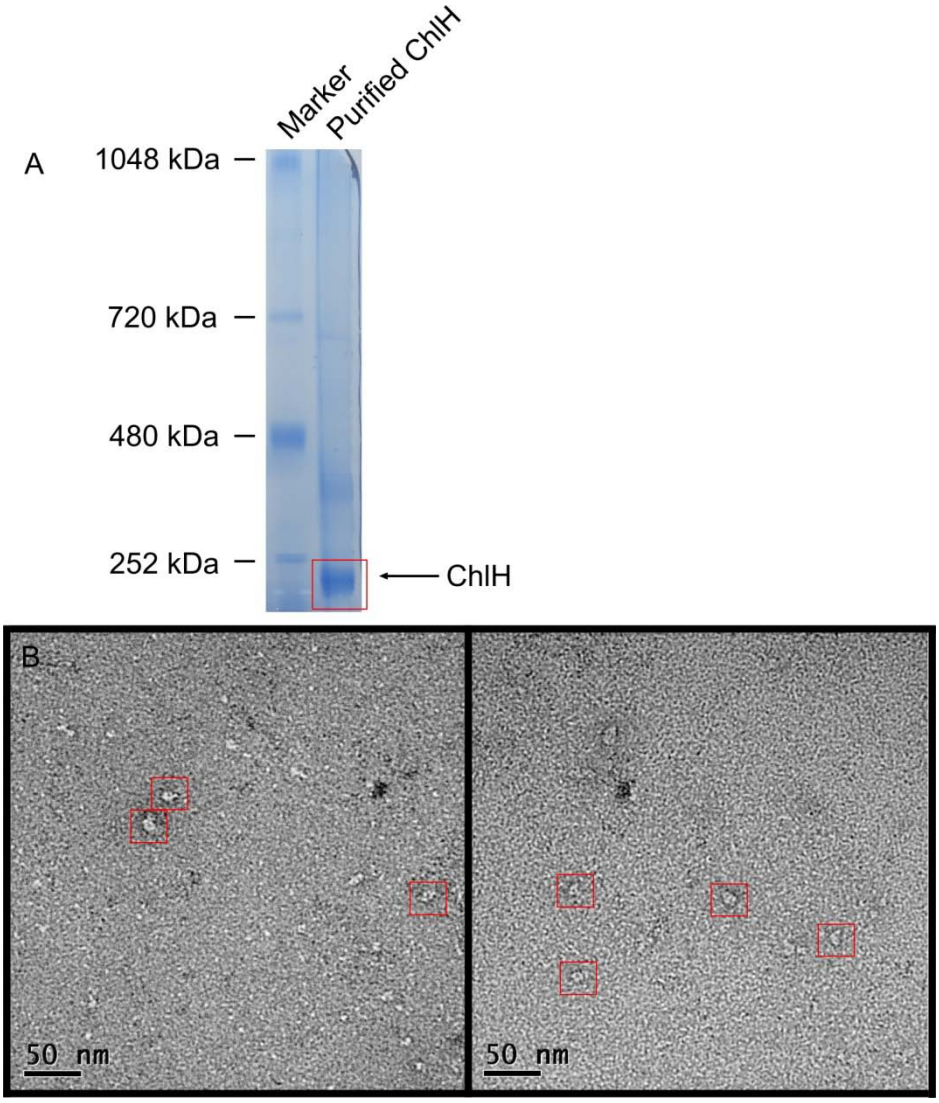

Figure 7 - EM images of ChlH extracted directly from native-PAGE

A, Native-PAGE of T. elongatus ChlH stained with Coomassie blue. An adjacent lane contained the same sample and was not stained. The gel was used as a reference indicating where protein should be extracted. B, EM grid of protein transferred directly from a native gel to the EM grid, as in Knispel et al. (2012).

4.3.6. Discussion

The Mg chelatase H subunit plays an essential role in (B)Chl biosynthesis by binding Proto prior to the insertion of Mg^{2+}. The H subunit must therefore form a transient complex with the I and D subunits of Mg chelatase. Once formed, the HID complex catalyses the formation of MgProto, a reaction that requires 14 $MgATP^{2+}$ (Reid and Hunter, 2004). The transient state kinetic study by Viney *et al.* (2007) showed that the key step in formation of a protein-bound MgProto product state is primarily the binding of $MgATP^{2+}$ as opposed to its hydrolysis. These kinetic experiments did not monitor release of MgProto, so perhaps it is this process that is coupled to nucleotide hydrolysis, rather than insertion of Mg^{2+}. The K_d data collected for *T. elongatus* ChlH for both substrate and product are similar to that of the *Synechocystis* homologue. The K_d for the substrate is higher than that of the product, which is to be expected. ChlH will preferentially bind D_{IX} and release the MgD_{IX} so it can be shuttled further along the pathway. Fig. 8 shows the *T. elongatus* ChlH EM structure that has been superimposed with the SAXS data on *Synechocystis* ChlH from Qian *et al*. (2012). The SAXS and EM data show that ChlH forms an extended, asymmetric molecular assembly. The radius of gyration, *Rg*, for the structure from the SAXS data is 46.9 Å (Qian *et al*., 2012), similar to the *R*g value of 47.8 Å determined for ribulose 1,5-bisphosphate carboxylase/oxygenase (Meisenberger *et al.,* 1984) a compact, globular protein of much greater molecular mass, 534 kDa (Knight, Andersson and Brändén, 1990). Although *Rg* values require a clear context to be interpretable in the form of a 3D molecular shape, this comparison supports the notion of ChlH as an open, asymmetrical structure.

The low resolution structural studies performed in this work cannot provide any direct mechanistic information, although it is interesting to note on the one hand the existence of a ~100 nm^3 cavity within the ChlH structure and on the other the likely need for an active site environment that promotes the Mg chelation reaction. This process has been studied in detail using density functional calculations, modelling the successive exchange of water molecules from the solvation shell surrounding the Mg^{2+} ion with the pyrrole nitrogens of the Proto substrate, deprotonation of the Proto, and distortion of the porphyrin ring (Shen and Ryde, 2005). It is possible that the ChlH protein helps to catalyze MgProto formation by exerting some control over the immediate solvation environment of porphyrin substrates and products,

accommodating distortion of the porphyrin ring and facilitating the deprotonation of the pyrrole nitrogens. The theoretical study of Shen and Ryde (2005) found that water is an unsuitable proton acceptor, which might necessitate the screening of that part of the active site involved in deprotonation from the bulk aqueous solvent. This presents a demanding requirement because Mg chelatase is a soluble complex located in the aqueous cytoplasmic compartment of the cell, or possibly at the interface between the membrane and cytoplasm. As already noted by Sirijovski *et al.* (2008) BchH proteins, such as that from *R. capsulatus,* also have the potential to form an enclosing structure (see Fig. 5 for a comparison with ChlH). Single particle reconstruction of this protein showed that apo-BchH has three lobes, with the "thumb" and "finger" domains coming into contact upon binding of Proto (Sirijovski *et al*., 2008). It was postulated that residues from both the N- and C-terminal regions are involved in binding Proto and that the majority of the porphyrin-binding residues are located within the N- terminus. Proteolysis studies identified a flexible linker region, proposed to lie at the junction between the N- and C-terminal domains and flanking Gly-734 (Sirijovski *et al*., 2008). The apo-ChlH and ChlH•D_{IX} structures, both filtered to 30 Å for ease of comparison in Fig. 5 do not show any evidence of large-scale alterations in conformation upon porphyrin binding, and a more detailed structural analysis is required to examine this point further. The one feature of ChlH of *T. elongatus* that can be identified is the N-terminal domain. This is the "head" region, assigned on the basis of labelling with a NTA-nanogold particle that binds to the N-terminal His_6 tag (Fig. 6). From estimates of the fraction of ChlH represented by the head domain, it has a molecular mass of 15.7 kDa, corresponding to ~152 amino acids at the N terminus followed by a short linker of a few residues. The large error in this estimation gives a range of 14.1–17.3 kDa for the molecular mass of this domain, which corresponds to the sequences running from the N terminus to either Gly-127 or Phe-156. In this region ChlH has the following sequence:

G^{127}SFSLAQIG^{135}QSKSVIANFMKKRKEKSG^{153}AG^{155}F

Gly-127 is conserved in all Mg chelatase H subunits, and a counterpart is also found in the CobN cobaltochelatase subunit from *Pseudomonas denitrificans* (Lundqvist *et al*., 2009). Although the positions of the other Gly residues vary slightly, ChlH sequences from diverse organisms contain in this region, in addition to a Gly-127 equivalent, two to four other Gly residues.

Although the overall isoelectric point for ChlH is 5.30, the sequence between Gly-127 and Phe-156 has a pI of 10.6. Such contrasting values are predicted for other ChlH sequences, and it is possible that this Gly-127-Phe-156 region controls the binding of ChlH to other subunits or to the membrane or is involved in mobility of the head domain, possibly opening or closing the cavity within ChlH. Having identified the N-terminal head region it would be fair to assume that the C-terminal fragment would constitute part of the cage domain. Shen *et al*., (2006) have shown that ABA/D_{IX} binding are independent of each other and a 45 kDa C-terminal fragment appears to be particularly important in ABA binding whereas the N-has a potential role in signal regulation (Wu *et al.*, 2009). It has also been shown that a C-terminal fragment (residues 631 to 999) is essential for chlorophyll biosynthesis (Wu *et al*., 2009). It would be interesting to know if the N-terminal head region plays an important role in the magnesium chelatase activity of ChlH; this interesting proposal will be addressed in Chapter 4.

The lumen enclosed by ChlH is ~100 nm^3 in volume, equivalent to a sphere 4.7 nm in diameter and much larger than required to sequester a Proto molecule of 1.4 × 1.4 nm. This discrepancy could arise from a pooling of negative stain in this cavity, which would lead to an overestimation of the enclosed volume, as seen in an EM and X-ray crystallographic analysis of the glycerol dehydrogenase complex (Ruzheinikov *et al*., 2001). Given the binding of ABA/Proto in the C-terminal domain it may be that the cage domain is involved in the binding of both ligands and may explain the apparently large volume of the lumen. Binding Proto in the cage may provide a stable environment for the photosensitive substrate. It is interesting to note that the hole adjacent to the flexible head domain is easily large enough to allow access of Proto to the lumen or exit of the MgProto product, so it is possible that the movement of the head domain of ChlH could play an important role in the catalytic cycle.

The multiple functions for the Mg chelatase H subunit could well necessitate a large, multidomain protein. Apart from its main role as the porphyrin-binding subunit of Mg chelatase, the H subunit is likely to play a regulatory role by virtue of its position at the branch point between heme and BChl biosynthesis. The need for regulatory mechanisms is clear because the levels of these pigments have to be carefully metered to ensure that they are neither deficient, which would impair assembly and repair of

the photosynthetic apparatus, nor overproduced, which could result in light-induced photodamage to the cell. The metabolic versatility of some photosynthetic bacteria imposes an additional regulatory load on the cell because several species can shift between aerobic/respiratory and anaerobic/photosynthetic growth modes, which require a reversible switching of flux down the heme and Bchl pathways. As an example, Willows *et al.* (2003) demonstrated that BchH is inactivated by light and oxygen as cells of *R. capsulatus* switch to aerobic growth. Furthermore, BchH increases the activity of the next enzyme in the Bchl pathway, S-adenosyl-L-methionine (magnesium protoporphyrin IX methyltransferase) (Hinchigeri *et al*, 1997; Johnson and Schmidt-Dannert, 2008), although this stimulation was not found in other work (Sawicki and Willows, 2007). BchH of *R. capsulatus* forms a complex with either BchM or BchJ proteins (Sawicki and Willows, 2010). Finally, green sulphur bacteria such as *Chlorobaculum tepidum* possess three homologs of BchH, designated as BchH, S, and T, no doubt linked to the more complicated pigment biosynthetic pathways in such bacteria, which lead to Chl *a*, Bchl *a*, and Bchl *c* (Gomez Maqueo Chew *et* al., 2009; Chew and Bryant, 2007). It was proposed that the three BchH homologs apportion the amounts of each pigment produced by the cell (Chew and Bryant, 2007). A detailed *in vitro* enzymological study of these *C. tepidum* BchH homologs, combined with BchI and D, showed that their Mg chelatase activity varied over 5 orders of magnitude. Moreover, two of the BchH homologs increased activity of the MgProto methyltransferase, but one of them decreased it (Johnson and Schmidt-Dannert, 2008).

ChlH in oxygenic photosynthetic organisms does not have to contend with multiple Chl/Bchl pathways in the same cell as in *Chlorobaculum* nor switches between aerobic/respiratory and anaerobic/photosynthetic growth as in *Rhodobacter*. The task of regulating flux down the Chl pathway remains, particularly in view of the fluctuating demands on the pathway placed by diurnal rhythms, variations in light intensity (Gibson *et al*., 1996; Harmer *et al*., 2000), and repair of damaged photosystem II complexes. A regulatory role for ChlH in higher plants was proposed several years ago (Gibson *et al*., 1996; Hudson *et al*., 1993), and it is established that ChlH stimulates activity of Mg Proto methyltransferase in *Synechocystis* (Shepherd and Hunter, 2004; Shepherd *et al*., 2003; Shepherd *et al*., 2005) and in tobacco (Alawady *et al*., 2005). As already noted, the Gun4 protein in higher plants and cyanobacteria can form a complex with ChlH (Larkin *et al*., 2003; Wilde *et al.*, 2004;

Alhikari *et al*., 2011), a process that heavily influences the activity of Mg chelatase (Davison *et al*., 2005). A wider role for Gun4 has been proposed, including regulation of 5-aminolevulinic acid synthesis and in photoprotection (Peter and Grimm, 2009). It is possible that these multiple regulatory and catalytic functions could account for the increased size and structural complexity of ChlH with respect to BchH apparent in the comparison of these structures in Fig. 5. The extra size and complexity of ChlH might confer properties on ChlH subunits from oxygenic photosynthetic organisms that are absent in BchH subunits. We propose that ChlH has adopted a caged structure, in comparison with BchH, as a response to the intracellular environment of Mg chelatase in *T. elongatus*, an oxygen-evolving photosynthetic organism. In view of the lability of MgProto, we suggest that ChlH encloses this product of magnesium chelation and chaperones it to the active site of the methyltransferase to ensure both efficient handover of MgProto and its protection from photooxidation. Given the sequence homology of the *T. elongatus* ChlH to the Mg chelatase H subunits of higher plants and algae, it is likely that an enclosed structure is required to discharge the catalytic, chaperoning, and regulatory functions of this H subunit in all oxygenic photosynthetic organisms.

The isolation of ChlH directly from Native-PAGE is a tantalising result for future work in this field. It is clear that Gun4 and ChlH form some type of complex (Larkin *et al*., 2003; Wilde *et al*., 2004; Alhikari *et al*., 2011) and this complex may be transient like that of I and D. Isolation from a gel and negative stain/cryo EM of these samples would give a good insight into the stimulation of MgCH by Gun4.

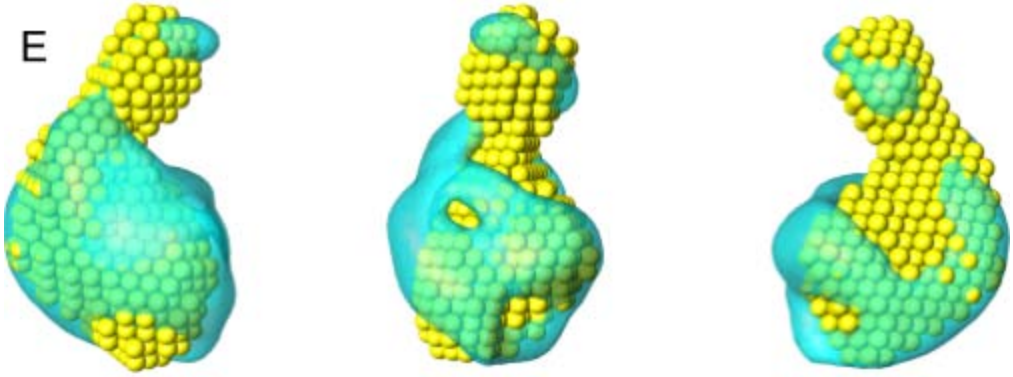

Figure 8 – Superposition of Synechocystis apo-ChlH SAXS representational model (yellow) with the 3D reconstruction of apo-ChlH from T. elongatus (cyan) from EM analysis

The superposition is viewed from three angles to emphasize the similarity between the two structural models. The handedness of the 3D reconstruction was selected arbitrarily for the best fit (Qian et al., 2012).

CHAPTER 4

Structural and functional characterisation of a mutant of the *Thermosynechococcus elongatus* ChlH protein with a deletion of the 15 kDa N-terminal domain.

5.1. Summary

Qian *et al*. (2012) recently solved the structure of a cyanobacterial magnesium chelatase H subunit at low resolution, using EM and SAXS. The reconstituted model shows a bi-lobed protein with a small ~15 kDa head region connected to the rest of the ChlH protein via a linker sequence. The flexibility of this linker region is suggested by the presence of several glycine residues, one of which is conserved amongst ChlH homologues. This linker region is connected to a globular body with a large lumen that is more than sufficient to accommodate a Proto molecule. Due to the number of different processes and functions proposed for ChlH it would be of much interest to elucidate the importance of the head region, at least in relation to its central role as the Proto binding subunit of magnesium chelatase. In this chapter *T. elongatus chlH* has been cloned in order to N-terminally truncate the native protein by the 160 residues that correspond to the proposed ~15 kDa head region. The structural and biochemical properties of this mutant have been investigated, with particular interest paid to porphyrin binding, catalysis of the MgCH reaction, association and binding with the Gun4 MgCH enhancer protein and the resulting structural changes that arise from this N-terminal deletion.

5.2. Introduction

MgCH is situated at the branchpoint of chlorophyll biosynthesis. It consists of three essential subunits; ChlI (~40 kDa), ChlD (~70 kDa) and ChlH (~140 kDa). I and D have been shown to form a double hexameric ring (Lundqvist *et al*., 2010) and I is the catalytic subunit known to be an ATPase of the AAA^+ (ATPases Associated with a variety of cellular Activities) family of proteins (Fodje *et al*., 2001). The N-terminus of

the D subunit is homologous to I and also contains a MIDAS (metal ion-dependent adhesion site) that has been suggested to be involved in divalent metal binding (Jensen *et al*., 1996). It has been suggested that the role of D in MgCH is to maintain a platform upon which I can coordinate with to initiate function (Axelsson *et al*., 2006).

The identification of the genes encoding MgCH was achieved by combining cell free extracts from three *E. coli* transformants overexpressing the product of each gene (Gibson *et al*., 1995). Subsequent characterisation of purified recombinant proteins enabled the elucidation of the role of ChlH and ChlI/ChlD as porphyrin binding and ATP/Mg^{2+} binding subunits respectively (Willows *et al.,* 1996; Jensen *et al*., 1998). The H protein has also been shown to stimulate the next enzyme along in the chlorophyll biosynthetic pathway MgProto methyltransferase (Shepherd *et al*., 2005; Alawady *et al*., 2005). Gun4, a protein involved in nuclear gene control, is a potential fourth subunit of the MgCH reaction. It binds ChlH and enhances the reaction through a method still yet to be resolved. It should be noted that Gun4 binds the substrate and product of the reaction (Larkin *et al*., 2003; Davison *et al*., 2005) and it may be through this that the reaction is enhanced.

Mutagenesis has been a crucial tool for identifying important residues and domains of enzymes with respect to activity, functionality and stability. In relation to MgCH subunits, Jensen *et al.* (2000) showed that cysteine residues in ChlI are important for ATPase activity and the formation of a ChlH•Proto complex. Olsson *et al*. (2004) characterised mutations in the *xantha-f* gene that encodes the ChlH subunit from barley, some of which were amino acid substitutions that led to lowered expression and downregulated chlorophyll biosynthesis. Other frameshift mutations resulted in truncated and, as a result, highly degraded proteins. The missense mutations found in barley, *xantha-f* ^{26} (M632R) and *xantha-f* ^{60} (P393L) were introduced into an H homologue from *Rba*. *capsulatus* (*xantha-f* ^{26} M591R and *xantha-f* ^{60} P341L) and the Mg chelatase activity of the purified recombinant protein was reduced by 52 % and 33% respectively (Olsson *et al*., 2004). The discovery of a *gun5* mutant in *Arabidopsis* has assigned a possible role of ChlH in plastid-to-nucleus signalling (Mochizuki *et al*., 2001) and the *gun5-1* and *cch* mutants, amino acid substitutions A990V and P642L respectively, showed weak phenotypes of decreased greening when compared to wild-type (Mochizuki *et al*., 2001). These mutations were made in the *Synechocystis chlH* (A942V and P595L, respectively) and cloned into an *E. coli* expression vector; both

mutant ChlHs retained WT porphyrin binding but resulted in a loss of MgCH activity *in vitro* that could be resurrected to WT levels by the addition of Gun4 (Davison and Hunter, 2011). Qian *et al*. (2012) showed that *T. elongatus* ChlH is a multi-lobed protein with a large globular body and a smaller lobe attached through a linker region. The linker is likely to be flexible due to a number of glycine residues which are typically associated with mobility and one residue (Gly127) is conserved throughout all H proteins sequenced to date. It has been postulated that the flexible linker region and head may have a role in the catalytic function of the H subunit (Qian *et al*., 2012). As in *gun5-1* and *cch* a large-scale truncation of the N-terminus of ChlH, by 63.2 kDa, maintained porphyrin binding to near WT levels but demonstrated abolition of MgCH activity (Qian *et al*., 2012). It can be assumed that structurally, tetrapyrrole binding in ChlH is much more robust than catalytic activity.

There is no high resolution structural information available for ChlH or any similar protein. A number of crystal trials have been conducted, by the Hunter group and collaborators, but ChlH appears to crystallise poorly under the conditions explored so far, with no diffraction. The possible flexibility of the linker region may prevent protein lattice formation and it may be argued that the head might prevent the protein packing to form crystals. If the head region was removed and the globular body domain retained its folded structure it may form crystals more easily and as a result give a higher chance of yielding highly-diffracting crystals. Whether or not this becomes possible, deletion of the head region should help to elucidate its structural and functional roles.

In this chapter an N-terminal 160-residue truncation of ChlH (hereafter ΔN160H with the sequence of the deleted region indicated by the cyan bar in Fig. 1) was constructed and the recombinant protein was purified. The porphyrin binding and enzymatic properties were studied along with the association with the enhancer protein Gun4. Finally structural properties of this ChlH deletion are discussed, and the potential for the acquisition of more detailed structural information.

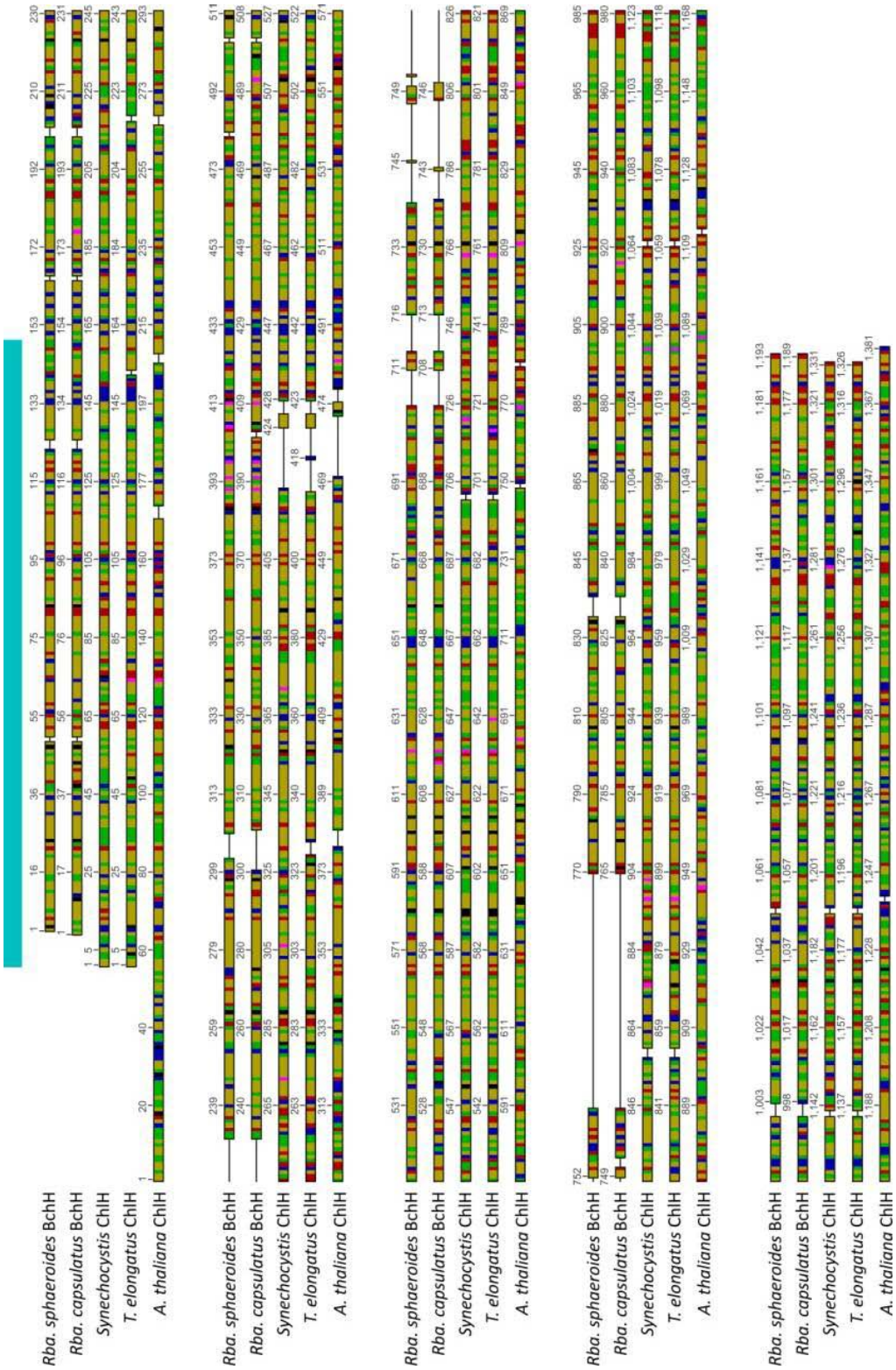

Figure 1 – Amino acid alingnment of Mg-chelatase ChlH/BchH porphyrin binding subunits

Amino acids are aligned according to their characteristics. Black, histidine; blue, positively charged; green, polar; magenta, cysteine; red, negatively charged; yellow, non-polar. The cyan bar indicates the proposed 160 residue N-terminal truncation. Compiled using Geneious software (Drummond, et al., (2010) Geneious v5.3, http://www.geneious.com).

5.3.Results

5.3.1. Overexpression and purification of *T. elongatus* ΔN160H

The pET9aHis[*ΔN160H*] (Table 2) construct, kindly donated by Dr. Amanda Brindley, was transformed into *E. coli* BL21 (DE3) cells and liquid cultures of this strain were induced to produce recombinant protein. SDS-PAGE of soluble and insoluble fractions from the culture showed that ΔN160H was found in both fractions. Wild-type ChlH, produced by overnight expression of the encoding gene, is primarily found in the soluble fraction of broken cells and the presence of insoluble and soluble ΔN160H indicates the formation of large protein aggregates. To enable large-scale purification of pure biochemically viable protein it is important to maximize soluble protein production. Expression trials (Fig. 2) were performed to limit production of insoluble protein possibly caused by the aggregation of high levels of truncated protein. Cells induced for 2 h, 4 h and overnight, together with cells grown overnight without induction, ΔN160H were harvested, disrupted then separated into soluble and insoluble fractions. Analysis of these fractions using SDS-PAGE shows that 2 hr induction of expression gives very limited protein production, as did overnight growth without induction. 4 hr and overnight induction produces high levels of ΔN160H protein ΔN160H in both soluble and insoluble fractions, highlighted with the red boxes in Fig. 2. Because of the tendency of ΔN160H to aggregate, a 4 hr induction was chosen to limit protein aggregation in both soluble and insoluble fractions.

Purification of ΔN160H from cells induced for 4 hrs was performed as described in section 2.10.1. Gel filtration chromatography indicated that the protein eluted in large soluble aggregates and this was confirmed by viewing the eluate using EM (Fig. 3); the uneven background is the result of non-specific negative staining. In an attempt to yield a homogenous population of protein molecules, the ΔN160H eluate was exchanged into buffers with a range of pH values, as described in section 2.11. Analytical HPLC gel filtration was performed to see if pH changes affected protein aggregation (Fig. 4). pH appears to have a limited effect on the aggregation of ΔN160H. The green trace, indicating a pH of 9.0, has the most positive effect on increasing the monomeric population of ΔN160H but a high number of other species of protein aggregates were also present.

Truncation of 160 residues from the N-terminus of ChlH may have exposed a hydrophobic patch that could promote aggregation. A detergent, n-Octyl-β-D-Glucoside (BOG), was used in an attempt to mitigate this effect; ΔN160H was exchanged (section 2.11) into buffer containing BOG, both above and below its a critical micellar concentration (CMC) of 20 – 25 mM. 2.5 mM BOG had little effect on aggregation of ΔN160H but 80 mM appeared to greatly increase the monomeric state of ΔN160H (Fig. 5). It is apparent from analytical gel filtration that detergent appears to have an effect on the aggregation states of ΔN160H. ChlH was also exchanged into buffer containing 0.75 mM n-dodecyl-β-D-maltopyranoside (DDM); 0.75 mM was chosen because DDM has a low CMC of 0.15 mM and the effects of BOG were only observed above the CMC. DDM appears to have a greater effect on the monomerisation of ΔN160H so after separation of soluble and membrane fractions it was added to the supernatant and to all buffers to a final concentration of 0.75 mM. In all the detergent trials the molecular weight appears to be slightly larger than WT ChlH and this is most likely the due to the interaction between the detergent and the protein. Fig. 6 shows a typical ΔN160H purification with 0.75 mM DDM and as expected ΔN160H is clearly smaller than the wild-type protein standard.

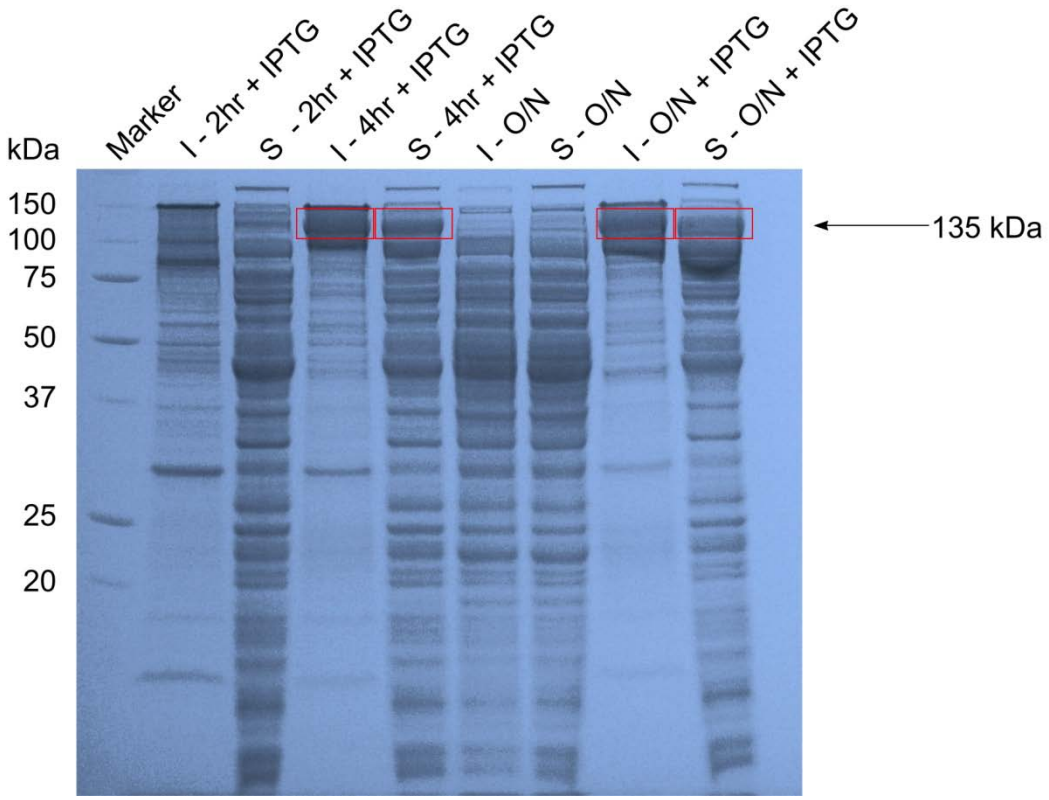

Figure 2 - Overexpression trials of ΔN160H

E. coli containing pET9a-His[ΔN160H] was grown at 37°C to an O.D.$_{600}$ of 0.7 and then incubated at 20°C for various periods of time, some induced with 0.4 mM IPTG. The insoluble (I) and soluble (S) fractions were separated by SDS-PAGE. ΔN160H has a predicted MW of 135 kDa. Induction with IPTG for 2 h does not result in the accumulation of recombinant ΔN160H protein in either the soluble or insoluble fraction. 4 h and overnight (O/N) induction with IPTG shows strong production in both insoluble and insoluble fractions. Growth overnight without IPTG induction shows no protein production.

Figure 3 - Electron micrograph of ΔN160H aggregates

Electron micrograph of initial recombinant ΔN160H purified from an E. coli soluble fraction by steps including gel filtration. Monomeric WT ChlH has a maximum dimension of 12 nm; the sizes of these proteins indicates that aggregation has occurred.

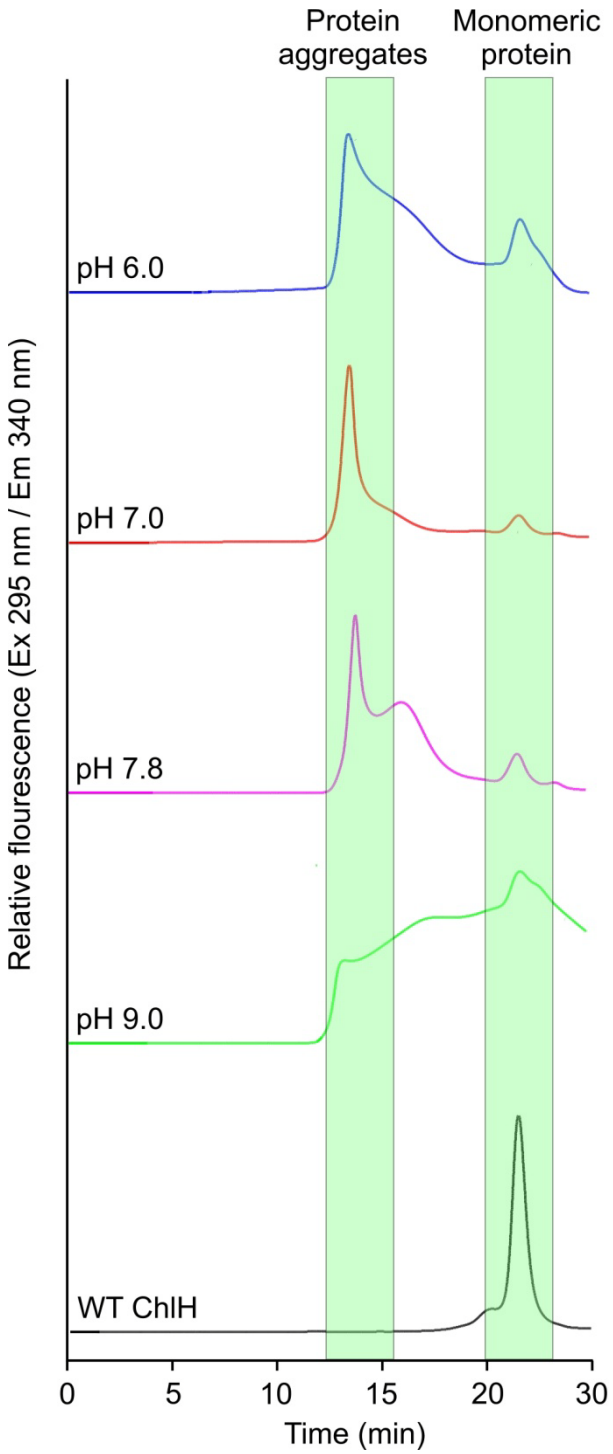

Figure 4 - Trials to prevent aggregation of ΔN160H by varying buffer pH

Analysis was performed using HPLC gel filtration chromatography, monitoring protein fluorescence. The green bars indicate the aggregated or monomeric protein populations. WT ChlH was purified using buffers with a pH of 7.8.

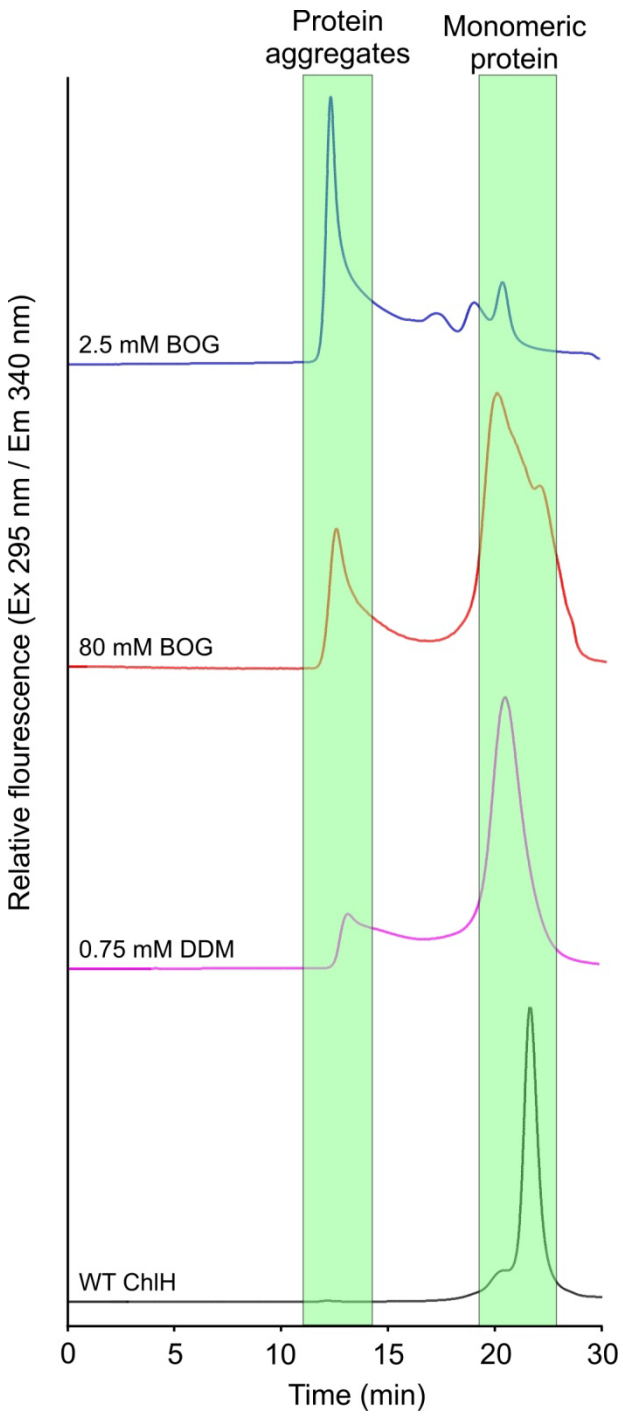

Figure 5 - Trials to prevent aggregation of ΔN160H by addition of detergent to buffers.

Analysis was performed using HPLC gel filtration chromatography monitoring protein fluorescence. Green bars indicate protein elution population as aggregated or monomeric.

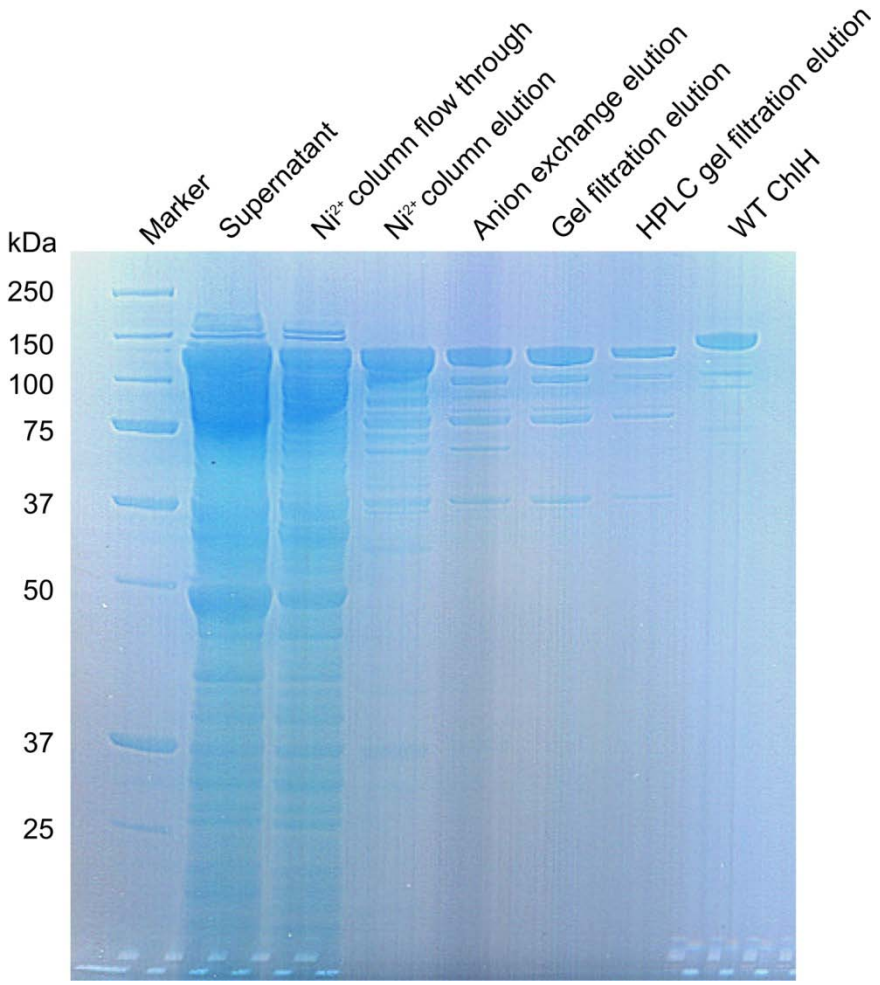

Figure 6 - SDS-PAGE demonstrating the purification of T. elongatus ΔN160H

E. coli containing the pET9a-His[ΔN160H] was grown at 37°C to an O.D.$_{600}$ of 0.7 and then incubated for 4 h at 20°C in medium supplemented with 0.4 mM IPTG. Cells were broken and the insoluble and soluble fractions separated. DDM was added to the supernatant to a final concentration of 0.75 mM. The soluble fraction was applied to Ni^{2+}, anion exchange and size exclusion chromatography columns sequentially (buffers all contained 0.75 mM DDM). WT ChlH was included to demonstrate a decrease in MW for the deletion mutant.

5.3.2. Single particle analysis of the ΔN160H protein

Purified ΔN160H was absorbed onto freshly glow-discharged carbon-coated copper grids that were subsequently negatively stained as described in Qian *et al*. (2012). Fig. 7*A* shows typical raw data for the clearly monomeric ΔN160H protein. Approximately 70 particles could be identified within a single 1K × 1K micrograph, and 20236 were picked in total. The particles were then treated using the IMAGIC-5 software package (van Heel *et al*. 1996). All particles were band-pass filtered to suppress low spatial frequencies according to values suggested in the IMAGIC-5 operation manual. The filtered particles were masked, normalized and centred for reference-free 2D classification (van Heel *et al*., 1981). After a few cycles of multi-reference alignment (MRA), a set of 25 characteristic 2D classes was built and used for consequent rounds of MRA (van Heel *et al*., 1985). A few iterations were performed until a stable 2D classification was obtained. 1349 2D classes were selected for Euler angle assignment and 3D reconstruction afterwards. An initial 3D model was produced, which was used for calculation of the Euler angles for the 2D classification data set. A mismatch between the calculated and assigned angles indicates an inaccurate model, so a new model was produced from the data set and re-projected so new Euler angles could be re-assigned. This iteration continued until a stable 3D model is generated; this model was visualised by UCFS Chimera (Pettersen *et al*., 2004). The threshold value for the volume of the reconstructed 3D model was adjusted to its predicted molecular weight, 135 kDa. In Fig. 7*D*, the 3D model generated from the averaged 2D classes has been rotated successively 90 degrees about the Z axis.

The ΔN160H structure shows a hollow globular protein with three connected lobes with a large open lumen. The lobes are connected to one another via linker regions and at least three large apertures are visible in the structures. Fig. 8 shows the superposition of the ΔN160H mutant with the previously published *T. elongatus* ChlH model (Qian *et al*., 2012). Both globular body regions are of a similar size and show evidence of openings into the hollow lumen in the same positions; ΔN160H appears to be missing the ‘head’ region observed in ChlH. The two models are not identical in their globular regions, which may be the result of a slight alteration in folding or it may be attributed to the 10 % error associated with negative staining.

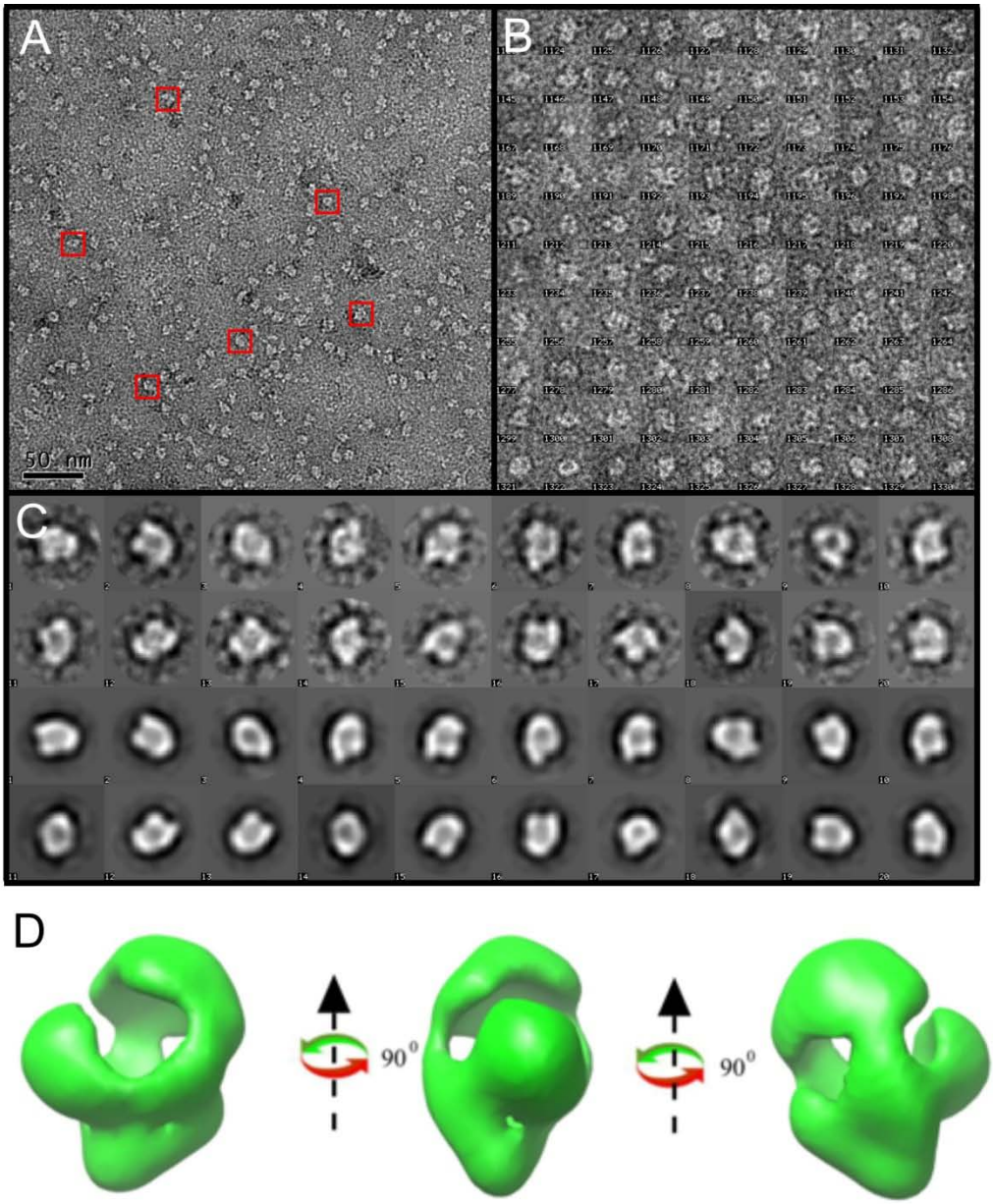

Figure 7 - Electron microscopy, classifications, reprojections and 3D model of negatively stained apo-ΔN160H

A, electron micrographs of ΔN160H. Scale bar = 50nm. B, 100 boxed single molecules of ΔN160H. The box size is 25 nm25 nm. C, Top two rows, 20 averaged 2D classes of apo-ΔN160H, bottom two rows, corresponding reprojections from the 3D model. D, 3D model of the MgCH ΔN160H mutant, calculated at a cutoff resolution of 30 Å.

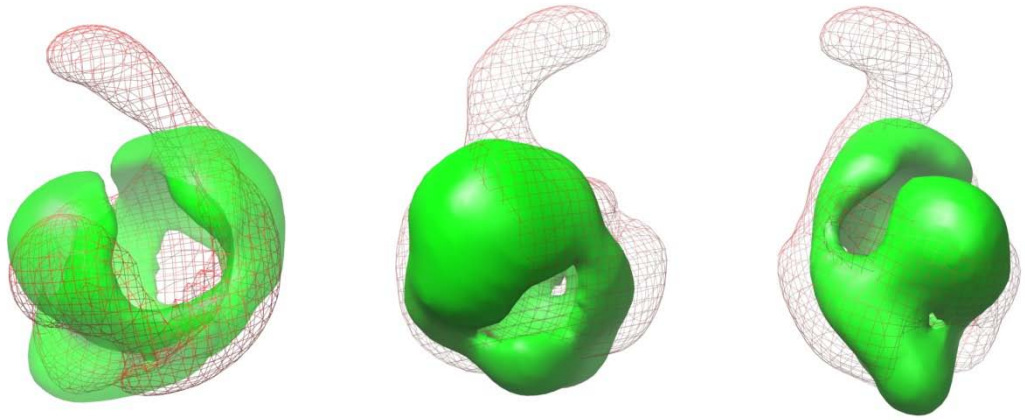

Figure 8 - Superposition of negatively stained apo-ΔN160H and WT apo-ChlH
Superimposition of single particle 3D reconstruction models. The hollow wire model represents the WT ChlH from T. elongatus and the solid green model represents the ΔN160H mutant.

5.3.3. Porphyrin binding studies

To identify if the ΔN160H mutant retains porphyrin binding functionality the dissociation constants between protein, substrate and product were determined using methodology described in 2.13. (Karger *et al*., 2001). Fig. 9 displays plots of integrated fluorescence as a function of tetrapyrrole concentration. In each case the binding titration data were fitted to equation 1, Chapter 3, in which a single type of binding site is assumed (Karger *et al*., 2001).

The calculated K_d values of ΔN160H for D_{IX} and MgD_{IX} were 1.06 ± 0.09 μM and 1.64 ± 0.08 μM respectively. These calculations are consistent with the published disassociation constants for wild-type *T. elongatus* ChlH of 1.48 ± 0.3 μM for D_{IX} and 2.12 ± 0.2 μM for MgD_{IX} (Qian *et al*., 2012). The data prented are from single titrations and the errors reflect the error in the K_d obtained using the equation.

5.3.4. Assaying the relationship between ΔN160H and Gun4

To ascertain if ΔN160H can form protein complexes with *T. elongatus* Gun4 clear native PAGE was used to identify any protein-protein interactions. 5 μM ChlH, 30 μM Gun4 and ChlH, Gun4 mixtures in molar ratios of 1:1, 1:2, 1:4 and 1:6 maintaining 5 μM ChlH were incubated at 50°C for ten minutes in native loading buffer and run on a gel at 4°C for 3 hours. Fig. 10*A* clearly shows monomeric ChlH just below the 242 kDa marker. The red boxes indicate high molecular weight complexes. ChlH forms an oligomeric complex with a MW of around 700 kDa. Given the MW of ChlH is ~150 kDa this would indicate that either a 4 or 5 × ChlH protein complex of 600 or 750 kDa respectively. In the samples with increasing Gun4 there is an increasing shift of this high MW band, although it is difficult to estimate the extent of this shift. It is also noteworthy that Gun4 forms high MW aggregates of approximately 500 kDa. The same conditions were used for ΔN160H and again analysed on native PAGE. ΔN160H also runs as a monomeric protein and another band is visible indicated by the arrow; the predicted MW of ~300 kDa is consistent with a dimer. ΔN160H does not appear to form the same high MW band that ChlH forms, though in Fig. 10*B*, lane 8 there is evidence of a high MW band with a similar migration to the complex seen with a 1:1 ratio of ChlH:Gun4. There is no difference in the migration between the ΔN160H:Gun4 in either the 1:4 or 1:6 ratio.

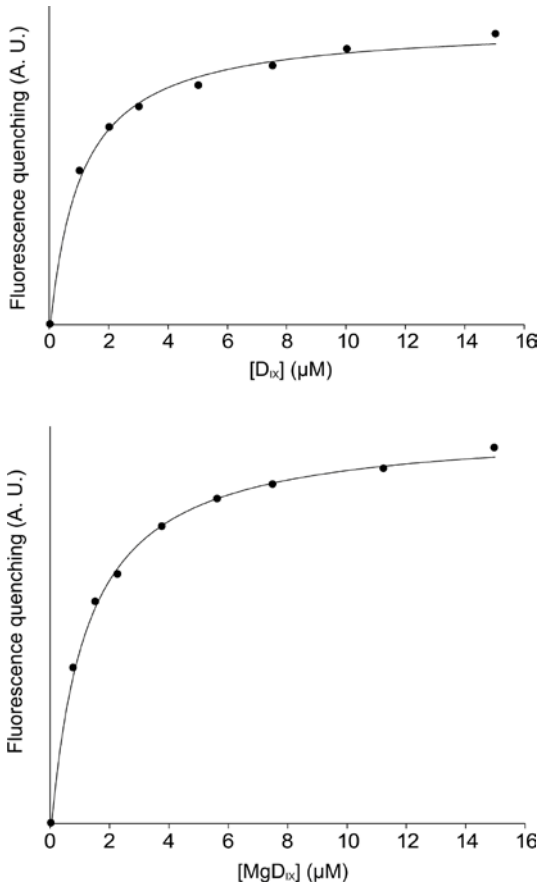

Figure 9 - ΔN160H fluorescence change upon porphyrin binding

Fluorescence quenching data for ΔN160H and the substrate, deuteroporphyrin IX (A) and product, Mg-deuteroporphyrin IX (B). The curve fits the experimental data to a single substrate binding model.

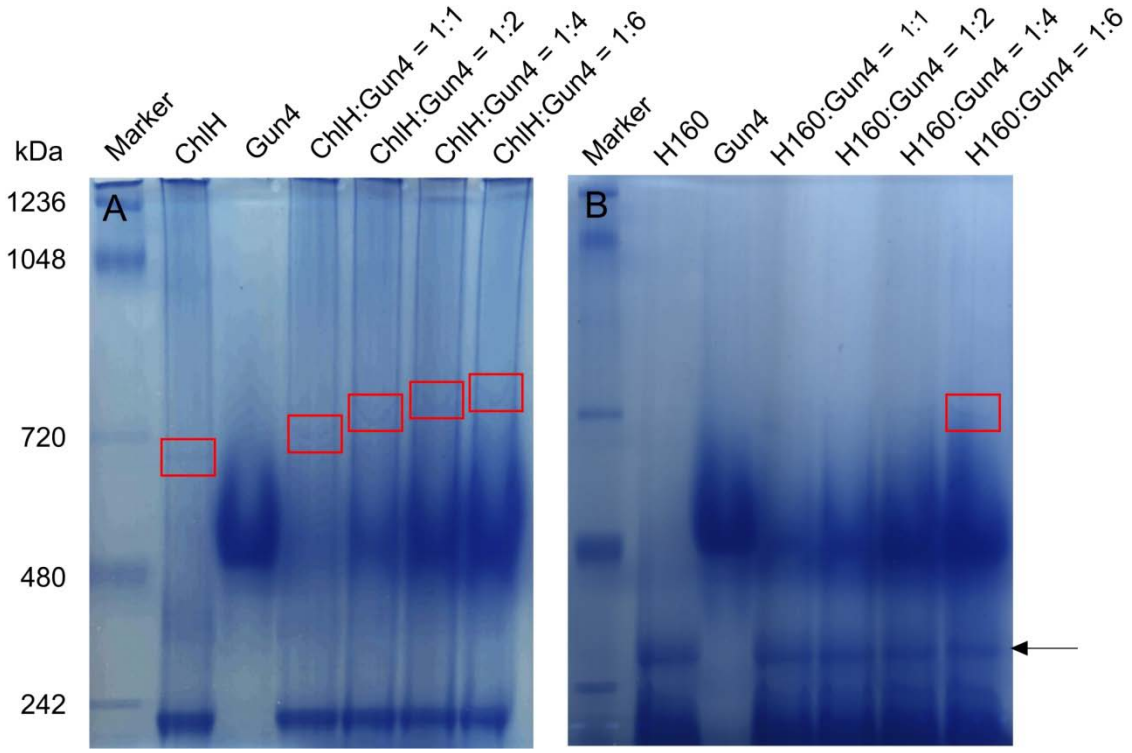

Figure 10 – Native gels showing complex formation between ChlH•Gun4 and ΔN160H•Gun4

3 – 8 % clear native PAGE. A, Lane 1, markers; Lane 2, T. elongatus ChlH; lane 3, T. elongatus Gun4 (30 μM): lanes 4 – 7, ChlH (5 μM) with increasing Gun4. B, as A, with ΔN160H rather than ChlH. Red boxes indicate visible protein complexes after Coomassie Brilliant Blue staining. The arrow indicates the appearance of another band only seen in ΔN160H native samples.

5.3.5. Kinetic Studies of ΔN160H

Qian *et al*., (2012) have shown that ChlH from *T. elongatus* is active in a MgCH assay with *Synechocystis* I and D subunits. Because the constructs for protein overexpression in *E. coli* are available for *Synechocystis I and D* and more importantly the production of active proteins has been proven (Jensen *et al*., 1998) it was decided to monitor ΔN160H MgCH activity using this heterologous system.

Recombinant proteins ChlI and ChlD from *Synechocystis* and ChlH and Gun4 form *T. elongatus* were purified following the protocol in Chapter 2.10, and the purity of the resulting preparations was analysed by SDS-PAGE (Fig. 11). ChlH and ΔN160H, with *Synechocystis* MgCH subunits ChlI and ChlD, were assayed for *in vitro* MgCH activity continuously for 1h whilst monitoring product fluorescence with an excitation wavelength of 420 nm and emission of 575 nm, as in Qian *et al*., (2012). The assays were performed with increasing concentrations of *T. elongatus* Gun4, and at two different temperatures as the proteins being assayed were native to two different species with different optimum growth temperatures. 34°C was chosen as this is the optimum temperature for *Synechocystis* subunits and 40°C was also chosen as this may allow the thermophilic *T. elongatus* porphyrin binding subunit and the Gun4 enhancer to achieve greater activity while avoiding denaturation of *Synechocystis* subunits. It was particularly important to have the higher temperature to allow ΔN160H the best possible chance of activity considering the extensive mutation.

Fig. 12*A* shows the steady-state rates for the ChlH (solid circles), I and D subunits at 34°C with increasing concentration of Gun4. As expected from previously published work on the effect of Gun4 on MgCH activity (Davison and Hunter, 2011) Gun4 increased the rate of reaction by around 3-fold. At 40°C the unenhanced rate is slightly higher than at 34°C, as would be expected, and at 1 μM Gun4 the rate is increased to ~0.4 μM min^{-1} of product (Fig. 12*B*). The ΔN160H mutant (Fig. 9, open circles) can be considered as inactive at both 34°C and 40°C in the absence of Gun4. ΔN160H is however revived with the addition of 1 μM Gun4 to a level that around half that of Gun4-free ChlH activity at 34°C and at 40°C the Gun4-assisted ΔN160H rate surpasses that of Gun4-free ChlH.

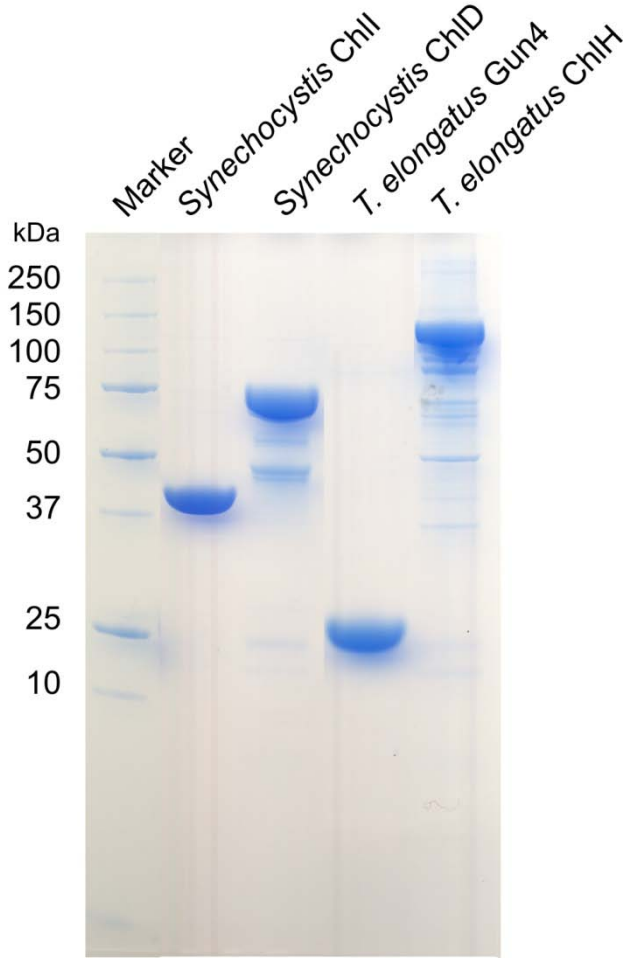

Figure 11 - Purification of various MgCH subunits for ΔN160H kinetic analysis

12 % SDS-PAGE analysis of MgCH subunits after purification.

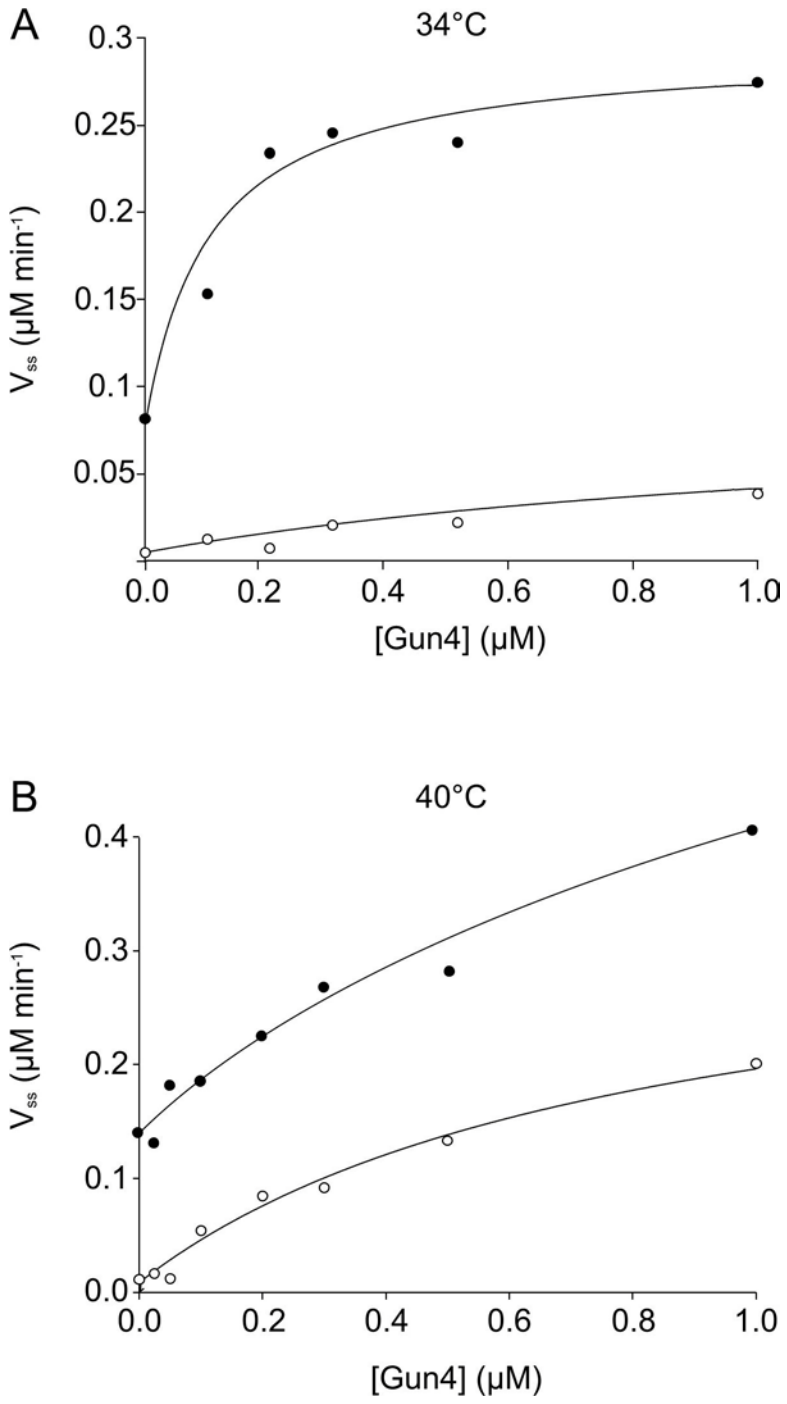

Figure 12 - Steady-state rate of ΔN160H compared to ChlH as a function of Gun4 concentration

Kinetic analysis of Synechocystis ChlI and ChlD incubated with 5 mM ATP, 15 mM $MgCl_2$, 8 μM D_{IX} and T. elongatus ChlH (solid circles) or ΔN160H (open circles) with increasing amounts of T. elongatus Gun4. Assays were performed at 34°C (A) and 40°C (B).

5.4.Discussion

Single particle reconstruction of ChlH reveals that the majority of the protein forms a hollow globular domain, which is attached to an N-terminal 160 residue 'head' domain (Qian *et al*., 2012). A truncation of ChlH (Fig. 1) was constructed to assess the role of this N-terminal domain. ChlH binds both the substrate and product of the MgCH reaction (Karger *et* al., 2001), but it has also been implicated in plastid-to-nucleus signalling (Mochizuki *et al*., 2001) and it stimulates the next enzyme along in the chlorophyll biosynthetic pathway (Shepherd *et al*., 2005; McLean and Hunter, 2009). A large N-terminal truncation of ChlH that removed the first 565 residues demonstrated the importance of the N-terminal third of ChlH for kinetic activity although normal tetrapyrrole binding was retained (Qian *et al*., 2012). Wu *et al*., (2009) have shown that a C-terminal fragment, residues 631 – 999, of ChlH in *Arabidopsis* is essential for MgCH activity. Creating an ΔN160H mutant would provide a number of insights into the role of the H subunit as the porphyrin binding subunit of MgCH. From the truncation, information regarding the validity of the N-terminal assignment by Qian *et al*., (2012) would be feasible as well as assigning a role in porphyrin and Gun4 binding or catalytic functioning.

From initial expression trials, ΔN160H appeared to express in both the soluble and insoluble fractions. Unlike highly stable ChlH, which is produced mainly in the soluble fraction from cultures induced overnight, a 4 h induction time was chosen to obtain the maximum yield of soluble protein. Preliminary purification of ΔN160H showed that deletion of the first 160 residues resulted in protein that elutes from size exclusion chromatography in the void volume. Soluble but highly aggregated clusters were seen when the sample was viewed using EM (Fig. 3). This aggregation is most likely due to the truncation exposing a hydrophobic patch and as a result the aggregation was only reduced when adding detergent (Figs. 4 and 5).

The reconstructed 3D model of ΔN160H reveals a globular hollow protein (Fig. 7) that is easily superimposed over the ChlH model. There is good similarity with the globular body and the head region is clearly missing in ΔN160H (Fig. 8). This observation provides confirmation that that the head domain is indeed encoded by a ~15 kDa N-terminal fragment. Moreover it is important to note that ΔN160H appears to maintain its hollow globular structure and the protein appears to be correctly folded. Any

significant change in functional properties is most likely to be due to the removal of the head region although it must be noted that such a significant truncation may alter the conformation of the rest of the protein to a certain degree.

The significantly higher number of 2D averaged classes obtained for ΔN160H (1349) when compared to ChlH (apo-ChlH, 75; substrate-bound ChlH, 92) (Qian *et al*., (2012) can be explained by the absence of the "head" region. This allows greater possible 3D distribution of the protein orientations compared with the asymmetric ChlH, where a several orientations and classes are excluded because of the head domain.

From the H•Gun4 binding assays it appears that the level of interaction between ΔN160H and Gun4 is considerably reduced when compared to ChlH. Lone ChlH is able to form a high MW complex of between 4 and 5 ChlH molecules, whereas ΔN160H forms a dimeric complex. It appears that when 4/5 ChlH molecules are in a complex the association with Gun4 is possible whereas dimeric ΔN160H does not show any interaction with Gun4. A ΔN160H•Gun4 complex does form when mixed in molar ratios of 1:4 and 1:6 and perhaps it is not until high concentrations of Gun4 are present that complexes are encouraged to form. Considering the ratio of H•Gun4 needed to form a complex is 1:4 and when taking into account the band size of 720 kDa, an H trimer with each ChlH binding ~4 Gun4 molecules fits best. However, a large complex comprising hollow ChlH proteins most likely contains fewer protein molecules than expected.

Fig. 12 (*closed circles*) shows assays for MgCH activity of *T. elongatus* ChlH and Gun4 with *Synechocystis* ChlI and ChlD. The increasing concentration of Gun4 significantly enhanced steady state chelation rates, as shown by Larkin *et al*., (2003) and Davison *et al*. (2005). The rates as a function of Gun4 concentration at 34°C and 40°C (Fig. 12*A* and *B* respectively) did not differ greatly which could be a result of a rate-limiting effect by mixing proteins from different species, or due to *Synechocystis* subunits having reached maximum activity at their optimum growth temperature of 34°C. ΔN160H shows has almost no activity at both temperatures ΔN160H (Fig. 12, *open circles*). The addition of Gun4 revives the enzyme somewhat and at 40 °C (Fig. 12, *B*) with a Gun4 concentration of 1 μM the assay is revived to a slightly higher rate than unenhanced ChlH. It is difficult to determine the extent the head deletion has on the catalytic activity. Although the H subunit is inactive in the absence of Gun4 this

could be a consequence of removal of the head domain, but altered folding caused by the large truncation cannot be discounted. The native gel analysis (Fig. 10) suggests that ΔN160H has lost some ability to form a complex with Gun4, but the enzyme assays are a more reliable indicator of a functional association and these indicate that the truncation does still allow the interaction with Gun4, especially at 40 °C.

The definite role of the first ~15 kDa of ChlH is difficult to pinpoint. What is clear is that protoporphyrin binding is associated with the globular body region, possibly within the lumen as proposed by Qian *et al*. (2012). As noted in Qian *et al*. (2012) the linker region between the head and the remaining globular protein has a contrasting pI when compared with ChlH as a whole. It may be this linker allows the type of Mg^{2+}-association with the membrane previously observed for the *Arabidopsis* ChlH (Gibson *et al*. 1996). Interesting future work would involve creating an inducible FLAG-tagged ΔN160H mutant in a WT *Synechocystis* background. Separating the thylakoid and soluble fractions under differing Mg^{2+} conditions, then western blotting with antibodies against ChlH and FLAG should indicate the locations of ChlH and ΔN160H and throw some light on the membrane association process. This would highlight if the ΔN160H is able to remain in the thylakoid fraction when compare to ChlH.

When considering any crystallographic possibilities of ChlH the head region of ChlH may disrupt any possible packing in protein lattice formation. This is a possible reason that there are no crystal structures of any of the ChlH/BchH/CobN proteins or any similar proteins in general. Removal of the head region might allow tighter packing of the proteins in a crystal lattice.

The ΔN160H truncation forms inclusion bodies when cultures are induced overnight and to some extent when induced for 4 h. The quality of the purification is also not to a high enough standard to allow crystal formation. A useful strategy for obtaining crystallographic information of H would be to determine a purification procedure that would enable large quantities of highly pure protein. One strategy to increase the purity of the protein could be to alter the pH in the anion exchange chromatography step. Although the pH of buffer in the gel filtration chromatography did not alter the aggregation state of the ΔN160H protein a great deal altering the pH in ion exchange often reduces the number of contaminating proteins in a purification step. Another option would be to try a cation exchange step either before or after anion exchange. If

ΔN160H does not bind strongly to a cation exchange column it may be that some of the contaminants do and thus are separable from recombinant protein. Gel filtration does improve the preparation and is necessary for the removal of any remaining aggregation. HPLC gel filtration improves the purification further but is not suitable for the large scale purification necessary for crystallisation trials. Another more appropriate gel filtration column with a void volume nearer the MW of ThrΔN160H may be of advantage. Finally it may be interesting to employ the thermophilic properties of the protein; *E. coli* grows at 37°C and *T. elongatus* grows optimally at 55°C. An incubation step after separating the insoluble and soluble fractions at a range of temperatures followed by an additional centrifugation step and analysis on SDS-PAGE may indicate a temperature at which contaminating *E. coli* proteins denature and ΔN160H remains intact.

CHAPTER 5

Characterisation of a thermophilic magnesium chelatase from *Thermosynechococcus elongatus*

6.1. Summary

The insertion of magnesium into Proto is catalysed by MgCH and commits the porphyrin to the synthesis of chlorophyll, as opposed to the synthesis of haem catalysed by ferrochelatase. MgCH is comprised of three subunits named BchH/ChlH, BchI/ChlI and BchD/ChlD depending on whether they are found in anoxygenic or aerobic phototrophs. MgCH from purple bacteria, cyanobacteria have been characterised kinetically and also structurally to some extent, although there are no high-resolution structures for the ChlH, I and D subunits. This problem might be overcome by using chelatase subunits from a thermophilic photosynthetic organism, but there are no reports of any thermophilic MgCH. In this chapter the ChlH, I and D subunits from *T. elongatus* are overproduced in *E. coli* and purified to yield an active enzyme. The temperature stability and kinetic parameters of this enzyme have been characterised.

6.2. Introduction

The formation of chlorophyll is likely to be regulated at the branch point of tetrapyrrole biosynthesis. Proto is a precursor of both chlorophyll and haem and the reactions catalysed by MgCH or ferrochelatase dictate the fate of this porphyrin. Ferrochelatase is either a monomeric or homodimeric enzyme of 34 - 54 kDa (Wu *et al*., 2001) and catalyses the chelation of divalent iron into Proto, in a process that does not require ATP. MgCH is a much more complicated enzyme consisting of three protein subunits that are all essential for activity (Gibson *et al*., 1995). The subunits are denoted BchH/ChlH, BchI/ChlI and BchD/ChlH (~140, ~40 and ~75 kDa respectively) depending on the mode of photosynthesis as either **a**noxygenic (Gibson *et al*., 1995**;** Petersen *et al*., 1998) or aerobic (Jensen *et al*., 1996a,; Kannangara *et al*., 1997;

Papenbrock *et al*., 1997; Guo *et al*., 1998). The H subunit binds both the substrate and product of the reaction (Karger *et al*., 2001). The H subunit is proposed to distort the tetrapyrrole ring in order to insert magnesium; this has been shown to be the case for iron insertion into haem by ferrochelatase (Lacerof *et al*., 2000; Al-Karadaghi *et al*., 2006). The I subunit is an ATPase from the AAA^+ family and like other proteins from this family I forms a nucleotide (ATP, ADP or adenosine 5´-[β,γ-imido]triphosphate)-dependent oligomeric complex (Fodje *et al*, 2001; Hansson *et al*., 2002; Reid *et al*., 2003). The N-terminal half of the D subunit is homologous to the I subunit, although D is not an ATPase; the C-terminal domain of D contains a MIDAS motif suggested to be involved in divalent metal ion binding (Jensen et al., 1996; Axelsson *et al*., 2006).

MgCH activity has been studied intensively since the 1990s and the recombinant enzyme has been characterised in a number of species (Jensen e*t al*., 1998; Guo *et al*., 1998; Gibson *et al*., 1999). In *Synechocystis* the optimum subunit ratio between ChlI and ChlD was found to be 2:1 with a molar excess of ChlD resulting in inhibition (Jensen *et al*., 1998). ChlH was found to have an optimum concentration double that of ChlI. Steady-state kinetics performed using a ratio of 4:2:1, ChlH:ChlI:ChlD, respectively, gave a V_{max} of 236 ± 36 pmol-$h^{-1}\mu g^{-1}$ and a K_m of 1.25 ± 0.28 µM for Proto, up to a concentration of 0.8 µM, when all other substrates were in excess (Jensen *et al*., 1998). At 0.8 µM Proto the rate was reduced to 92 pmol-$h^{-1}\mu g^{-1}$. Jensen *et al*., (1998) interpreted this reduction as a possible consequence of aggregation of Proto molecules, limiting the availability for the enzyme, rather than substrate inhibition. A V_{max} of 95 ± 3 pmol-$h^{-1}\mu g^{-1}$ and a K_m of 4.9 ± 0.2 mM was estimated for $MgCl_2$ and V_{max} of 50 ± 3 pmol-$h^{-1}\mu g^{-1}$ and a K_m of 0.49 ± 0.1 mM was observed for ATP (Jensen *et al*., 1998). A more detailed steady-state study showed that the k_{cat} of the *Synechocystis* MgCH is 0.8 min^{-1} (Reid and Hunter, 2004).

In the purple bacterium *Rba. sphaeroides,* kinetic information showed that the optimum ratio of the three MgCH subunits was 36:4:1 of BchH, BchI and BchD, respectively (Gibson *et al*., 1999). A high molar excess of BchD inhibits the *Rba. sphaeroides* MgCH (Gibson *et al*., 1999). Using the ratio of 36:4:1 (BchH: BchI: BchD) the V_{max} was 32.1 ± 1.0 pmol-$h^{-1}\mu g^{-1}$ and the K_m for Proto was 0.15 ± 0.05 µM. Above 1 µM porphyrin appears to inhibit the chelation reaction, but again this may be due to Proto aggregation (*c.f.* Jensen *et al*., 1998). The V_{max} for Mg^{2+} was 43.4 ± 1.4 pmol-$h^{-1}\mu g^{-1}$ with a K_m of 3.3 ± 0.48 mM and the maximum rate achieved with

increasing ATP gave a V_{max} of 22.1± 0.7 pmol-$h^{-1}$$\mu g^{-1}$ and a K_m of 0.12 ± 0.02 mM (Gibson *et al*., 1999).

The aim of this chapter is to provide the first kinetic information for a MgCH from a thermophilic source, comparing the data with those already available for the *Synehcocystis* and *Rba. sphaeroides* enzymes mentioned above. Apart from widening our knowledge of MgCH enzymes generally, one benefit of this work is that it establishes that all three subunits are active, so they all become candidates for future structural studies.

6.3.Results

6.3.1. Cloning the *T. elongatus* chlD gene

Previous studies have noted the low levels of expression of the *chlD* gene from *Synechocystis* in *E. coli* using the pET9aHis$_6$ expression vector (Dr. Paul Davison, personal communication). This is also the case when expressing *gun4* gene in this vector, although in this case cloning the gene into the pGEX-4t-1 vector overcame this problem (Dr. Paul Davison, personal communication). Bearing this in mind, the *tsr1414* gene encoding *T. elongatus* ChlD was cloned into both pET9a-His$_6$ and pGEX using the primers pET-DF and pET-DR and GEX-DF and GEX-DR respectively (see Chapter 2, table 4). Cloning was performed using the Clontech method described in section 2.7.10. *ChlD* was cloned into pET9a-His$_6$ with a *Nde*I site at the 5’ end of the gene and a *Bam*HI site at the 3’ end. When cloning in pGEX, an *Eco*RI site was located at the 5’ end of the gene with a *Not*I at the 3’ end of the gene. The insertion of the *chlD* gene was confirmed by DNA sequencing and the plasmids were named pET9a-His$_6$[*TchlD*] and pGEX[*TchlD*] (fig. 1).

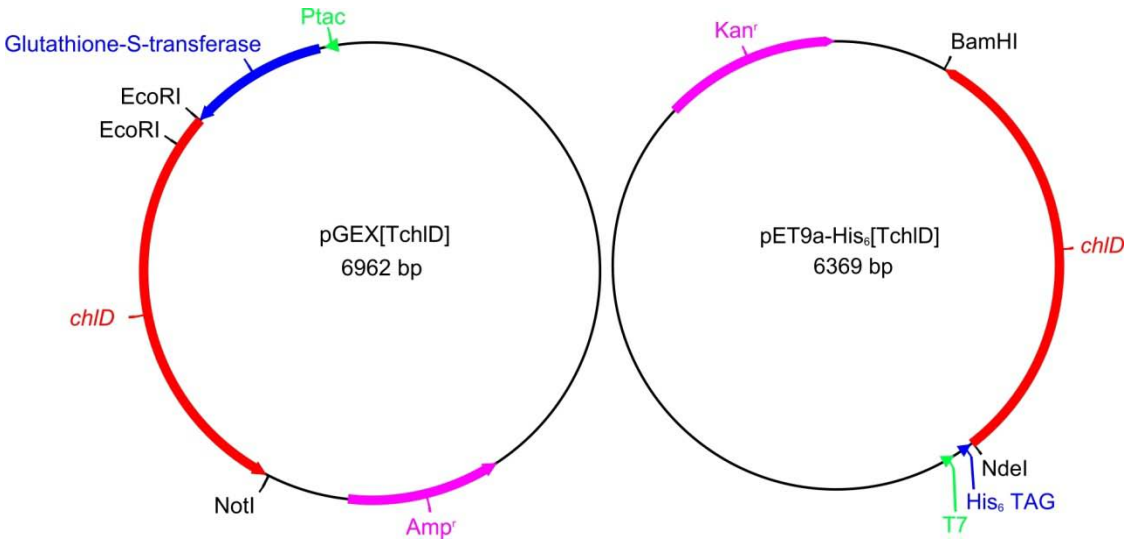

Figure 1 – Plasmid maps of pGEX and pET9a-His$_6$ vectors containing chlD. *Constructs containing the ChlD encoding gene showing restriction sties and relevant antibiotic selection.*

6.3.2. Expression trials of ChlD

Both the pET9a-His$_6$[TchlD] and pGEX[TchlD] plasmids were individually transformed into the *E. coli* Bl21(DE3) expression strain and grown on LB agar with antibiotic selection. Single colonies of both transformants were then inoculated into 6 different rich media (50 ml cultures) and induced to express protein as in section 2.8.1. The cells were harvested by centrifugation and lysed by sonication. The soluble and insoluble fractions were separated and expression of ChlD was analysed using SDS-PAGE (fig. 2).The pET9a-His$_6$[TchlD] transformants grown in the auto-inducing media (AIM) (Formedium) appeared to express the most soluble ChlD. This growth medium and plasmid were therefore used for further growth and expression of ChlD.

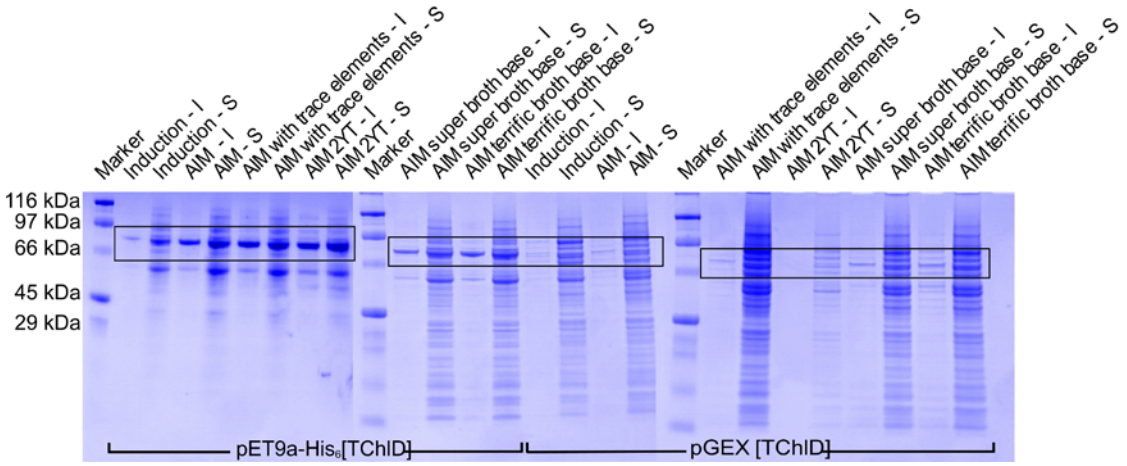

Figure 2 – Expression trial of ChlD in using two different expression plasmids in 6 various types of commercial rich media

Both pET9a-His$_6$[TchlD] and pGEX[TchlD] were transformed into six different types of rich media (induction indicates the use of standard LB broth) and induced to overproduce protein. The cells were broken and analysed using SDS-PAGE for ChlD expression. I represents insoluble fraction and S indicates soluble fraction.

6.3.3. Purification of MgCH subunits

The plasmids containing the *T. elongatus chlH* and *chlI* genes were kindly provided by Dr. Paul Davison. Cells were transformed with pET9a-His$_6$[*TchlH*], pET9a-His$_6$[*TchlI*] and pET9a-His$_6$[*TchlD*] and grown as described in section 2.12. The cells were harvested by centrifugation and lysed using sonication. The soluble and insoluble fractions were separated and the proteins were purified as in section 2.10. SDS-PAGE (Fig. 3) shows that all proteins had a typical purity of 90% or higher.

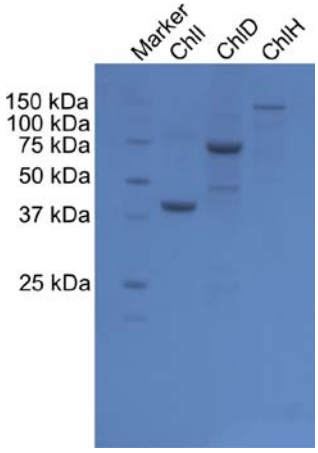

Figure 3 – Analysis of purity of recombinant T. elongatus MgCH subunit proteins

SDS-PAGE of I, D and H subunits after final purification steps.

6.3.4. Analytical gel filtration

The size exclusion chromatography analysis in Qian *et al*. (2012) and Chapter 3 showed that ChlH from *T. elongatus* eluted in one main peak from with an estimated MW of 150 kDa. The predicted molecular weight of ChlH is 150 kDa so these gel filtration data suggest a monomeric protein, as seen with the *Synechocystis* ChlH (Karger *et al.*, 2001).

Purified ChlD was analysed by HPLC gel filtration chromatography in the absence of $MgCl_2$ or nucleotide. ChlD eluted in one major peak with a retention time of 16.5 mins (Fig. 4). Using a calibration curve this gave an estimated molecular weight of 500 kDa. ChlD has a predicted molecular weight of 73 kDa so this would indicate 7 ChlD monomers in a complex,

When ChlI was analysed by gel filtration on the same column the elution profile indicated a species smaller than for ChlH or ChlD, possibly arising from a monomer or a dimer although the elution was outside the range for estimation of the size of the species.

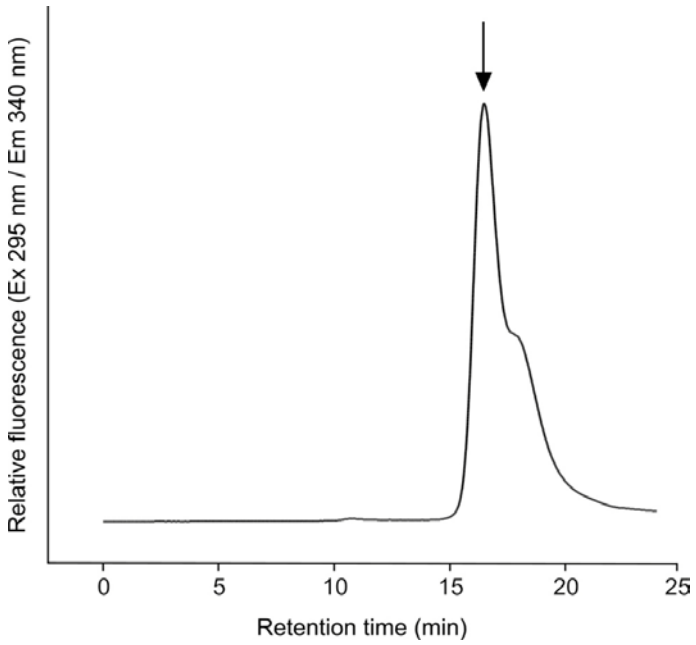

Figure 4 –HPLC gel filtration elution profile of ChlD

Elution profile of purified ChlD from a calibrated Biosep S4000 gel filtration column. The arrow indicates an estimated molecular weight of 500 kDa.

6.3.5. Optimisation of the I:D subunit ratio for steady-state MgCH assays

The MgCH I and D subunits associate in an ATP-dependent reaction to form a complex (Jensen *et al*., 1999; Gibson *et al*., 1999). A cryo-EM study of a ~660 kDa complex formed *in vitro* from *Rba. capsulatus* subunits suggests a stoichiometry of 6:6 (Elmlund *et al*., 2008).

To ensure kinetic analysis of the MgCH was under optimum conditions, initial tests were performed to determine optimal concentrations of the I and D subunits. Because ChlI is the catalytic subunit with ATPase activity and D has a supposed role as support/scaffold unit for I it seemed most appropriate to vary the concentration of D rather than I. All the MgCH assays were performed as previously published for *Synechocystis* MgCH (Reid and Hunter, 2004) but at a temperature of 45°C. Continuous, fluorometric MgCH assays were performed at a range of ChlD concentrations, with 1 µM ChlH and 0.1 µM ChlI. The steady state rates were observed and either duplicate or triplicate results plotted as a mean with standard deviation about the mean (Fig. 5). The optimum concentration of ChlD appeared to be 0.1 µM which gave a maximum rate of 0.045 ± 0.001µM min^{-1}. This concentration gave an ID ratio of 1:1. The published MgCH kinetics from *Synechocystis* describe an optimal ID ratio of 2:1; at this ratio this system has an activity marginally below optimum in the present study (Fig. 5) with a maximum rate of 0.042 ± 0.001µM min^{-1}.

When the concentration of D in the assay is increased so that I and D are no longer equimolar, excess D inhibits the reaction. At a D concentration five times that of optimum no chelation reaction is observed, in agreement with previous studies (Jensen *et al*., 1998; Gibson *et al*., 1999).

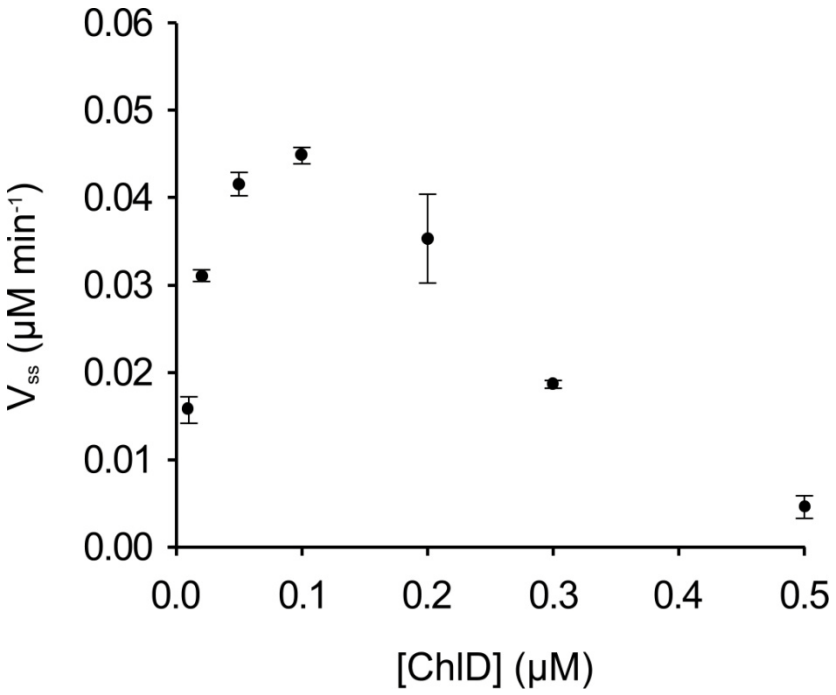

Figure 5 – MgCH assays with increasing amounts of the ChlD subunit

MgCH assays performed at 45°C with increasing concentration of ChlD. Assays were performed with 8 µM D_{IX}, 15 mM $MgCl_2$ and 5 mM ATP. ChlH was at a concentration of 1 µM and ChlI was 0.1 µM.

6.3.6. Setting the optimal ChlH concentration

The optimum concentration of the ChlH subunit was determined, using the previously determined optimal concentrations for ChlI and ChlD of 0.1 µM (Fig. 6). A saturating concentration of ChlH was obtained at around 1 µM, giving a maximum rate of 0.054 ± 0.005 µM min^{-1}. These data can be described by the Hill equation with a three-parameter function giving an estimated V_{max} of 0.039 ± 0.006 µM min^{-1} with a K_m of 0.64 ± 0.078 µM and *h* of 6.2 ± 3.4. Similar curves have been interpreted as showing positive cooperativity in the interaction between H and ID (Sawacki and Willows, 2008). Full activity was observed at 1 µM ChlH, so a ChlH:ChlI:ChlD subunit ratio of 10:1:1, was chosen as the concentration for kinetic analysis of the enzyme.

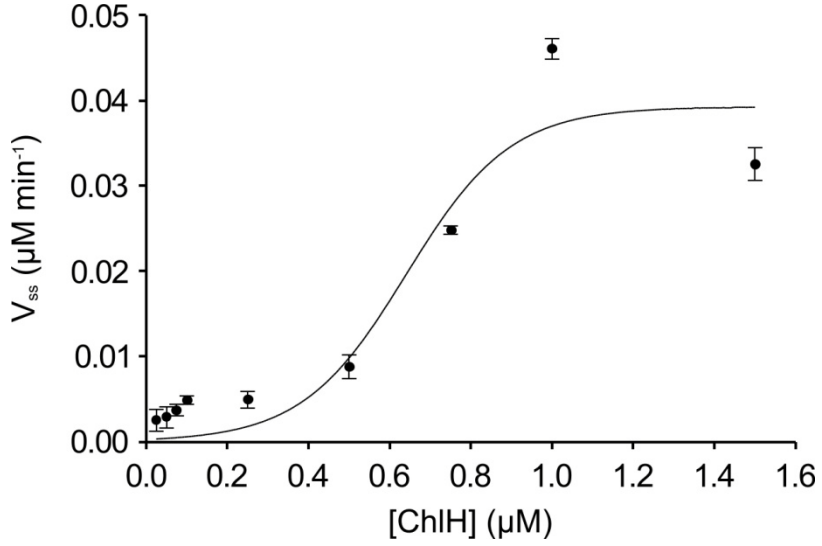

Figure 6 – MgCH assays with increasing amounts of the ChlH subunit

MgCH assays with increasing concentration of ChlH. Assays were performed with 8 µM D_{IX}, 15 mM $MgCl_2$ and 5 mM ATP. ChlI and ChlD were at a concentration of 0.1 µM at a temperature of 45°C.

6.3.7. Measurements of steady-state kinetic parameters for the three substrates

To estimate the V_{max} and K_m of MgCH for D_{IX}, continuous magnesium chelation assays were performed at a range of porphyrin concentrations with the previously optimised subunit ratio of 10:1:1. The concentrations of $MgCl_2$ and ATP were maintained at the presumed saturating level of 15 mM and 5 mM respectively. It was observed that a saturating concentration of D_{IX} was reached at 2.5 µM with a steady state rate of 0.05 µM min^{-1} and further increases in the concentration of D_{IX} inhibit chelatase activity (Fig. 7). The V_{max} and K_m were therefore estimated from the rising portion of the curve (Fig 7 inset) as V_{max} = 0.052 ± 0.006 µM min^{-1} and K_m = 0.43 ± 0.17 µM. The substrate inhibition constant (K_i) was calculated to be 4.56 ± 0.54 µM using the equation:

$$v = \frac{V'a}{K'_m + a + a^2/K_{si}}$$

Where v is velocity, K'_m is the mechalis-menton constant, a is the substrate and K_{si} is the inhibition constant.

The ATP dependence of the MgCH catalysed reaction was investigated. As the substrate for MgCH is actually $MgATP^{2-}$, the $MgCl_2$ concentration was always maintained with a 15 mM excess over the ATP concentration to ensure a constant free Mg^{2+} concentration of 15 mM. This was presumed to be a saturating concentration of Mg^{2+}. The D_{IX} concentration was 5 µM. A maximum steady state rate of 0.047 µM min^{-1} was observed. The data (Fig. 8) were fitted to a single rectangular hyperbola with characterising parameters V_{max} = 0.064 ± 0.0112 µM min^{-1} and K_m = 1.8 ± 0.81 µM.

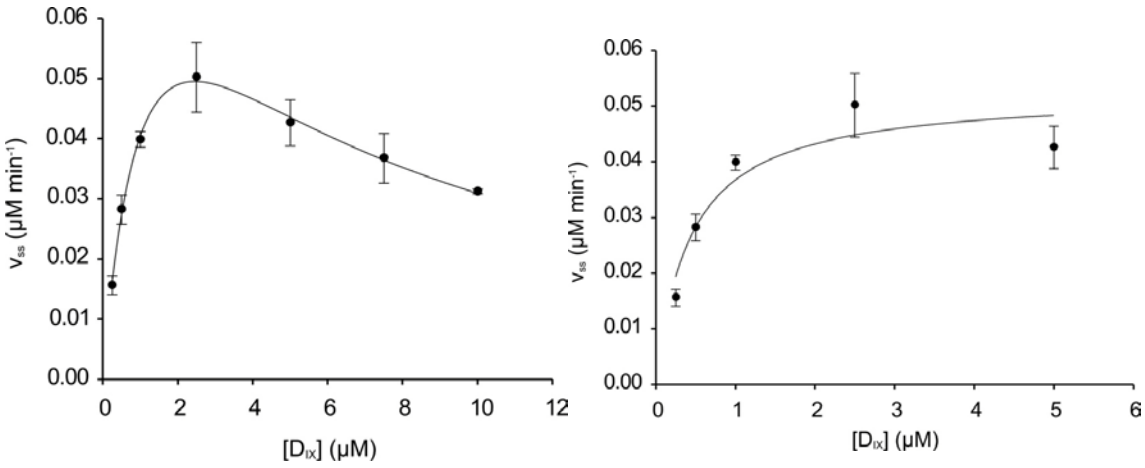

Figure 7 – MgCH assays with increasing amounts of D_{IX}

Left panel: substrate inhibition is seen with D_{IX} concentrations above 5 µM. Right panel: the steady-state activity up to saturation can be fitted to estimate kinetic parameters. Assays were performed with 15 mM $MgCl_2$ and 5 mM ATP at a temperature of 45°C. The curve was fitted to a substrate inhibition model.

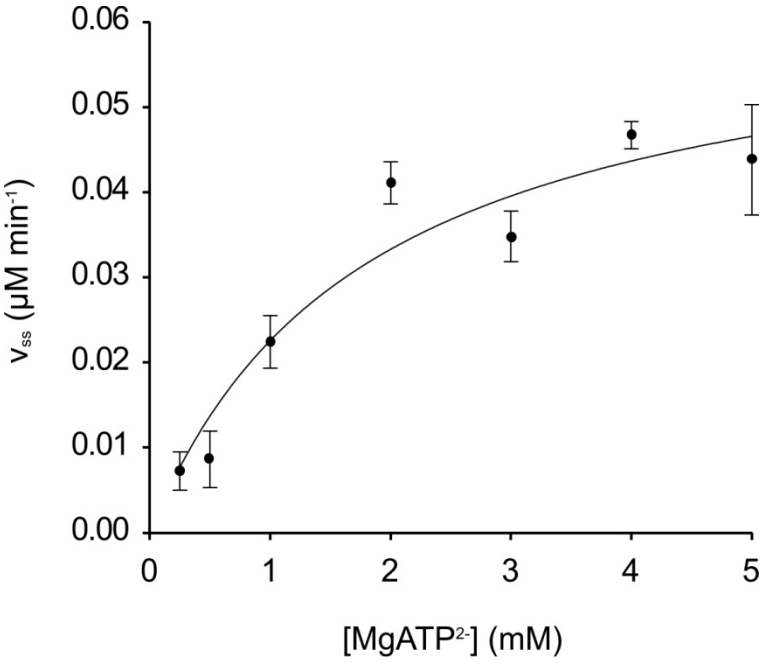

Figure 8 – MgCH assays with increasing amounts of $MgATP^{2-}$

MgCH assays with increasing concentration of $MgATP^{2-}$. Assays were performed at 45°C with 5 µM D_{IX}, ensuring the free Mg^{2+} was maintained at 15 mM.

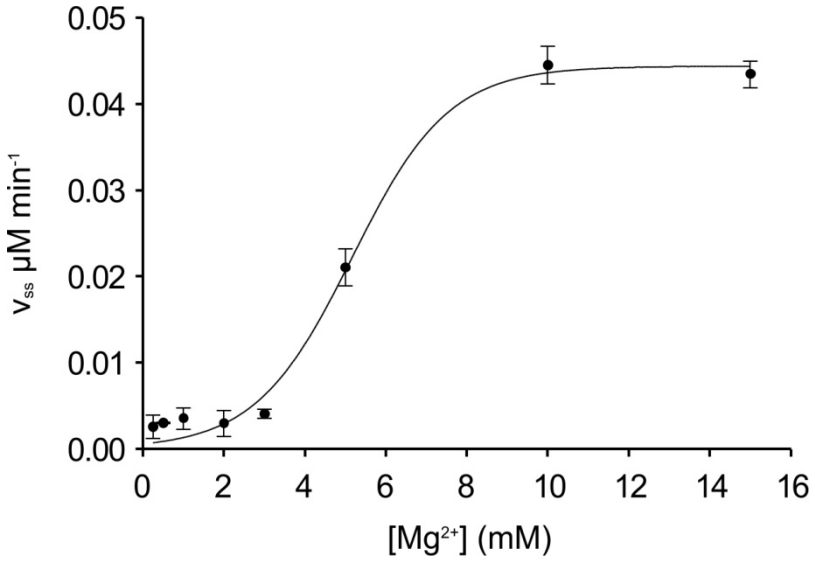

Figure 9 – MgCH assays with increasing amounts of Mg^{2+}

MgCH assays with increasing concentration of $MgCl_2$. Assays were performed at 45 °C with ATP maintained at 5 mM and the D_{IX} concentration at 5 µM.

The MgCH dependence on free magnesium was investigated at saturating concentrations of the other two substrates (ATP, 5 mM and D_{IX} 5 µM). The data were fitted to the Hill equation with a three-parameter function giving an estimated V_{max} of 0.045 ± 0.003 µM min^{-1} with a K_m of 5.11 ± 0.35 mM and *h* of 4.37 ± 1.35 (Fig. 9).

6.3.8. Analysis of MgCH subunits by circular dichroism spectroscopy

Circular dichroism (CD) spectroscopy was carried out in the UV region (section 2.15) to provide some evidence for the correct folding of the recombinant ChlH, I and D subunits from *T. elongatus*. The CD spectra were similar for all three subunits, indicating a high proportion of α-helices, rather than random coils, suggesting that all three subunits are folded (Fig. 10). Fig. S1 in the supplementary data section shows examples of CD spectra of particular secondary structural features. Elipcitiy was calculated using the equation:

$$[\theta] = \frac{(\theta \text{ x } m)}{c \text{ x } l \text{ x } 10000}$$

Where θ is optical rotation, *m* is molecular weight, *c* is concentration of protein in experiment (g/ml) and *l* is the pathlength used.

6.3.9. Thermostability of MgCH subunits

The thermostability of the MgCH subunits was investigated to reveal how much tolerance the subunits have for high temperatures in relation to structural integrity. CD was performed where a chosen wavelength, 222 nm, was monitored during a thermal ramp (Fig. 11). Over a time of approximately 3 hours, the temperature was monitored from 5°C until the there was no more change in absorbance at 222 nm indicating the protein was fully unfolded. From this the first derivative was taken to estimate the T_m.

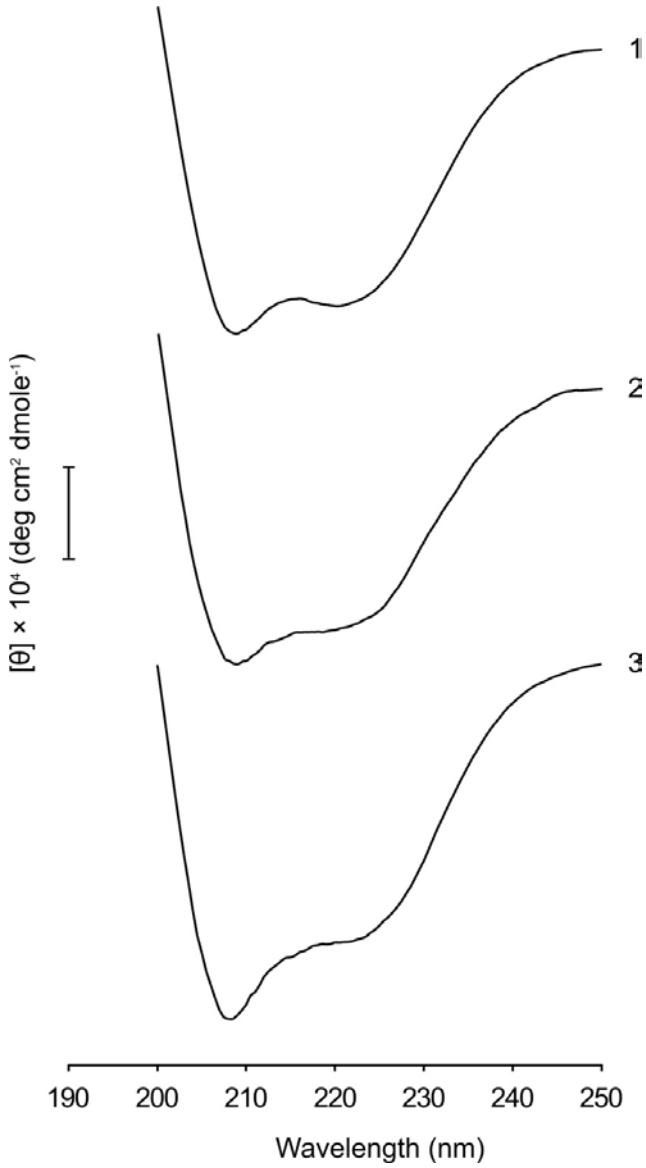

Figure 10 - UV CD analysis of the MgCH subunits from T. elongatus

Far UV CD spectra were recorded on a Jasco J-810 spectropolarimeter at room temperature. The numbered spectra correspond to samples containing: 1, ChlI; 2, ChlH; 3, ChlD. Spectra have been stacked for clarity, the y axis scale bar corresponds to 10 mdeg cm^2 dmole^{-1}.

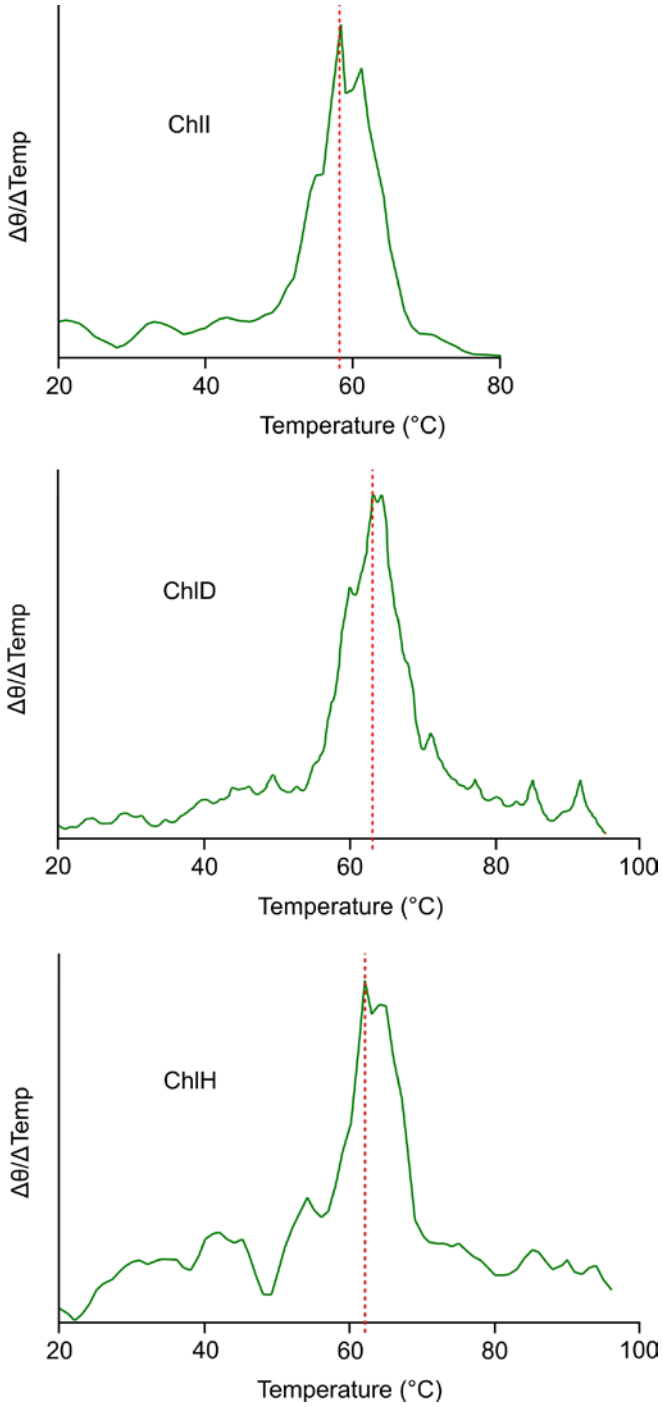

Figure 11 – CD analysis monitoring change in wavelength at 222 nm with increasing temperature to measure thermal stability

The CD signal was measured at 222 nm in chelatase buffer with increasing temperature, with the data plotted as the first derivative. The red dashed line indicates the T_m of the protein.

Table 1 – T_m for the MgCH subunits from Synechocystis and T. elongatus

The data for the Synechocystis I and D subunits were kindly made available by Nathan Adams (N.B. P. Adams, Ph.D. thesis, 2012). For the analysis of Synechocystis ChlH see the supplementary data section Fig. S2.

Subunit	*Synechocystis*	*T. elongatus*
ChlH	43°C	62°C
ChlI	47°C	58°C
ChlD	41°C	63°C

It is clear from the thermal melt data that as expected the *T. elongatus* subunits have a far greater tolerance for high temperatures when compared to *Synechocystis.* Interestingly however, the most tolerant subunit from each organism is not the same, H and D from both organisms behave similarly whereas the *Synechocystis* I subunit is far more robust with respect to the other *Synechocystis* subunits, than the *T. elongatus* homologue is with respect to the thermophilic H and D subunits.

6.4. Discussion

SDS-PAGE analysis of all three MgCH subunits from the thermophile *T. elongatus* shows that all three proteins are essentially pure after gel filtration chromatography. The analytical gel filtration of ChlD is interesting as there is no monomer observed and all protein migrates in large complexes.

The optimal ratio of the ID complex of 1:1 from kinetic data is consistent with the current structural BchI:BchD model from cryo-EM analysis (Elmlund, 2008). In previously published work the ID ratio has varied to quite a degree. In BchID complexes from *Rba. sphaeroides* the optimum ratio for steady-state kinetic studies has been reported to be 4:1 respectively (Gibson *et al.*, 1999). In *Synechocystis* an optimum ratio of 2:1 was determined (Jensen *et al.*, 1998) and was used in all later studies from this laboratory. The reported need for a small excess of ChlI over ChlD (the 2:1 ratio of Jensen *et al.*, 1998) may arise from a small proportion of inactive I subunit or from weak binding between ChlI and ChlD requiring an excess of protein to drive complex formation. It should also be noted that in this study and in published

work (Jensen *et al.*, 1998; Gibson *et al.*, 1999) anything over a 1:1 molar ratio of D to I leads to inhibition. Perhaps the I subunit interacts with H, and excess D starts to intervene and prevent this association.

The H subunit concentration found to be optimal was around 1 µM leading to an optimal subunit ratio of 10:1:1. The initial characterisation of the *Synechocystis* MgCH showed that a ratio of 4:2:1 (H: I: D) was optimal (Jensen et al., 1998), compared to a ratio of 36:4:1 for *Rba. sphaeroides* (Gibson *et al.*, 1999), in good agreement with the current study. An analysis of ChlH mutant subunits showed saturation of activity at a H to I ratio of 2:0.2 (Davison *et al.*, 2011), which is consistent with the data in this chapter.

When optimising the concentration of ChlH in the assay, a sigmoid curve appears to describe the data well. This could indicate a cooperative interaction between H and the ID complex. The Hill coefficient of 6.2 ± 3.4 is consistent with positive cooperativity. Sawacki and Willows (2008) have also described cooperativity with BchH and the BchI•BchD complex; they offered the explanation that more than one H will interact at any one time. Alternatively, these data could arise from a mixture of binding reactions between H and D_{IX} and HD_{IX} and the ID complex.

ChlH appears to be inhibited by high concentrations of D_{IX} (over 5 µM) similar to the work of Jensen *et al.*, (1998), who observed inhibition with Proto concentrations over 0.8 µM. The estimated inhibition constant (K_i) in the present work is 4.56 µM. One explanation of this phenomenon could be that the high temperatures of the assay promote aggregation of D_{IX} rendering it unavailable for the enzyme.

The kinetic parameters of MgCH from different species vary significantly. The k_{cat} for *Synechocystis* MgCH when using the porphyrin binding subunit concentration as a reference is 0.8 min^{-1} (Reid and Hunter, 2004). The *Rba. capsulatus* MgCH has a turnover number of 5.1 min^{-1} in relation to BchD concentration which Sawacki and Willows (2008) note is ~6 times higher than that of *Synechocystis.* This is somewhat misleading when regarding the ratio of H and D in both experiments. When the *Synechocystis* MgCH turnover number is calculated in relation to the concentration of ChlD it is 3 min^{-1}, which is comparable with the purple bacterial enzyme.

Because the ChlH subunit in this work is at a much higher concentration than that used by Reid and Hunter (2004), the k_{cat} for *Synechocystis* MgCH was recalculated on the basis of the ChlI concentration and it was estimated to be 1.5 min^{-1}(Reid and Hunter, 2004). On this basis the *T. elongatus* k_{cat} is 0.52 min^{-1}. This is still *ca.* 10-fold lower than the value determined for *Rba. capsulatus* but relatively close to the k_{cat} of *Synechocystis* with a ~3 fold difference. *Rba. sphaeroides* utilises Bchl for light harvesting whereas in cyanobacteria phycobilisomes are heavily involved in energy capture. These differing physiological demands on the Bchl and haem branches of tetrapyrrole biosynthesis could contribute to the differing k_{cat} values, but without knowledge of the same values for the ferrochelatases, and the numbers of enzyme molecules present, no valid comparisons can be made.

CHAPTER 6

Evidence for in vivo interactions between MgCH subunits

7.1.Summary

Three subunits are essential for the activity of MgCH, the enzyme involved in the insertion of a magnesium ion into protoporphyrin. These consist of H, a porphyrin binding subunit, and an ATP/Mg^{2+} binding complex formed by the I and D subunits. It is thought that H binds to porphyrin and this then interacts transiently with the H I•D complex to perform the chelation reaction. Apart from mechanistic studies the evidence for the formation of a MgCH complex is limited to an *in vitro* column assay in which non-tagged ChlI and ChlH subunits were observed to bind to a Ni^{2+} agarose column with immobilised His-tagged ChlD subunits. Analysis of column eluates using western blots and immunodetection showed that HID complexes can form under these conditions (Davison and Hunter, 2011). This chapter presents the first evidence for an *in vivo* MgCH complex in *Synechocystis*, as well as presenting additional information on the presence of the ChlI subunit in different cellular locations. The importance for the selection of buffers used in this type of assay is also discussed.

7.2.Introduction

Assays in which a target protein is genetically modified to encode an affinity chromatography tag and then isolated on the appropriate resin to analyse any co-purified proteins are an extremely useful tool. Pull-down assays can give insights into proteins and/or co-factors that interact with the target protein.

The three essential subunits of MgCH, the porphyrin binding subunit, H; the AAA^+ ATPase I and the D subunit, have been shown to form a complex *in vitro* using a column binding assay (Davison and Hunter, 2011). Recombinant His_6-tagged ChlD

was immobilised on Ni^{2+} charged chelating Sepharose and following a washing step recombinant non-tagged ChlI was applied to the column. After another washing step, non-tagged ChlH was then applied; any unbound subunits were removed by a final wash and the column was eluted with buffer containing 300 mM imidazole. Western blotting of eluates showed that ChlI, ChlD and ChlH had all bound to the column.

This approach is advantageous in the respect that the best possible conditions are provided for the complex to form. The MgCH subunits were already assumed to form a complex and the use of large quantities of highly pure proteins gives the opportunity to show that they do indeed interact *in vitro*. Although this procedure yielded encouraging results it does not provide any information on how well the proteins interact, nor does it show whether or not such interactions occur inside the cell.

Another approach is to use pull-down assays where a gene encoding an affinity tagged target protein is recombined into a non-essential location in the genome of the organism. Then, the tagged protein can act as *in vivo* bait to trap any interacting partner subunits. An inducible promoter can confer some extra control over the timing of the interaction. The non-essential site within the *Synechocystis* genome chosen for the work in this chapter was the *psbAII* gene; the photosystem II D1 protein is encoded by three genes *psbAI*, *psbAII* and *psbAIII*. These are semi-induced under high light conditions (Hihara *et al*., 2001). The deletion of the *psbAII* gene (*slr1311*) does not result in a mutant phenotype (Dr. Roman Sobotka, personal communication) and so a mutant was created that contains a ChlI protein with an N-terminal 3 X FLAG peptide sequence (DYKDDDDK) and integrated into this D1 site. It should be noted that the native gene encoding ChlI was retained, so there are two copies of the protein present, one tagged and the other native.

Pull-down assays with this mutant were performed under different buffer conditions and the eluate analysed for proteins that co-purified with FLAG-ChlI. This chapter reports the first isolation of the full ChlHID MgCH complex *in vivo* and the importance of the buffers used to achieve the desired results will be discussed.

7.3.Results

The *Synechocystis* FLAG-ChlI mutant was kindly donated by Dr. Roman Sobotka. The mutant was grown on BG-11 agar plates under high light and used to inoculate 4 x 125 ml starter cultures of BG-11 liquid medium and grown as in 2.8.2. under high light (50 µmol photons m^{-2} s^{-1}) for 2 days. 4 x 1.25 L flasks of BG-11 were inoculated with these starter cultures and again grown under high light until an OD740 of ~1 was reached. The cells were pelleted and resuspended in buffer containing 25mM HEPES (pH7.4), 5mM CaCl2, 10mM $MgCl_2$, 20% glycerol and 5 mM ATP. The cells were broken by bead beating and the soluble and insoluble fractions were separated by centrifugation.

It is known that ChlI is expressed in *E. coli* as a soluble protein (Jensen *et al.*, 1998) (Gibson *et al.*, 1995) and so, following cell breakage and centrifugation of the extract, the supernatant fraction of *Synechocystis* was chosen for further analysis. This fraction was loaded onto an anti-FLAG M2 affinity column, which was washed with 10 ml of HEPES buffer and then resuspended in 1 ml of buffer and allowed to settle. Another 1 ml of buffer was added as a final wash and the column was then eluted by incubation in 1 ml thylakoid HEPES buffer containing 100 µg pure FLAG peptide on a roller-mixer for 1 hour at room temperature. The eluted material was separated from the column by passage through a cellulose acetate membrane and the purification was analysed by SDS-PAGE (fig. 1)

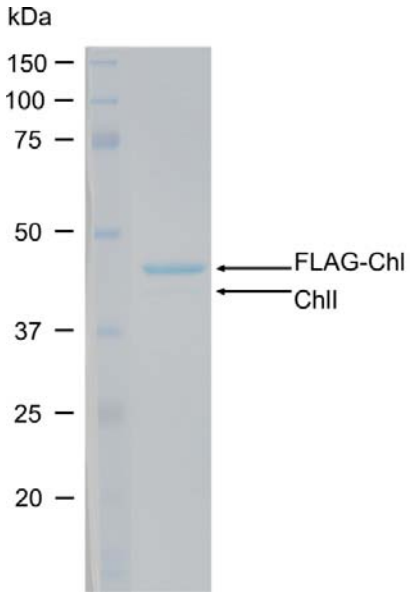

Figure 1 - SDS-PAGE showing the purification of FLAG-ChlI

The soluble fraction of Synechocystis containing the FLAG-ChlI gene was purified on an affinity column using HEPES buffer and the eluate analysed by SDS-PAGE. The upper band is most likely FLAG-ChlI and the lower band the WT ChlI.

Fig. 1 demonstrates that FLAG-tagged ChlI can be purified from the soluble fraction of *Synechocystis*. Two bands of protein are eluted from the purification and because the FLAG-ChlI gene was added to a WT background it is likely that the upper band is FLAG-ChlI and the lower band is WT ChlI that has co-purified alongside the tagged protein.

FLAG peptides have a high content of acidic residues such as aspartic acid, which could influence the binding of SDS, and affect the relative mobility giving the protein a larger apparent MW. What is clear from the SDS-PAGE is that the FLAG-ChlI purification is very efficient in HEPES buffer, increasing the likelihood of any co-purification being the result of a specific interaction, rather than contamination, Thus, the co-purification of FLAG-ChlI and ChlI supports the existence of an I_2 complex, or possibly an even higher order of assembly.

To identify other interesting proteins are present in the purification the starting cell supernatant and the column eluate were blotted (section 2.9.3.) and probed with an antibody raised against ChlH. Fig. 2 shows the western blot probed with anti-ChlH and it is clear that the supernatant contains ChlH, as expected. Other bands are seen lower down the gel lane, indicating that there is either some degradation of the H subunit, detected by the antibody to ChlH, and/or some non-specific cross-reaction with FLAG-ChlI, perhaps because the FLAG-ChlI is expressed at a relatively high level and so there will be much more protein produced in the cell. There is no evidence for ChlH in

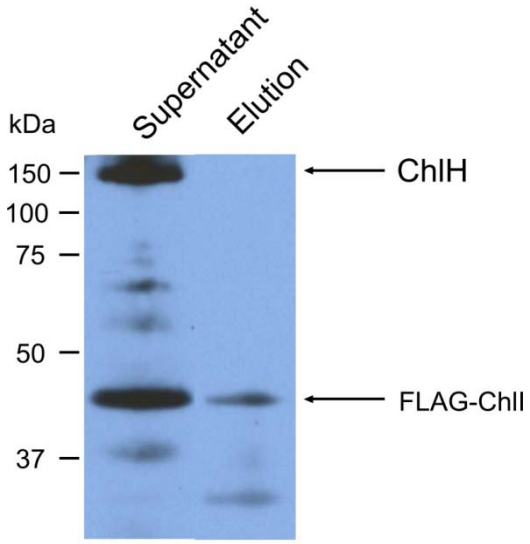

Figure 2 – Western blot of a FLAG-ChlI pull down assay, probed with anti-ChlH antibodies

The cell supernatant and eluate fractions are labelled, as are the positions of the ChlH and FLAG-ChlI signals.

the eluate indicating that FLAG-ChlI and ChlH did not co-elute using this HEPES buffer system. The western blot of FLAG-ChlI purification was stripped and probed with anti-ChlI antibodies. Fig. 3 shows that two bands are present in both the supernatant and the elution. The FLAG-ChlI band that appeared in Fig. 2 can be assumed to be the same as the upper band in Fig. 3 due to the correspondence in size.

The correspondence in migration on SDS-PAGE between the two bands in Figs. 1 and 3 suggests that the two Coomassie-stained bands in Fig. 1 are most likely the WT ChlI and FLAG-ChlI, emphasising the fact that ChlI does form complexes in the cytoplasm of *Synechocystis*.

The absence of other bands from the SDS-PAGE analysis in Fig. 1 suggested that the pull-down is perhaps not performed at the correct pH that HEPES can buffer at. With this in mind the purification was attempted again with another 4 × 1.25 L of culture.a lower pH; 25mM MES pH (6.5), 10mM $CaCl_2$, 20 mM $MgCl_2$, 20% glycerol and 5 mM ATP was used for the resuspension and washing of the column. In this assay the thylakoids were also analysed for the presence of interesting proteins. The thylakoids were resuspended in thylakoid buffer, as far as possible avoiding contamination with cell debris, and solubilised by the addition of β-DDM to a final concentration of 2 % (w/v) at room temperature for an hour. The solubilised material and remaining cell debris were separated by centrifugation. The supernatant and solubilised thylakoids were applied to separate anti-FLAG M2 affinity gel columns and washed and eluted as previously. Fig. 4 shows western blots of both soluble fraction and solubilised thylakoids analysed with different antibodies. It is clear that as seen previously FLAG-ChlI and WT ChlI co-purify from the cell. It is interesting to note that similar levels of FLAG-ChlI are present in both the soluble and membrane

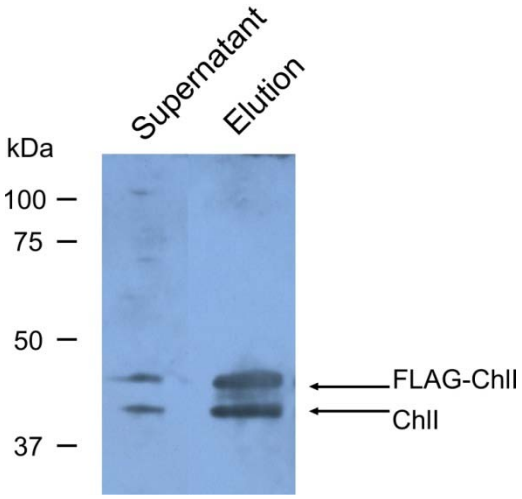

Figure 3 – Western blot of FLAG-ChlI pull down assay and labelling with anti-ChlI

WT and FLAG-ChlI is indicated in both supernatant and elution.

fractions. WT ChlI co-purifies with FLAG-ChlI to a greater extent when the soluble fraction is used, consistent with the idea that WT ChlI is mainly found into the soluble fraction of *Synechocystis*. A large amount of ChlD with a migration of the correct molecular weight has also co-purified with FLAG-ChlI, as seen in the middle two blots, but only using the soluble fraction; no detectable signal was obtained using the solublised membranes. Finally incubation of the blot with antibodies to ChlH also gave a faint but visible band of the correct molecular weight for ChlH, again with the soluble fraction. Less ChlH was seen from the purification when compared to D and I. Because the stripping of the blot in Fig. 3 also removed some protein from the nitrocellulose membrane used in Fig. 4 was incubated with different antibodies and the bands visualised sequentially without using a stripping protocol in between each antibody incubation.

Because the proteins co-purified with FLAG-ChlI were generally found in the soluble fraction SDS-PAGE was used to analyse the protein content of the pull-down from this fraction allowing any interesting bands to be excised and analysed using mass spectrometry. Fig. 5 shows the SDS-PAGE of the second FLAG-ChlI pull-down assay, which used MES buffer rather than the HEPES buffer. This second type of purification is clearly not as efficient at removing contaminants when compared to the previous experiment (Fig. 1) it is clear that a large number of proteins co-purify with FLAG-ChlI. As previously described using MES buffer WT *Synechocystis* soluble and insoluble fractions were also analysed by SDS-PAGE as a negative control for the

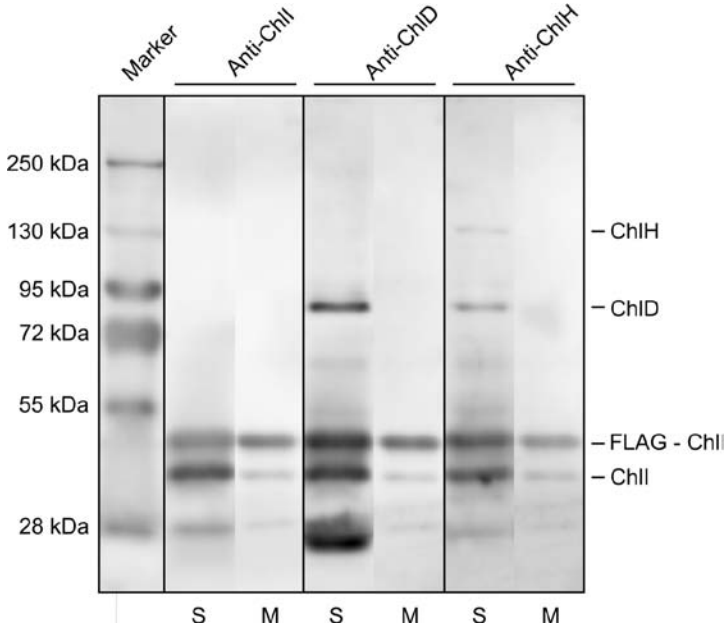

Figure 4 – Western blot of FLAG-ChlI pull-down assay using MES buffer

Blots were analysed with antibodies targeted to ChlI, ChlD and ChlH consecutively. S represents the soluble fraction and M represents the thylakoid membranes. The proteins likely to be identified are highlighted on the right. The purification was performed in 25mM MES pH (6.5), 10mM $CaCl_2$, 20 mM $MgCl_2$, 20% glycerol and 5 mM ATP.

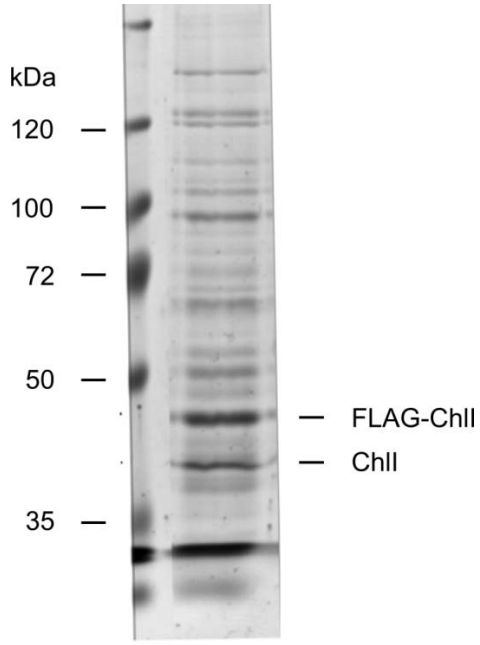

Figure 5 – SDS-PAGE analysis of FLAG-ChlI pull-down assay prepared using MES buffer, and stained with Coomassie blue

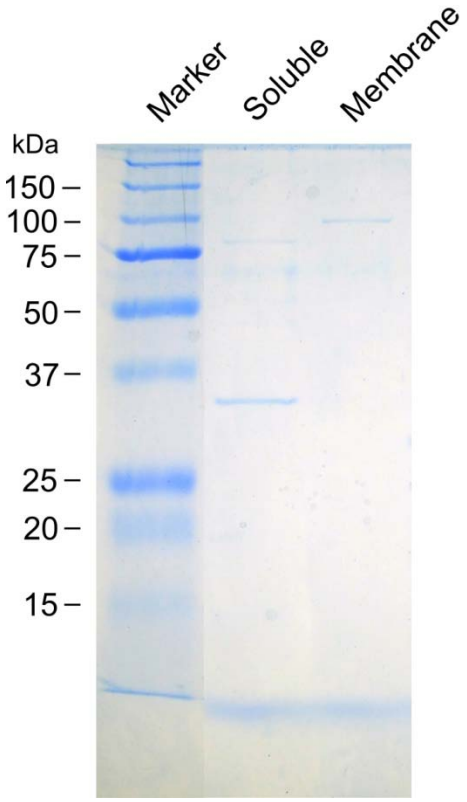

Figure 6 - SDS-PAGE analysis of WT Synechocystis soluble and membrane fractions prepared using MES buffer, and stained with Coomassie blue

FLAG-ChlI pull-down assays (Fig. 6). The control gel shows one major band in the soluble fraction with an estimated molecular weight of ~35 kDa and a fainter band of around 80 kDa. The membrane fraction has one band with an estimated molecular weight of ~100 kDa. The band in the soluble fraction of ~35 kDa was confirmed to be tryptophanyl-tRNA synthetase by mass spectrometry (personal communication, Dr Philip J. Jackson).

Mass spectrometry (MS) was performed on both the soluble and membrane FLAG-ChlI elutions to identify which proteins were present. In both cases proteins were derivatised by S-carbamidomethylation and digested by trypsin in the presence of SDS. The tryptic peptide fragments were prepared for MS analysis by solid phase extraction using a combination of cation exchange and C18 reversed-phase media. The peptides were analysed using nano-LC/MS-MS in conjunction with ultra high resolution time of flight MS. This enabled high mass accuracy in both the MS and tandem MS spectra.

Table 1 displays proteins identified from MS analysis of the pull-downs from both soluble and membrane fractions. These results show that ChlI has been purified from both fractions and the soluble fraction also contains Δ-aminolevulinic acid dehydratase, also known as porphobilinogen synthase, which is involved in the first committed step of tetrapyrrole biosynthesis.

Protein	Score
Soluble fraction	
Magnesium-chelatase subunit chlI; - Synechocystis sp	420
Soluble hydrogenase 42 kD subunit; - Synechocystis sp	281
DNA-directed RNA polymerase subunit alpha; - Synechocystis sp	188
Polyribonucleotide nucleotidyltransferase; - Synechocystis sp	157
Elongation factor Tu; - Synechocystis sp	155
Delta-aminolevulinic acid dehydratase; - Synechocystis sp	148
Hemolysin; - Synechocystis sp	142
DNA-binding protein HU; - Synechocystis sp	114
DNA-directed RNA polymerase subunit beta; - Synechocystis sp	98
Slr1195 protein; - Synechocystis sp	89
Sll0518 protein; - Synechocystis sp	76
Ribonuclease D; - Synechocystis sp	74
Circadian clock protein kinase kaiC; - Synechocystis sp	73
50S ribosomal protein L7/L12; - Synechocystis sp	72
Ribose-phosphate pyrophosphokinase; - Synechocystis sp	71
D-fructose 1,6-bisphosphatase class 2/sedohept - Synechocystis sp	69
SOS function regulatory protein; - Synechocystis sp	68
DNA-directed RNA polymerase subunit beta'; - Synechocystis sp	63
Single-stranded DNA-binding protein; - Synechocystis sp	60
Sll1109 protein; - Synechocystis sp	55
Ribulose bisphosphate carboxylase large chain; - Synechocystis sp	53
Urease subunit beta; - Synechocystis sp	52
Asparaginyl-tRNA synthetase; - Synechocystis sp	50
30S ribosomal protein S2; - Synechocystis sp	48
Naphthoate synthase; - Synechocystis sp	45
Slr1855 protein; - Synechocystis sp	45
Fructose-bisphosphate aldolase class 2; - Synechocystis sp	43
Carbamoyl-phosphate synthase large chain; - Synechocystis sp38	37
Sll0359 protein; - Synechocystis sp	37
Slr1363 protein; - Synechocystis sp	36
Slr0443 protein; - Synechocystis sp	36
Tryptophanyl-tRNA synthetase; - Synechocystis sp	36
30S ribosomal protein S5; - Synechocystis sp	35
Glycogen synthase 1; - Synechocystis sp	34
Acetohydroxy acid synthase; - Synechocystis sp	33
50S ribosomal protein L13; - Synechocystis sp	33
Ssl0242 protein; - Synechocystis sp	32
30S ribosomal protein S18; - Synechocystis sp	32
30S ribosomal protein S1 homolog A; - Synechocystis sp	31
Phycobilisome 32.1 kDa linker polypeptide, phy - Synechocystis sp	31
Slr1926 protein; - Synechocystis sp	30
Acyl-[acyl-carrier-protein]--UDP-N-acetylgluco - Synechocystis sp	29
Acetolactate synthase small subunit; - Synechocystis sp	29
Sll1830 protein; - Synechocystis sp	29
DNA topoisomerase 1; - Synechocystis sp	27
Carbamoyl-phosphate synthase small chain; - Synechocystis sp	26
Phosphoglycerate kinase; - Synechocystis sp	25
Sll1033 protein; - Synechocystis sp	24
Cysteine synthase; - Synechocystis sp	24
General secretion pathway protein G; - Synechocystis sp	24
Sll1130 protein; - Synechocystis sp	23
UPF0296 protein ssl2874; - Synechocystis sp	22
Thylakoid fraction	
Magnesium-chelatase subunit chlI; - Synechocystis sp	155
Sll0359 protein; - Synechocystis sp	49
Na-activated K transporter subunit KtrA; - Synechocystis sp	26

Table 1 - Proteins identified by nano-LC-MS/MS and database searching in FLAG-ChlI pull-down assays

Peptides identified by database searching are shown alongside their score.

7.4.Discussion

Significant conclusions can be drawn regarding MgCH and with regard to the method and success of pull-down assays the work presented here offers scope. It is clear that the H, I and D subunits MgCH do indeed form a complex that can be isolated from *Synechocystis* using FLAG-tagged ChlI as bait. The interaction was tighter than expected; the MgCH interaction is usually thought to be transient but this eluted complex was formed and remained intact through 120 column volumes of wash buffer.

The MgCH from *Synechocystis* is almost completely soluble with only a small fraction of WT ChlI co-purifying from the thylakoid membranes. The high expression of FLAG-ChlI in the membrane fraction is an artefact of the high over-expression, arising from the effects of the high light growth conditions and the use of a light-inducible promoter that drives expression of the FLAG-ChlI construct. It would appear that ChlI forms a complex with other ChlI subunits when purified with ATP, which appears to be stable at both pH 6.5 and 7.4. It would be interesting to repeat the purification using the HEPES buffer (pH 7.4) with the addition of an HPLC gel filtration step to analyse the molecular mass of the ChlI aggregates in the eluate. Subsequent analysis by EM and native gels could reveal the type of association between ChlI *in vivo* in the presence of ATP and confirm whether the sample is heptameric as seen by Reid and Hunter (2003) with a ChlI aggregate reconstituted *in vitro*. It would also be useful to determine if this ChlI•ChlI interaction is ATP dependent as has previously been seen.

The band for co-purified ChlD appears to be less intense than that seen for WT and FLAG-ChlI, and the ChlH band is weaker still. Unfortunately, with the protocol developed here, it would be impossible to visualise the MgCH complex directly by EM. The impurities that remain in the pull-down assay using MES buffer (pH 6.5) would prevent any clear image of anything that would be useful. New strategies will be needed to provide enough HID complexes for structural analysis. Crystallisation appears to be impossible, but single particle reconstruction only requires ~10,000 molecules for a low resolution structure with negatively stained material, so it is still possible that, with the correct affinity-based protocol, a chelatase complex can be isolated and analysed structurally.

The co-purification of Δ-aminolevulinic acid dehydratase with ChlI is interesting and should be investigated further. MgCH is involved in regulation of Chl in plants (reviewed by Masuda and Fujita, 2008) and is presumably involved in cyanobacterial Chl regulation as well. The co-purification of these two proteins may provide a regulation mechanism in *Synechocystis*.

What is clear is that for further work in this area a number of approaches would be best used to further this research. Western blotting has been a resilient and trustworthy tool for studying co-purification of interacting proteins. With the development of more sensitive mass spectrometers and more genomes being sequenced it is obvious that MS will continue to become more important (Hall *et al*., 2012).

The work in this chapter demonstrates that the MgCH enzyme forms a complex *in vivo*. It is also clear that pH of the buffers used is of great importance and much thought should be put into designing experiments with the desired outcome in mind. It would appear that with some preliminary work a highly tailored buffer may be found that would allow the isolation of relatively pure MgCH complex that would be appropriate for more rigorous downstream applications and analysis.

To identify binding partners in the MgCH enzyme all three subunits could be labelled, each with a different tag, to enable serial affinity steps. It would also be important to C-terminally tag proteins if the N-terminal domains are important for complex formation.

CHAPTER 7

General Discussion

Magnesium chelatase is a fascinating enzyme to study in terms of its physical attributes that are known and those that are proposed and discussed. It is the first step of chlorophyll biosynthesis committing porphyrins to become pigments that are the hub of energy capture and transfer. In higher plants MgCH has been shown to play a key role in the regulation of Chl biosynthesis and help manage the amount of Chl and haem made (Masuda and Fujita, 2008) and it makes sense that this would be the same in cyanobacteria and photosynthetic bacteria. The high level of complexity of MgCH is an indication of the importance and how intricate the reaction it catalyses is. The ferrochelatase, catalysing the insertion of Fe^{2+} into Proto on the other branch to that of Mg^{2+} chelation, is a single protein enzyme that often forms a dimer. This reaction is ATP independent whereas Mg^{2+} chelation uses 15 ATP molecules (Reid and Hunter, 2004).

The H subunit which is the tetrapyrrole binding protein of MgCH (Karger *et al*., 2001) has been shown in this thesis (Chapter 3) to be a bi-lobed protein with a small "head" region connected to a large hollow "body" through a linker region. The structures that have been modelled of both BchH and ChlH differ significantly forming an open and caged body, respectively. They also appear to behave differently upon the binding of Proto. At the level of resolution presented in this thesis there appears to be little change upon the binding of Proto, unlike that of BchH (Sirijovski *et al*., 2008).

The H subunit is a large protein (~ 150 kDa) when compared to other tetrapyrrole binding proteins (ferrochelatase (~54 kDa) binds Proto, methyltransferase (~25 kDa) binds MgProto and Gun4 (~ 25 kDa) binds both Proto and MgProto (Davison *et* al., 2005)). It has also been suggested that there is no specific amino acid motif that is required for MgProto binding and that a particular fold is required (Kindgren *et al*., 2011). All these proteins must have this particular fold enabling tetrapyrrole binding and it may be assumed that the fold requires residues that make up perhaps a significant portion of even the smallest Proto binding proteins. H has also been shown

to be involved in other roles including an anti-sigma factor (Osanai *et al*., 2009) and its controversial role in the binding of abscisic acid (Wu *et al.*, 2009; Müller and Hansson, 2009; Tsuzuki *et al*., 2011). H also binds the MgCH enhancer protein Gun4 (Chapter 4, Fig. 10) and is also likely to have a role in regulation of the branch of Chl biosynthesis since it up stimulates the steady-state rate of the next enzyme along in the pathway (Hinchigeri *et al*., 1997; Shepherd *et al*., 2005). All these functions obviously result in a large amount of sequence that makes ChlH a multi-functional protein.

Mutational studies have indicated mutations of the protein that are important for catalytic activity (Olsson *et al*., 2004) and it is also known that the N-terminal 565 residues are essential for MgCH function. Chapter 4 discusses an N-terminal deletion of ChlH that while catalytically dead, is recoverable with Gun4. This indicates that the identified "head" region is not essential for chelation but may be important and may also perform another function. Due to the unchanged K_d for both substrate and product it can be assumed that the head is not involved in tetrapyrrole binding. A *Synechocystis* mutant with this mutation would be interesting to monitor for any changes in phenotype of both MgCH capacity and other perhaps surprising characteristics.

The characterisation of a thermophilic MgCH gives evidence that it functions much the same as that of a mesophilic MgCH. CD analysis on secondary structure of each subunit with respect to temperature also highlights similar properties regarding structural integrity in relation to growth temperature of the organism. From the kinetic analysis of a thermophilic enzyme we know that all subunits are catalytically active. Often, thermophilic proteins have a higher chance of forming crystals and due to the low amount of structural information available for the MgCH this may be a fruitful avenue to explore.

The evidence proving that MgCH does form a complex *in vivo* is compelling to the isolation of a MgCH or ID complex that can be visualised by EM. Another exciting opportunity would be to take advantage of the new techniques that are being developed in MS. Carol Robinson's group are developing MS techniques that are able to provide detailed structural information of complexes (Hall *et al*., 2012). Unlike EM and SAXS that are typically used for complex assessment which are both of low resolution MS would provide detailed information not only of structural characteristic but also of binding dynamics. With isolation of proteins from cells the worry of creating artefacts

is also reduced. A limiting problem facing this currently is the quantity of material needed for these particular MS techniques. The future may allow more sensitive MS what will give a higher chance of obtaining results in this field.

Supplementary Information

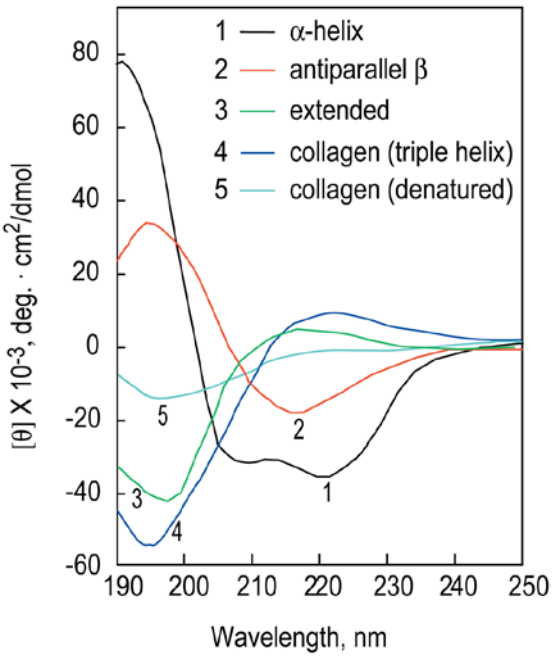

Figure S1 – Typical CD spectra of particular secondary structural features including α-helices and random coil

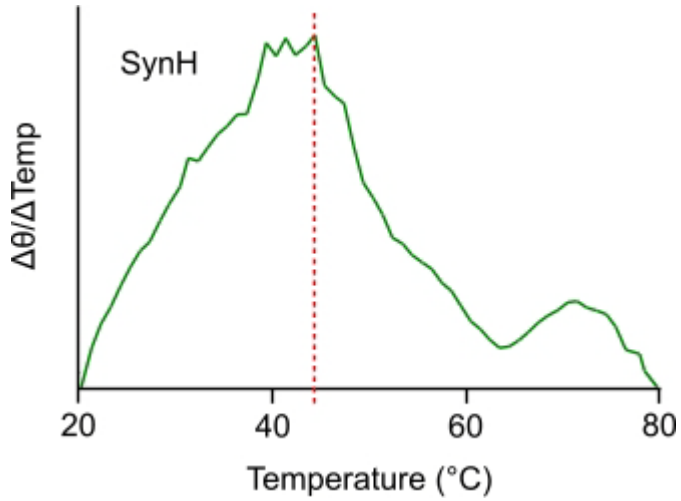

Figure S2 – CD analysis monitoring change in wavelength at 222 nm with increasing temperature to measure thermal stability

The CD signal was measured at 222 nm in chelatase buffer with increasing temperature, with the data plotted as the first derivative. The red dashed line indicates the T_m of the protein.

References

Addlesee, H. A. and Hunter, C. N. (1999). Physical mapping and functional assignment of the geranylgeranyl-bacteriochlorophyll reductase gene, *bchP*, of *Rhodobacter sphaeroides*. *Journal of Bacteriology* **181,** 7248-7255.

Adhikari, N. D.; Froehlich, J. E.; Strand, D. D.; Buck, S. M.; Kramer, D. M.; Larkin, R. M. (2011). GUN4-porphyrin complexes bind the ChlH/GUN5 subunit of Mg-Chelatase and promote chlorophyll biosynthesis in *Arabidopsis*. *Plant Cell* **23,** 1449-1467.

Adl, S. M.; Simpson, A. G.; Farmer, M. A.; Andersen, R. A.; Anderson, O. R.; Barta, J. R.; Bowser, S. S.; Brugerolle, G.; Fensome, R. A.; Fredericq, S.; James, T. Y.; Karpov, S.; Kugrens, P.; Krug, J.; Lane, C. E.; Lewis, L. A.; Lodge, J.; Lynn, D. H.; Mann, D. G.; McCourt, R. M.; Mendoza, L.; Moestrup, O.; Mozley-Standridge, S. E.; Nerad, T. A.; Shearer, C. A.; Smirnov, A. V.; Spiegel, F. W.; Taylor, M. F. (2005). The new higher level classification of eukaryotes with emphasis on the taxonomy of protists. *J Eukaryot. Microbiol* **52,** 399-451.

Al-Karadaghi, S.; Hansson, M.; Nikonov, S.; Jonsson, B.; Hederstedt, L. (1997). Crystal structure of ferrochelatase: the terminal enzyme in heme biosynthesis. *Structure* **5,** 1501-1510.

Al-Karadaghi, S.; Franco, R.; Hansson, M.; Shelnutt, J. A.; Isaya, G.; Ferreira, G. C. (2006). Chelatases: distort to select? *Trends Biochem Sci* **31,** 135-142.

Alawady, A.; Reski, R.; Yaronskaya, E.; Grimm, B. (2005). Cloning and expression of the tobacco CHLM sequence encoding Mg protoporphyrin IX methyltransferase and its interaction with Mg chelatase. *Plant Mol Biol* **57,** 679-691.

Ausubel, F. M., Brent, R., Kingston, R. E., Moore, D. D., Seidman, J. G., Smith, J. A., Struhl, K. (1987) *Current Protocols in Molecular Biology*. Wiley-Interscience, New York.

Avissar, Y. J. and Beale, S. I. (1989). Biosynthesis of Tetrapyrrole Pigment Precursors : Pyridoxal Requirement of the Aminotransferase Step in the Formation of delta-Aminolevulinate from Glutamate in Extracts of *Chlorella vulgaris*. *Plant Physiol* **89,** 852-859.

Axelsson, E.; Lundqvist, J.; Sawicki, A.; Nilsson, S.; Schroder, I.; Al-Karadaghi, S.; Willows, R. D.; Hansson, M. (2006). Recessiveness and dominance in barley mutants deficient in Mg-chelatase subunit D, an AAA protein involved in chlorophyll biosynthesis. *Plant Cell* **18,** 3606-3616.

Barber, J. (1998). Photosystem two. *Biochim. Biophys. Acta* **1365,** 269-277.

Battersby, A. R.; Fookes, C. J. R.; Gustafson-Potter, K. E.; Matcham, G. W. J.; McDonald, E. (1979). Proof by synthesis that unrearranged hydroxymethylbilane is the product from deaminase and the substrate for cosynthetase in the biosynthesis of uro'gen-III. *J. Chem. Soc., Chem. Commun.* , 1155-1158.

Battersby, A. R.; Fookes, C. J. R.; Matcham, G. W. J.; McDonald, E. (1979). Order of assembly of the four pyrrole rings during biosynthesis of the natural porphyrins. *J. Chem. Soc., Chem. Commun.* , 539-541.

Battersby, A. R.; Fookes, C. J. R.; Hart, G.; Matcham, G. W. J.; Pandey, P. (1983). Biosynthesis of porphyrins and related macrocycles. Part 21. The interaction of deaminase and its product (hydroxymethylbilane) and the relationship between deaminase and cosynthetase. *J. Chem Soc Perkin Trans* 3041-3047.

Battersby, A. R. (1994). How nature builds the pigments of life: the conquest of vitamin B12. *Science* **264,** 1551-1557.

Beale, S. I. and Castelfranco, P. A. (1974). The Biosynthesis of delta-Aminolevulinic Acid in Higher Plants: II. Formation of C-delta-Aminolevulinic Acid from Labeled Precursors in Greening Plant Tissues. *Plant Physiol* **53,** 297-303.

Beale, S. I. (1990). Biosynthesis of the Tetrapyrrole Pigment Precursor, delta-Aminolevulinic Acid, from Glutamate. *Plant Physiol* **93,** 1273-1279.

Beale, S. I. (1999). Enzymes of chlorophyll biosynthesis. *Photosynthesis Research* **60,** 43-73.

Bollivar, D. W. and Beale, S. I. (1995). Formation of the isocyclic ring of chlorophyll by isolated *Chlamydomonas reinhardtii* chloroplasts. *Photosynthesis Research* **43,** 113-124.

Bollivar, D. W. and Beale, S. I. (1996). The chlorophyll biosynthetic enzyme Mg-protoporphyrin IX monomethyl ester (oxidative) cyclase: characterization and partial purification from *Chlamydomonas reinhardtii* and *Synechocystis* sp. PCC 6803. *Plant Physiology* **112,** 105-114.

Boynton, T. O.; Gerdes, S.; Craven, S. H.; Neidle, E. L.; Phillips, J. D.; Dailey, H. A. (2011). Discovery of a gene involved in a third bacterial protoporphyrinogen oxidase activity through comparative genomic analysis and functional complementation. *Appl Environ Microbiol* **77,** 4795-4801.

Bricker, T. M. (1992). Oxygen evolution in the absence of the 33-kilodalton manganese-stabilizing protein. *Biochemistry* **31,** 4623-4628.

Brindley, A. A.; Raux, E.; Leech, H. K.; Schubert, H. L.; Warren, M. J. (2003). A story of chelatase evolution: identification and characterization of a small 13-15-kDa "ancestral" cobaltochelatase (CbiXS) in the archaea. *J Biol Chem* **278,** 22388-22395.

Buick, R. (2008). When did oxygenic photosynthesis evolve? *Philosophical Transactions of the Royal Society B: Biological Sciences* **363,** 2731-2743.

Chen, W.; Russell, C. S.; Murooka, Y.; Cosloy, S. D. (1994). 5-Aminolevulinic acid synthesis in *Escherichia coli* requires expression of *hemA*. *J Bacteriol.* **176,** 2743-2746.

Chen, W.; Wright, L.; Li, S.; Cosloy, S. D.; Russell, C. S.; Lee, S. (1996). Expression of glutamyl-tRNA reductase in *Escherichia coli*. *Biochimica et Biophysica Acta* **1309,** 109-121.

Chereskin, B. M.; Castelfranco, P. A.; Dallas, J. L.; Straub, K. M. (1983). Mg-2,4-divinyl pheoporphyrin a5: the product of a reaction catalyzed *in vitro* by developing chloroplasts. *Archives of Biochemistry and Biophysics* **226,** 10-18.

Chew, A. G. and Bryant, D. A. (2007). Chlorophyll biosynthesis in bacteria: the origins of structural and functional diversity. *Annu. Rev. Microbiol* **61,** 113-129.

Chow, K. S.; Singh, D. P.; Roper, J. M.; Smith, A. G. (1997). A single precursor protein for ferrochelatase-I from *Arabidopsis* is imported in vitro into both chloroplasts and mitochondria. *J Biol Chem* **272,** 27565-27571.

Chow, K. S.; Singh, D. P.; Walker, A. R.; Smith, A. G. (1998). Two different genes encode ferrochelatase in *Arabidopsis*: mapping, expression and subcellular targeting of the precursor proteins. *Plant J* **15,** 531-541.

Coomber, S. A.; Chaudhri, M.; Connor, A.; Britton, G.; Hunter, C. N. (1990). Localized transposon Tn5 mutagenesis of the photosynthetic gene cluster of *Rhodobacter sphaeroides*. *Mol Microbiol* **4,** 977-989.

Dailey, H. A. (1982). Purification and characterization of membrane-bound ferrochelatase from *Rhodopseudomonas sphaeroides*. *J Biol Chem* **257,** 14714-14718.

Dailey, T. A.; Boynton, T. O.; Albetel, A. N.; Gerdes, S.; Johnson, M. K.; Dailey, H. A. (2010). Discovery and Characterization of HemQ: an essential heme biosynthetic pathway component. *J Biol Chem* **285,** 25978-25986.

Davison, P. A.; Schubert, H. L.; Reid, J. D.; Iorg, C. D.; Heroux, A.; Hill, C. P.; Hunter, C. N. (2005). Structural and biochemical characterization of Gun4 suggests a mechanism for its role in chlorophyll biosynthesis. *Biochemistry* **44,** 7603-7612.

Davison, P. A. and Hunter, C. N. (2011). Abolition of magnesium chelatase activity by the gun5 mutation and reversal by Gun4. *FEBS Lett* **585,** 183-186.

Dawson, R. M. C. (1969) *Data for biochemical research*. Oxford University Press, New York .

de Armas-Ricard, M.; Levican, G.; Katz, A.; Moser, J.; Jahn, D.; Orellana, O. (2011). Cellular levels of heme affect the activity of dimeric glutamyl-tRNA reductase. *Biochem Biophys Res Commun.* **405,** 134-139.

Drummond, A. J.; Ashton, B.; Buxton, S.; Markowitz, S.; Cheung, M.; Moir, R.; Stones-Havas, S.; Sturrock, S.; Thierer, T.; Wilson, A. (2010). Geneious v5.3. *www. genious. com*.

Duke, S. O.; Lydon, J.; Becerril, J. M.; Sherman, T. D.; Lehnen, L. P.; Matsumoto, H. (1991). Protoporphyrinogen oxidase-inhibiting herbicides. *Science* **39,** 465-473.

Elliott, T.; Avissar, Y. J.; Rhie, G. E.; Beale, S. I. (1990). Cloning and sequence of the *Salmonella typhimurium* hemL gene and identification of the missing enzyme in hemL mutants as glutamate-1-semialdehyde aminotransferase. *J Bacteriol* **172,** 7071-7084.

Ellsworth, R. K. and Aronoff, S. (1969). Investigations of the biogenesis of chlorophyll *a*. IV. Isolation and partial characterization of some biosynthetic intermediates between Mg-protoporphine IX monomethyl ester and Mg-vinylpheoporphine a_5, obtained from *Chlorella* mutants. *Archives of Biochemistry and Biophysics* **130,** 374-383.

Erskine, P. T.; Norton, E.; Cooper, J. B.; Lambert, R.; Coker, A.; Lewis, G.; Spencer, P.; Sarwar, M.; Wood, S. P.; Warren, M. J.; Schoolingin-Jordan, P. M. (1999). X-ray structure of 5-aminolevulinic acid dehydratase from *Escherichia coli* complexed with the inhibitor levulinic acid at 2.0 angstrom resolution. *Biochemistry* **38,** 4266-4276.

Erskine, P. T.; Newbold, R.; Roper, J.; Coker, A.; Warren, M. J.; Shoolingin-Jordan, P. M.; Wood, S. P.; Cooper, J. B. (1999). The Schiff base complex of yeast 5-aminolaevulinic acid dehydratase with laevulinic acid. *Protein Sci* **8,** 1250-1256.

Falk, J. E. (1964) Porphyrins and metalloporphyrins; their general, physical and coordination chemistry, and laboratory methods . Elsevier Pub. Co., Amsterdam, New York .

Ferreira, K. N.; Iverson, T. M.; Maghlaoui, K.; Barber, J.; Iwata, S. (2004). Architecture of the photosynthetic oxygen-evolving center. *Science* **303,** 1831-1838.

Fodje, M. N.; Hansson, A.; Hansson, M.; Olsen, J. G.; Gough, S.; Willows, R. D.; Al Karadaghi, S. (2001). Interplay between an AAA module and an integrin I domain may regulate the function of magnesium chelatase. *J Mol Biol* **311,** 111-122.

Freer, A.; Prince, S.; Sauer, K.; Papiz, M.; Hawthornthwaite-Lawless, A.; McDermott, G.; Cogdell, R.; Isaacs, N. W. (1996). Pigment-pigment interactions and energy transfer in the antenna complex of the photosynthetic bacterium *Rhodopseudomonas acidophila*. *Structure* **4,** 449-462.

Fujita, Y. and Bauer, C. E. (2000). Reconstitution of light-independent protochlorophyllide reductase from purified Bch1 and BchN-BchB subunits - *In vitro* confirmation of nitrogenase-like features of a bacteriochlorophyll biosynthesis enzyme. *J Biol Chem* **275,** 23583-23588.

Gaubier, P.; Wu, H. J.; Laudie, M.; Delseny, M.; Grellet, F. (1995). A chlorophyll synthetase gene from *Arabidopsis thaliana*. *Mol Gen. Genet.* **249,** 58-64.

Gibson, K. D.; Laver, W. G.; Neuberger, A. (1958). Initial stages in the biosynthesis of porphyrins. 2. The formation of d-aminolaevulic acid from glycine and succinyl-coenzyme A by particles from chicken erythrocytes. *Biochem. J.* **70,** 70-81.

Gibson, L. C.; Marrison, J. L.; Leech, R. M.; Jensen, P. E.; Bassham, D. C.; Gibson, M.; Hunter, C. N. (1996). A putative Mg chelatase subunit from Arabidopsis thaliana cv C24. Sequence and transcript analysis of the gene, import of the protein into chloroplasts, and in situ localization of the transcript and protein. *Plant Physiol* **111,** 61-71.

Gibson, L. C.; Jensen, P. E.; Hunter, C. N. (1999). Magnesium chelatase from *Rhodobacter sphaeroides*: initial characterization of the enzyme using purified subunits and evidence for a BchI-BchD complex. *Biochem J* **337 (Pt 2),** 243-251.

Gibson, L. C. D.; Willows, R. D.; Kannangara, C. G.; von Wettstein, D.; Hunter, C. N. (1995). Magnesium-protoporphyrin chelatase of *Rhodobacter sphaeroides*: reconstitiution of activity by combining the products of the *bchH*, *-I* and *-D* genes expressed in *Escherichia coli*. *Proc Natl Acad Sci U S A* **92,** 1941-1944.

Gill, S. C. and von Hippel, P. H. (1989). Calculation of protein extinction coefficients from amino acid sequence data. *Anal Biochem* **182,** 319-326.

Gomez Maqueo, C. A.; Frigaard, N. U.; Bryant, D. A. (2009). Mutational analysis of three bchH paralogs in (bacterio-)chlorophyll biosynthesis in *Chlorobaculum tepidum*. *Photosynth Res* **101,** 21-34.

Guo, R.; Luo, M.; Weinstein, J. D. (1998). Magnesium-Chelatase from Developing Pea Leaves. *Plant Physiology* **116,** 605-615.

Hall, Z.; Politis, A.; Robinson, C. V. (2012). Structural modeling of heteromeric protein complexes from disassembly pathways and ion mobility-mass spectrometry. *Structure* **20,** 1596-1609.

Hall, Z.; Politis, A.; Robinson, C. V. (2012). Structural Modeling of Heteromeric Protein Complexes from Disassembly Pathways and Ion Mobility-Mass Spectrometry. *Structure* **20,** 1596-1609.

Hanahan, D. and In: Glover, D. M. ed. (1985) *DNA cloning: A practical approach* . IRL Press, McLean, Virginia , p. 109 .

Hansson, A.; Kannangara, C. G.; von, W. D.; Hansson, M. (1999). Molecular basis for semidominance of missense mutations in the XANTHA-H (42-kDa) subunit of magnesium chelatase. *Proc Natl Acad Sci U S A* **96,** 1744-1749.

Hansson, A.; Willows, R. D.; Roberts, T. H.; Hansson, M. (2002). Three semidominant barley mutants with single amino acid substitutions in the smallest magnesium chelatase subunit form defective AAA+ hexamers. *Proc Natl Acad Sci U S A* **99,** 13944-13949.

Harmer, S. L.; Hogenesch, J. B.; Straume, M.; Chang, H. S.; Han, B.; Zhu, T.; Wang, X.; Kreps, J. A.; Kay, S. A. (2000). Orchestrated transcription of key pathways in *Arabidopsis* by the circadian clock. *Science* **290,** 2110-2113.

Hart, G. J.; Miller, A. D.; Battersby, A. R. (1988). Evidence that the pyrromethane cofactor of hydroxymethylbilane synthase (porphobilinogen deaminase) is bound through the sulphur atom of a cysteine residue. *Biochem J* **252,** 909-912.

Hennig, M.; Grimm, B.; Contestabile, R.; John, R. A.; Jansonius, J. N. (1997). Crystal structure of glutamate-1-semialdehyde aminomutase: an alpha2- dimeric vitamin B6-dependent enzyme with asymmetry in structure and active site reactivity. *Proc Natl Acad Sci USA* **94,** 4866-4871.

Heyes, D. J. and Hunter, C. N. (2005). Making light work of enzyme catalysis: protochlorophyllide oxidoreductase. *Trends In Biochemical Sciences* **30,** 642-649.

Heyes, D. J.; Menon, B. R. K.; Sakuma, M.; Scrutton, N. S. (2008). Conformational Events during Ternary Enzyme-Substrate Complex Formation Are Rate Limiting in the Catalytic Cycle of the Light-Driven Enzyme Protochlorophyllide Oxidoreductase. *Biochemistry* **47,** 10991-10998.

Higuchi, M. and Bogorad, L. (1975). The purification and properties of uroporphyrinogen I synthases and uroporphyrinogen III cosynthase. Interactions between the enzymes. *Ann. N. Y. Acad Sci* **244,** 401-418.

Hihara, Y.; Kamei, A.; Kanehisa, M.; Kaplan, A.; Ikeuchi, M. (2001). DNA microarray analysis of cyanobacterial gene expression during acclimation to high light. *Plant Cell* **13,** 793-806.

Hinchigeri, S. B.; Hundle, B.; Richards, W. R. (1997). Demonstration that the BchH protein of *Rhodobacter capsulatus* activates S-adenosyl-L-methionine:magnesium protoporphyrin IX methyltransferase. *FEBS Lett* **407,** 337-342.

Hoggins, M.; Dailey, H. A.; Hunter, C. N.; Reid, J. D. (2007). Direct Measurement of Metal Ion Chelation in the Active Site of Human FerrochelataseGÇá. *Biochemistry* **46,** 8121-8127.

Hollingshead, S.; Kopecna, J.; Jackson, P. J.; Canniffe, D. P.; Davison, P. A.; Dickman, M. J.; Sobotka, R.; Hunter, C. N. (2012). Conserved Chloroplast Open-reading Frame ycf54 Is Required for Activity of the Magnesium Protoporphyrin Monomethylester Oxidative Cyclase in *Synechocystis* PCC 6803. *J Biol Chem* **287,** 27823-27833.

Hoober, J. K.; Kahn, A.; Ash, D. E.; Gough, S.; Kannangara, C. G. (1988). Biosynthesis of delta-aminolevulinate in greening barley leaves. IX. Structure of the substrate, mode of gabaculine inhibition, and the catalytic mechanism of glutamate 1-semialdehyde aminotransferase. *Carlsberg. Res Commun.* **53,** 11-25.

Hu, G.; Yalpani, N.; Briggs, S. P.; Johal, G. S. (1998). A porphyrin pathway impairment is responsible for the phenotype of a dominant disease lesion mimic mutant of maize. *Plant Cell* **10,** 1095-1105.

Huang, D. D.; Wang, W. Y.; Gough, S. P.; Kannangara, C. G. (1984). delta-Aminolevulinic acid-synthesizing enzymes need an RNA moiety for activity. *Science* **225,** 1482-1484.

Huang, D. D. and Wang, W. Y. (1986). Chlorophyll biosynthesis in *Chlamydomonas* starts with the formation of glutamyl-tRNA. *J Biol Chem* **261,** 13451-13455.

Hudson, A.; Carpenter, R.; Doyle, S.; Coen, E. S. (1993). Olive: a key gene required for chlorophyll biosynthesis in *Antirrhinum majus*. *EMBO J* **12,** 3711-3719.

Hunter, G. A.; Al-Karadaghi, S.; Ferreira, G. C. (2011). Ferrochelatase: The convergence of the porphyrin biosynthesis and iron transport pathways. *J Porphyr. Phthalocyanines.* **15,** 350-356.

Ishikawa, A.; Okamoto, H.; Iwasaki, Y.; Asahi, T. (2001). A deficiency of coproporphyrinogen III oxidase causes lesion formation in *Arabidopsis*. *Plant J* **27,** 89-99.

Jacobs, N. J. and Jacobs, J. M. (1981). Protoporphyrinogen oxidation in *Rhodopseudomonas sphaeroides*, a step in heme and bacteriochlorophyll synthesis. *Archives of Biochemistry and Biophysics* **211,** 305-311.

Jaffe, E. K. (2004). The porphobilinogen synthase catalyzed reaction mechanism. *Bioorganic Chemistry* **32,** 316-325.

Jahn, D. (1992). Complex-formation between glutamyl-tRNA synthetase and glutamyl-transfer RNA reductase during the tRNA dependent synthesis of 5-aminolevulinic acid in *Chlamydomonas reinhardtii*. *FEBS Letters* **314,** 77-80.

Jensen, P. E.; Gibson, L. C.; Henningsen, K. W.; Hunter, C. N. (1996). Expression of the chlI, chlD, and chlH genes from the Cyanobacterium *Synechocystis* PCC6803 in Escherichia coli and demonstration that the three cognate proteins are required for magnesium-protoporphyrin chelatase activity. *J Biol Chem* **271,** 16662-16667.

Jensen, P. E.; Willows, R. D.; Petersen, B. L.; Vothknecht, U. C.; Stummann, B. M.; Kannangara, C. G.; von, W. D.; Henningsen, K. W. (1996). Structural genes for Mg-chelatase subunits in barley: Xantha-f, -g and -h. *Mol Gen. Genet.* **250,** 383-394.

Jensen, P. E.; Gibson, L. C.; Hunter, C. N. (1998). Determinants of catalytic activity with the use of purified I, D and H subunits of the magnesium protoporphyrin IX chelatase from *Synechocystis* PCC6803. *Biochem J* **334 (Pt 2),** 335-344.

Jensen, P. E.; Gibson, L. C.; Hunter, C. N. (1999). ATPase activity associated with the magnesium-protoporphyrin IX chelatase enzyme of *Synechocystis* PCC6803: evidence

for ATP hydrolysis during Mg2+ insertion, and the MgATP-dependent interaction of the ChlI and ChlD subunits. *Biochem J* **339 (Pt 1),** 127-134.

Jensen, P. E.; Gibson, L. C.; Shephard, F.; Smith, V.; Hunter, C. N. (1999). Introduction of a new branchpoint in tetrapyrrole biosynthesis in *Escherichia coli* by co-expression of genes encoding the chlorophyll-specific enzymes magnesium chelatase and magnesium protoporphyrin methyltransferase. *FEBS Lett* **455,** 349-354.

Jensen, P. E.; Reid, J. D.; Hunter, C. N. (2000). Modification of cysteine residues in the ChlI and ChlH subunits of magnesium chelatase results in enzyme inactivation. *Biochem J* **352 Pt 2,** 435-441.

Johnson, C. H. and Golden, S. S. (1999). Circadian programs in cyanobacteria: adaptiveness and mechanism. *Annual Review of Microbiology* **53,** 389-409.

Jordan, P. M. (1991). The biosynthesis of 5-aminoleavelunic acid and its transformation into uroporphyrinogen III. *Biosynthesis of Tetrapyrroles* **19,** 1-86.

Kaneko, T.; Matsubayashi, T.; Sugita, M.; Sugiura, M. (1996). Physical and gene maps of the unicellular cyanobacterium *Synechococcus* sp strain PCC6301 genome. *Plant Molecular Biology* **31,** 193-201.

Kaneko, T. and Tabata, S. (1997). Complete genome structure of the unicellular cyanobacterium *Synechocystis* sp. PCC6803. *Plant And Cell Physiology* **38,** 1171-1176.

Kannangara, C. G.; Gough, S. P.; Bruyant, P.; Hoober, J. K.; Kahn, A.; von Wettstein, D. (1988). $tRNA^{glu}$ as a cofactor in d-aminolevulinate biosynthesis: steps that regulate chlorophyll synthesis. *Trends Biochem Sci* **13,** 139-143.

Kannangara, C. G.; Vothknecht, U. C.; Hansson, M.; von, W. D. (1997). Magnesium chelatase: association with ribosomes and mutant complementation studies identify barley subunit Xantha-G as a functional counterpart of *Rhodobacter* subunit BchD. *Mol Gen. Genet.* **254,** 85-92.

Karger, G. A.; Reid, J. D.; Hunter, C. N. (2001). Characterization of the binding of deuteroporphyrin IX to the magnesium chelatase H subunit and spectroscopic properties of the complex. *Biochemistry* **40,** 9291-9299.

Karlberg, T.; Lecerof, D.; Gora, M.; Silvegren, G.; Labbe-Bois, R.; Hansson, M.; Al Karadaghi, S. (2002). Metal Binding to *Saccharomyces cerevisiae* Ferrochelatase. *Biochemistry* **41,** 13499-13506.

Kato, K.; Tanaka, R.; Sano, S.; Tanaka, A.; Hosaka, H. (2010). Identification of a gene essential for protoporphyrinogen IX oxidase activity in the cyanobacterium *Synechocystis* sp. PCC6803. *Proc Natl Acad Sci U S A* **107,** 16649-16654.

Kikuchi, G.; Kumar, A. M.; Talmage, P.; Shemin, D. (1958) The enzymatic synthesis of d-aminolevulinic acid. *J Biol Chem* **233**, 1214-1219.

Kindgren, P.; Eriksson, M. J.; Benedict, C.; Mohapatra, A.; Gough, S. P.; Hansson, M.; Kieselbach, T.; Strand, A. (2011). A novel proteomic approach reveals a role for Mg-protoporphyrin IX in response to oxidative stress. *Physiol Plant* **141,** 310-320.

Knight, S.; Andersson, I.; Branden, C. I. (1990). Crystallographic analysis of ribulose 1,5-bisphosphate carboxylase from spinach at 2.4 A resolution. Subunit interactions and active site. *J Mol Biol* **215,** 113-160.

Knispel, R. W.; Kofler, C.; Boicu, M.; Baumeister, W.; Nickell, S. (2012). Blotting protein complexes from native gels to electron microscopy grids. *Nat Methods* **9,** 182-184.

Koch, M.; Breithaupt, C.; Kiefersauer, R.; Freigang, J.; Huber, R.; Messerschmidt, A. (2004). Crystal structure of protoporphyrinogen IX oxidase: a key enzyme in haem and chlorophyll biosynthesis. *EMBO Journal* **23,** 1720-1728.

Koncz, C.; Mayerhofer, R.; Koncz-Kalman, Z.; Nawrath, C.; Reiss, B.; Redei, G. P.; Schell, J. (1990). Isolation of a gene encoding a novel chloroplast protein by T-DNA tagging in *Arabidopsis thaliana*. *EMBO J* **9,** 1337-1346.

Kondo, T.; Mori, T.; Lebedeva, N. V.; Aoki, S.; Ishiura, M.; Golden, S. S. (1997). Circadian rhythms in rapidly dividing cyanobacteria. *Science* **275,** 224-227.

Kruse, E.; Mock, H. P.; Grimm, B. (1995). Coproporphyrinogen III oxidase from barley and tobacco – sequence analysis and initial expression studies. *Planta* **196,** 796-803.

Kruse, E.; Mock, H. P.; Grimm, B. (1995). Reduction of coproporphyrinogen oxidase level by antisense RNA synthesis leads to deregulated gene expression of plastid proteins and affects the oxidative defense system. *EMBO J* **14,** 3712-3720.

Kucho, K.; Okamoto, K.; Tsuchiya, Y.; Nomura, S.; Nango, M.; Kanehisa, M.; Ishiura, M. (2005). Global analysis of circadian expression in the cyanobacterium *Synechocystis* sp. strain PCC 6803. *J Bacteriol* **187,** 2190-2199.

Laemmli, U. K. (1970). Cleavage of structural proteins during the assembly of the head of bacteriophage T4. *Nature* **227,** 680-685.

Larkin, R. M.; Alonso, J. M.; Ecker, J. R.; Chory, J. (2003). GUN4, a regulator of chlorophyll synthesis and intracellular signaling. *Science* **299,** 902-906.

Lecerof, D.; Fodje, M.; Hansson, A.; Hansson, M.; Al-Karadaghi, S. (2000). Structural and mechanistic basis of porphyrin metallation by ferrochelatase. *J Mol Biol* **297,** 221-232.

Leeper, F. J. (1987). Intermediate Steps in the Biosynthesis of Chlorophylls. In: *Chlorophyll metabolism* , pp. 407-431.

Lermontova, I.; Kruse, E.; Mock, H. P.; Grimm, B. (1997). Cloning and characterization of a plastidal and a mitochondrial isoform of tobacco protoporphyrinogen IX oxidase. *Proc. Natl. Acad. Sci. U. S. A* **94,** 8895-8900.

Li, J. M.; Brathwaite, O.; Cosloy, S. D.; Russell, C. S. (1989). 5-Aminolevulinic acid synthesis in *Escherichia coli*. *J Bacteriol* **171,** 2547-2552.

Liu, L. N.; Chen, X. L.; Zhang, Y. Z.; Zhou, B. C. (2005). Characterization, structure and function of linker polypeptides in phycobilisomes of cyanobacteria and red algae: an overview. *Biochim Biophys Acta* **1708,** 133-142.

Louie, G. V.; Brownlie, P. D.; Lambert, R.; Cooper, J. B.; Blundell, T. L.; Wood, S. P.; Warren, M. J.; Woodcock, S. C.; Jordan, P. M. (1992). Structure of porphobilinogen deaminase reveals a flexible multidomain polymerase with a single catalytic site. *Nature* **359,** 33-39.

Louie, G. V.; Brownlie, P. D.; Lambert, R.; Cooper, J. B.; Blundell, T. L.; Wood, S. P.; Malashkevich, V. N.; Hadener, A.; Warren, M. J.; ShoolinginJordan, P. M. (1996). The three-dimensional structure of *Escherichia coli* porphobilinogen deaminase at 1.76 Å resolution. *Proteins-Structure Function and Genetics* **25,** 48-78.

Lundqvist, J.; Elmlund, H.; Wulff, R. P.; Berglund, L.; Elmlund, D.; Emanuelsson, C.; Hebert, H.; Willows, R. D.; Hansson, M.; Lindahl, M.; Al-Karadaghi, S. (2010). ATP-induced conformational dynamics in the AAA+ motor unit of magnesium chelatase. *Structure* **18,** 354-365.

Luo, J. and Lim, C. K. (1993). Order of uroporphyrinogen III decarboxylation on incubation of porphobilinogen and uroporphyrinogen III with erythrocyte uroporphyrinogen decarboxylase. *Biochem J* **289 (Pt 2),** 529-532.

Mac, M.; Tang, X. S.; Diner, B. A.; McCracken, J.; Babcock, G. T. (1996). Identification of histidine as an axial ligand to P700+. *Biochemistry* **35,** 13288-13293.

Martins, B. M.; Grimm, B.; Mock, H. P.; Huber, R.; Messerschmidt, A. (2001). Crystal structure and substrate binding modeling of the uroporphyrinogen-III decarboxylase from *Nicotiana tabacum*. Implications for the catalytic mechanism. *J Biol Chem* **276,** 44108-44116.

Masuda, T.; Suzuki, T.; Shimada, H.; Ohta, H.; Takamiya, K. (2003). Subcellular localization of two types of ferrochelatase in cucumber. *Planta* **217,** 602-609.

Masuda, T. (2008). Recent overview of the Mg branch of the tetrapyrrole biosynthesis leading to chlorophylls. *Photosynthesis Research* **96,** 121-143.

Masuda, T. and Fujita, Y. (2008). Regulation and evolution of chlorophyll metabolism. *Photochem Photobiol. Sci* **7,** 1131-1149.

Mathews, M. A.; Schubert, H. L.; Whitby, F. G.; Alexander, K. J.; Schadick, K.; Bergonia, H. A.; Phillips, J. D.; Hill, C. P. (2001). Crystal structure of human uroporphyrinogen III synthase. *EMBO J* **20,** 5832-5839.

Matringe, M.; Camadro, J. M.; Labbe, P.; Scalla, R. (1989). Protoporphyrinogen oxidase as a molecular target for diphenyl ether herbicides. *Biochem J* **260,** 231-235.

Matringe, M. and Scalla, R. (1991). Effects of acifluorfen-methyl on cucumber cotyledons: Porphyrin accumulation. *Pestic Biochem Physiol* **32,** 164-172.

Matringe, M.; Camadro, J. M.; Joyard, J.; Douce, R. (1994). Localization of ferrochelatase activity within mature pea chloroplasts. *J Biol Chem* **269,** 15010-15015.

Mayer, S. M.; Rieble, S.; Beale, S. I. (1994). Metal requirements of the enzymes catalyzing conversion of glutamate to delta-aminolevulinic acid in extracts of *Chlorella vulgaris* and *Synechocystis* sp. PCC 6803. *Archives of Biochemistry and Biophysics* **312,** 203-209.

McLean, S. and Hunter, C. N. (2009). An enzyme-coupled continuous spectrophotometric assay for magnesium protoporphyrin IX methyltransferases. *Anal Biochem* **394,** 223-228.

Medlock, A.; Swartz, L.; Dailey, T. A.; Dailey, H. A.; Lanzilotta, W. N. (2007). Substrate interactions with human ferrochelatase. *Proceedings of the National Academy of Sciences* **104,** 1789-1793.

Mehta, P. K. and Christen, P. (1994). Homology of 1-aminocyclopropane-1-carboxylate synthase, 8-amino-7-oxononanoate synthase, 2-amino-6-caprolactam racemase, 2,2-dialkylglycine decarboxylase, glutamate-1-semialdehyde 2,1-

aminomutase and isopenicillin-N-epimerase with aminotransferases. *Biochem Biophys Res Commun.* **198,** 138-143.

Meisenberger, O.; Pilz, I.; Bowien, B.; Pal, G. P.; Saenger, W. (1984). Small angle x-ray study on the structure of active and inactive ribulose bisphosphate carboxylase from *Alcaligenes eutrophus*. Evidence for a configurational change. *J Biol Chem* **259,** 4463-4465.

Metz, J. G.; Nixon, P. J.; Rogner, M.; Brudvig, G. W.; Diner, B. A. (1989). Directed alteration of the D1 polypeptide of photosystem II: evidence that tyrosine-161 is the redox component, Z, connecting the oxygen-evolving complex to the primary electron donor, P680. *Biochemistry* **28,** 6960-6969.

Miller, E. M. and Nickoloff, J. A. (1995). *Escherichia coli* electrotransformation. *Methods Mol Biol* **47,** 105-113.

Minamizaki, K.; Mizoguchi, T.; Goto, T.; Tamiaki, H.; Fujita, Y. (2007). Identification of two homologous genes, chlAI and chlAII, that are differentially involved in isocyclic ring formation of chlorophyll a in the cyanobacterium *Synechocystis* sp. PCC 6803. *Journal of Biological Chemistry* M708954200.

Mochizuki, N.; Brusslan, J. A.; Larkin, R.; Nagatani, A.; Chory, J. (2001). *Arabidopsis* genomes uncoupled 5 (GUN5) mutant reveals the involvement of Mg-chelatase H subunit in plastid-to-nucleus signal transduction. *Proc Natl Acad Sci U S A* **98,** 2053-2058.

Mock, H. P. and Grimm, B. (1997). Reduction of Uroporphyrinogen Decarboxylase by Antisense RNA Expression Affects Activities of Other Enzymes Involved in Tetrapyrrole Biosynthesis and Leads to Light-Dependent Necrosis. *Plant Physiol* **113,** 1101-1112.

Mock, H. P.; Keetman, U.; Kruse, E.; Rank, B.; Grimm, B. (1998). Defense responses to tetrapyrrole-induced oxidative stress in transgenic plants with reduced uroporphyrinogen decarboxylase or coproporphyrinogen oxidase activity. *Plant Phisiology* **113,** 1112.

Moser, J.; Schubert, W. D.; Beier, V.; Bringemeier, I.; Jahn, D.; Heinz, D. W. (2001). V-shaped structure of glutamyl-tRNA reductase, the first enzyme of tRNA-dependent tetrapyrrole biosynthesis. *EMBO J* **20,** 6583-6590.

Muller, A. H. and Hansson, M. (2009). The barley magnesium chelatase 150-kd subunit is not an abscisic acid receptor. *Plant Physiol* **150,** 157-166.

Murphy, M. J. and Siegel, L. M. (1973). Siroheme and sirohydrochlorin. The basis for a new type of porphyrin-related prosthetic group common to both assimilatory and dissimilatory sulfite reductases. *J Biol Chem* **248,** 6911-6919.

Nakamura, Y.; Kaneko, T.; Sato, S.; Ikeuchi, M.; Katoh, H.; Sasamoto, S.; Watanabe, A.; Iriguchi, M.; Kawashima, K.; Kimura, T.; Kishida, Y.; Kiyokawa, C.; Kohara, M.; Matsumoto, M.; Matsuno, A.; Nakazaki, N.; Shimpo, S.; Sugimoto, M.; Takeuchi, C.; Yamada, M.; Tabata, S. (2002). Complete genome structure of the thermophilic cyanobacterium *Thermosynechococcus elongatus* BP-1. *DNA Res* **9,** 123-130.

Naylor, G. W.; Addlesee, H. A.; Gibson, L. C. D.; Hunter, C. N. (1999). The photosynthesis gene cluster of *Rhodobacter sphaeroides*. *Photosynthesis Research* **62,** 121-139.

Neuwald, A. F.; Aravind, L.; Spouge, J. L.; Koonin, E. V. (1999). AAA+: A class of chaperone-like ATPases associated with the assembly, operation, and disassembly of protein complexes. *Genome Res* **9,** 27-43.

Nomata, J.; Mizoguchi, T.; Tamiaki, H.; Fujita, Y. (2006). A second nitrogenase-like enzyme for bacteriochlorophyll biosynthesis: reconstitution of chlorophyllide a reductase with purified X-protein (BchX) and YZ-protein (BchY-BchZ) from *Rhodobacter capsulatus*. *J Biol Chem* **281,** 15021-15028.

O'Neill, G. P.; Chen, M. W.; Soll, D. (1989). delta-Aminolevulinic acid biosynthesis in Escherichia coli and *Bacillus subtilis* involves formation of glutamyl-tRNA. *FEMS Microbiol Lett* **51,** 255-259.

Olsson, U.; Sirijovski, N.; Hansson, M. (2004). Characterization of eight barley xantha-f mutants deficient in magnesium chelatase. *Plant Physiol Biochem* **42,** 557-564.

Osanai, T.; Kanesaki, Y.; Nakano, T.; Takahashi, H.; Asayama, M.; Shirai, M.; Kanehisa, M.; Suzuki, I.; Murata, N.; Tanaka, K. (2005). Positive regulation of sugar catabolic pathways in the cyanobacterium *Synechocystis* sp. PCC 6803 by the group 2 sigma factor sigE. *J Biol Chem* **280,** 30653-30659.

Osanai, T.; Imashimizu, M.; Seki, A.; Sato, S.; Tabata, S.; Imamura, S.; Asayama, M.; Ikeuchi, M.; Tanaka, K. (2009). ChlH, the H subunit of the Mg-chelatase, is an anti-sigma factor for SigE in *Synechocystis* sp. PCC 6803. *Proc Natl Acad Sci U S A* **106,** 6860-6865.

Oster, U.; Bauer, C. E.; Rudiger, W. (1997). Characterization of chlorophyll a and bacteriochlorophyll a synthases by heterologous expression in *Escherichia coli*. *J Biol Chem* **272,** 9671-9676.

Papenbrock, J.; Grafe, S.; Kruse, E.; Hanel, F.; Grimm, B. (1997). Mg-chelatase of tobacco: identification of a Chl D cDNA sequence encoding a third subunit, analysis of the interaction of the three subunits with the yeast two-hybrid system, and reconstitution of the enzyme activity by co-expression of recombinant CHLD, CHLH and CHLI. *Plant J* **12,** 981-990.

Papenbrock, J.; Mock, H. P.; Hruse, E.; Grimm, B. (1999). Expression studies in tetrapyrrole biosynthesis: inverse maxima of magnesium chelatase and ferrochelatase activity during cyclic photoperiods. *Planta* **208,** 264-273.

Perry, S. E.; Li, H. M.; Keegstra, K. (1991). In vitro reconstitution of protein transport into chloroplasts. *Methods Cell Biol* **34,** 327-344.

Pesaresi, P.; Masiero, S.; Eubel, H.; Braun, H. P.; Bhushan, S.; Glaser, E.; Salamini, F.; Leister, D. (2006). Nuclear photosynthetic gene expression is synergistically modulated by rates of protein synthesis in chloroplasts and mitochondria. *Plant Cell* **18,** 970-991.

Peter, E. and Grimm, B. (2009). GUN4 is required for posttranslational control of plant tetrapyrrole biosynthesis. *Mol Plant* **2,** 1198-1210.

Peter, E.; Salinas, A.; Wallner, T.; Jeske, D.; Dienst, D.; Wilde, A.; Grimm, B. (2009). Differential requirement of two homologous proteins encoded by sll1214 and sll1874 for the reaction of Mg protoporphyrin monomethylester oxidative cyclase under aerobic and micro-oxic growth conditions. *Biochimica et Biophysica Acta (BBA) - Bioenergetics* **1787,** 1458-1467.

Petersen, B. L.; Jensen, P. E.; Gibson, L. C.; Stummann, B. M.; Hunter, C. N.; Henningsen, K. W. (1998). Reconstitution of an active magnesium chelatase enzyme complex from the bchI, -D, and -H gene products of the green sulfur bacterium *Chlorobium vibrioforme* expressed in *Escherichia coli*. *J Bacteriol* **180,** 699-704.

Petoukhov, M. V.; Eady, N. A.; Brown, K. A.; Svergun, D. I. (2002). Addition of missing loops and domains to protein models by x-ray solution scattering. *Biophys J* **83,** 3113-3125.

Pettersen, E. F.; Goddard, T. D.; Huang, C. C.; Couch, G. S.; Greenblatt, D. M.; Meng, E. C.; Ferrin, T. E. (2004). UCSF Chimera--a visualization system for exploratory research and analysis. *J Comput. Chem* **25,** 1605-1612.

Phillips, J. D.; Whitby, F. G.; Kushner, J. P.; Hill, C. P. (2003). Structural basis for tetrapyrrole coordination by uroporphyrinogen decarboxylase. *EMBO J* **22,** 6225-6233.

Pontier, D.; Albrieux, C.; Joyard, J.; Lagrange, T.; Block, M. A. (2007). Knock-out of the magnesium protoporphyrin IX methyltransferase gene in *Arabidopsis*. Effects on chloroplast development and on chloroplast-to-nucleus signaling. *J Biol Chem* **282,** 2297-2304.

Pontoppidan, B. and Kannangara, C. G. (1994). Purification and partial characterisation of barley glutamyl-tRNA^{Glu} reductase, the enzyme that directs

glutamate to chlorophyll biosynthesis. *European Journal of Biochemistry* **225,** 529-537.

Porra, R. J. and Lascelles, J. (1968). Studies on ferrochelatase. The enzymic formation of haem in proplastids, chloroplasts and plant mitochondria. *Biochem J* **108,** 343-348.

Porra, R. J.; Schafer, W.; Gad'on, N.; Katheder, I.; Drews, G.; Scheer, H. (1996). Origin of the two carbonyl oxygens of bacteriochlorophyll a. Demonstration of two different pathways for the formation of ring E in *Rhodobacter sphaeroides* and *Roseobacter denitrificans*, and a common hydratase mechanism for 3-acetyl group formation. *Eur J Biochem* **239,** 85-92.

Qian, P.; Marklew, C. J.; Viney, J.; Davison, P. A.; Brindley, A. A.; Soderberg, C.; Al-Karadaghi, S.; Bullough, P. A.; Grossmann, J. G.; Hunter, C. N. (2012). Structure of the cyanobacterial Magnesium Chelatase H subunit determined by single particle reconstruction and small-angle X-ray scattering. *J Biol Chem* **287,** 4946-4956.

Reid, J. D.; Siebert, C. A.; Bullough, P. A.; Hunter, C. N. (2003). The ATPase activity of the ChlI subunit of magnesium chelatase and formation of a heptameric AAA+ ring. *Biochemistry* **42,** 6912-6920.

Reid, J. D. and Hunter, C. N. (2004). Magnesium-dependent ATPase activity and cooperativity of magnesium chelatase from *Synechocystis* sp. PCC6803. *J Biol Chem* **279,** 26893-26899.

Rieble, S. and Beale, S. I. (1991). Purification of glutamyl-tRNA reductase from *Synechocystis* sp. PCC 6803. *Journal of Biological Chemistry* **266,** 9740-9745.

Rimington, C. and Miles, P. A. (1951). A study of the porphyrins excreted in the urine by a case of congenital porphyria. *Biochem J* **50,** 202-206.

Rippka, R.; Deruelles, J.; Waterbury, J. B.; Herdman, M.; Stanier, R. Y. (1979). Generic assignments, strain histories and properties of pure cultures of cyanobacteria. *Journal of General Microbiology* **111,** 1-61.

Roper, J. M. and Smith, A. G. (1997). Molecular localisation of ferrochelatase in higher plant chloroplasts. *Eur J Biochem* **246,** 32-37.

Rudiger W (1997). Chlorophyll metabolism: From outer space down to the molecular level. *Phytochem.* **46,** 1151-1167.

Rudiger, W.; Benz, J.; Guthoff, C. (1980). Detection and partial characterization of activity of chlorophyll synthetase in etioplast membranes. *Eur J Biochem* **109,** 193-200.

Ruzheinikov, S. N.; Burke, J.; Sedelnikova, S.; Baker, P. J.; Taylor, R.; Bullough, P. A.; Muir, N. M.; Gore, M. G.; Rice, D. W. (2001). Glycerol dehydrogenase. structure, specificity, and mechanism of a family III polyol dehydrogenase. *Structure* **9,** 789-802.

Sambrook, J., Fritsch, E. F., Maniatis, T. (1989) *Molecular Cloning. A Laboratory Manual*. Cold Spring Harbour Laboratory Press, New York.

Santana, M. A.; Pihakaski-Maunsbach, K.; Sandal, N.; Marcker, K. A.; Smith, A. G. (1998). Evidence that the plant host synthesizes the heme moiety of leghemoglobin in root nodules. *Plant Physiol* **116,** 1259-1269.

Sawicki, A. and Willows, R. D. (2007). S-adenosyl-L-methionine:magnesium-protoporphyrin IX O-methyltransferase from *Rhodobacter capsulatus*: mechanistic insights and stimulation with phospholipids. *Biochem J* **406,** 469-478.

Sawicki, A. and Willows, R. D. (2008). Kinetic analyses of the magnesium chelatase provide insights into the mechanism, structure, and formation of the complex. *J Biol Chem* **283,** 31294-31302.

Sawicki, A. and Willows, R. D. (2010). BchJ and BchM interact in a 1 : 1 ratio with the magnesium chelatase BchH subunit of *Rhodobacter capsulatus*. *FEBS J* **277,** 4709-4721.

Scalla, R.; Matringe, M.; Camadro, J. M.; Labbe, P. (1990). Recent advances in the mode of action of diphenyl ether and related herbicides. *Z Naturforsch* **45c,** 503-511.

Schagger, H.; Cramer, W. A.; von, J. G. (1994). Analysis of molecular masses and oligomeric states of protein complexes by blue native electrophoresis and isolation of membrane protein complexes by two-dimensional native electrophoresis. *Anal Biochem* **217,** 220-230.

Schmid, H. C.; Oster, U.; Kogel, J.; Lenz, S.; Rudiger, W. (2001). Cloning and characterisation of chlorophyll synthase from *Avena sativa*. *Biol Chem* **382,** 903-911.

Schon, A.; Krupp, G.; Gough, S.; Berry-Lowe, S.; Kannangara, C. G.; Soll, D. (1986). The RNA required in the first step of chlorophyll biosynthesis is a chloroplast glutamate tRNA. *Nature* **322,** 281-284.

Schubert, H. L.; Phillips, J. D.; Heroux, A.; Hill, C. P. (2008). Structure and mechanistic implications of a uroporphyrinogen III synthase-product complex. *Biochemistry* **47,** 8648-8655.

Senior, N. M.; Brocklehurst, K.; Cooper, J. B.; Wood, S. P.; Erskine, P.; Shoolingin-Jordan, P. M.; Thomas, P. G.; Warren, M. J. (1996). Comparative studies on the 5-aminolaevulinic acid dehydratases from *Pisum sativum*, *Escherichia coli* and *Saccharomyces cerevisiae*. *Biochem J* **320 (Pt 2),** 401-412.

Shen, G.; Boussiba, S.; Vermaas, W. F. (1993). Synechocystis sp PCC 6803 strains lacking photosystem I and phycobilisome function. *Plant Cell* **5,** 1853-1863.

Shen, Y. and Ryde, U. (2005). Reaction mechanism of porphyrin metallation studied by theoretical methods. *Chemistry* **11,** 1549-1564.

Shen, Y. Y.; Wang, X. F.; Wu, F. Q.; Du, S. Y.; Cao, Z.; Shang, Y.; Wang, X. L.; Peng, C. C.; Yu, X. C.; Zhu, S. Y.; Fan, R. C.; Xu, Y. H.; Zhang, D. P. (2006). The Mg-chelatase H subunit is an abscisic acid receptor. *Nature* **443,** 823-826.

Shepherd, M.; Reid, J. D.; Hunter, C. N. (2003). Purification and kinetic characterization of the magnesium protoporphyrin IX methyltransferase from *Synechocystis* PCC6803. *Biochem J* **371,** 351-360.

Shepherd, M. and Hunter, C. N. (2004). Transient kinetics of the reaction catalysed by magnesium protoporphyrin IX methyltransferase. *Biochem J* **382,** 1009-1013.

Shepherd, M.; McLean, S.; Hunter, C. N. (2005). Kinetic basis for linking the first two enzymes of chlorophyll biosynthesis. *FEBS J* **272,** 4532-4539.

Shioi, Y. and Takamiya, K. (1992). Monovinyl and divinyl protochlorophyllide pools in etiolated tissues of higher plants. *Plant Physiology* **100,** 1291-1295.

Shoolingin-Jordan, P. M. (1995). Porphobilinogen deaminase and uroporphyrinogen III synthase: structure, molecular biology, and mechanism. *J Bioenerg Biomembr.* **27,** 181-195.

Singh, D. P.; Cornah, J. E.; Hadingham, S.; Smith, A. G. (2002). Expression analysis of the two ferrochelatase genes in *Arabidopsis* in different tissues and under stress conditions reveals their different roles in haem biosynthesis. *Plant Molecular Biology* **50,** 773-788.

Sirijovski, N.; Olsson, U.; Lundqvist, J.; Al-Karadaghi, S.; Willows, R. D.; Hansson, M. (2006). ATPase activity associated with the magnesium chelatase H-subunit of the chlorophyll biosynthetic pathway is an artefact. *Biochem J* **400,** 477-484.

Sirijovski, N.; Lundqvist, J.; Rosenback, M.; Elmlund, H.; Al-Karadaghi, S.; Willows, R. D.; Hansson, M. (2008). Substrate-binding model of the chlorophyll biosynthetic magnesium chelatase BchH subunit. *J Biol Chem* **283,** 11652-11660.

Smith, A. G.; Marsh, O.; Elder, G. H. (1993). Investigation of the subcellular location of the tetrapyrrole-biosynthesis enzyme coproporphyrinogen oxidase in higher plants. *Biochem J* **292 (Pt 2),** 503-508.

Sobotka, R.; McLean, S.; Zuberova, M.; Hunter, C. N.; Tichy, M. (2008). The C-terminal extension of ferrochelatase is critical for enzyme activity and for functioning of the tetrapyrrole pathway in Synechocystis strain PCC 6803. *J Bacteriol* **190,** 2086-2095.

Sobotka, R.; Komenda, J.; Bumba, L.; Tichy, M. (2005). Photosystem II Assembly in CP47 Mutant of *Synechocystis* sp. PCC 6803 Is Dependent on the Level of Chlorophyll Precursors Regulated by Ferrochelatase. *Journal of Biological Chemistry* **280,** 31595-31602.

Sobotka, R.; Tichy, M.; Wilde, A.; Hunter, C. N. (2011). Functional Assignments for the Carboxyl-Terminal Domains of the Ferrochelatase from *Synechocystis* PCC 6803: The CAB Domain Plays a Regulatory Role, and Region II Is Essential for Catalysis. *Plant Physiology* **155,** 1735-1747.

Soper, T. S. and Manning, J. M. (1982). Inactivation of pyridoxal phosphate enzymes by gabaculine. Correlation with enzymic exchange of beta-protons. *J Biol Chem* **257,** 13930-13936.

Spiller, S. C.; Castelfranco, A. M.; Castelfranco, P. A. (1982). Effects of Iron and Oxygen on Chlorophyll Biosynthesis : I. *In vivo* observations on iron and oxygen-deficient plants. *Plant Physiol* **69,** 107-111.

Srivastava, A. and Beale, S. I. (2005). Glutamyl-tRNA Reductase of *Chlorobium vibrioforme* Is a Dissociable Homodimer That Contains One Tightly Bound Heme per Subunit. *The Journal of Bacteriology* **187,** 4444-4450.

Suzuki, J. Y. and Bauer, C. E. (1995). A prokaryotic origin for light-dependent chlorophyll biosynthesis of plants. *Proc Natl Acad Sci U S A* **92,** 3749-3753.

Suzuki, J. Y.; Bollivar, D. W.; Bauer, C. E. (1997). Genetic analysis of chlorophyll biosynthesis. *Annu Rev Genet.* **31,** 61-89.

Tripathy, B. C. and Rebeiz, C. A. (1986). Chloroplast biogenesis. Demonstration of the monovinyl and divinyl monocarboxylic routes of chlorophyll biosynthesis in higher plants. *Journal of Biological Chemistry* **261,** 13556-13564.

Tripathy, B. C. and Rebeiz, C. A. (1988). Chloroplast biogenesis 60. Conversion of divinyl protochlorophyllide to monovinyl protochlorophyllide in green(ing) barley, a dark monovinyl/light divinyl plant species. *Plant Physiology* **87,** 89-94.

Tsukamoto, I.; Yoshinaga, T.; Sano, S. (1979). The role of zinc with special reference to the essential thiol groups in delta-aminolevulinic acid dehydratase of bovine liver. *Biochim Biophys Acta* **570,** 167-178.

van Heel, M.; Harauz, G.; Orlova, E. V.; Schmidt, R.; Schatz, M. (1996). A new generation of the IMAGIC image processing system. *J Struct Biol* **116,** 17-24.

Verdecia, M. A.; Larkin, R. M.; Ferrer, J. L.; Riek, R.; Chory, J.; Noel, J. P. (2005). Structure of the Mg-chelatase cofactor GUN4 reveals a novel hand-shaped fold for porphyrin binding. *PLoS Biol* **3,** e151.

von Gromoff, E. D.; Alawady, A.; Meinecke, L.; Grimm, B.; Beck, C. F. (2008). Heme, a plastid-derived regulator of nuclear gene expression in *Chlamydomonas*. *Plant Cell* **20,** 552-567.

Walker, C. J.; Mansfield, K. E.; Smith, K. M.; Castelfranco, P. A. (1989). Incorporation of atmospheric oxygen into the carbonyl functionality of the protochlorophyllide isocyclic ring. *Biochem J* **257,** 599-602.

Walker, C. J. and Weinstein, J. D. (1991). Further characterization of the magnesium chelatase in isolated developing cucumber chloroplasts : substrate specificity, regulation, intactness, and ATP requirements. *Plant Physiol* **95,** 1189-1196.

Warren, M. J. and Jordan, P. M. (1988). Investigation into the nature of substrate binding to the dipyrromethane cofactor of *Escherichia coli* porphobilinogen deaminase. *Biochemistry* **27,** 9020-9030.

Warren, M. J.; Smith, A. G.; Heyes, D. J.; Neil Hunter, C. (2009). Biosynthesis of Chlorophyll and Barteriochlorophyll. In: *Tetrapyrroles* Springer New York, pp. 235-249.

Watanabe, N.; Che, F. S.; Iwano, M.; Takayama, S.; Yoshida, S.; Isogai, A. (2001). Dual targeting of spinach protoporphyrinogen oxidase II to mitochondria and

chloroplasts by alternative use of two in-frame initiation codons. *J Biol Chem* **276,** 20474-20481.

Whitby, F. G.; Phillips, J. D.; Kushner, J. P.; Hill, C. P. (1998). Crystal structure of human uroporphyrinogen decarboxylase. *EMBO J* **17,** 2463-2471.

Wilde, A.; Mikolajczyk, S.; Alawady, A.; Lokstein, H.; Grimm, B. (2004). The gun4 gene is essential for cyanobacterial porphyrin metabolism. *FEBS Lett* **571,** 119-123.

Wilks, H. M. and Timko, M. P. (1995). A light-dependent complementation system for analysis of NADPH:protochlorophyllide oxidoreductase: identification and mutagenesis of two conserved residues that are essential for enzyme activity. *Proc Natl Acad Sci U S A* **92,** 724-728.

Willows, R. D.; Gibson, L. C.; Kanangara, C. G.; Hunter, C. N.; von, W. D. (1996). Three separate proteins constitute the magnesium chelatase of *Rhodobacter sphaeroides*. *Eur J Biochem* **235,** 438-443.

Willows, R. D.; Lake, V.; Roberts, T. H.; Beale, S. I. (2003). Inactivation of Mg chelatase during transition from anaerobic to aerobic growth in *Rhodobacter capsulatus*. *J Bacteriol* **185,** 3249-3258.

Willows, R. D.; Hansson, A.; Birch, D.; Al-Karadaghi, S.; Hansson, M. (2004). EM single particle analysis of the ATP-dependent BchI complex of magnesium chelatase: an AAA+ hexamer. *J Struct Biol* **146,** 227-233.

Witty, M.; Wallace-Cook, A. D.; Albrecht, H.; Spano, A. J.; Michel, H.; Shabanowitz, J.; Hunt, D. F.; Timko, M. P.; Smith, A. G. (1993). Structure and expression of chloroplast-localized porphobilinogen deaminase from pea (Pisum sativum L.) isolated by redundant polymerase chain reaction. *Plant Physiol* **103,** 139-147.

Wu, C. K.; Dailey, H. A.; Rose, J. P.; Burden, A.; Sellers, V. M.; Wang, B. C. (2001). The 2.0 A structure of human ferrochelatase, the terminal enzyme of heme biosynthesis. *Nat Struct Biol* **8,** 156-160.

Wu, F. Q.; Xin, Q.; Cao, Z.; Liu, Z. Q.; Du, S. Y.; Mei, C.; Zhao, C. X.; Wang, X. F.; Shang, Y.; Jiang, T.; Zhang, X. F.; Yan, L.; Zhao, R.; Cui, Z. N.; Liu, R.; Sun, H. L.; Yang, X. L.; Su, Z.; Zhang, D. P. (2009). The magnesium-chelatase H subunit binds abscisic acid and functions in abscisic acid signaling: new evidence in *Arabidopsis*. *Plant Physiol* **150,** 1940-1954.

Yamamoto, H.; Nomata, J.; Fuita, Y. (2008). Functional expression of nitrogenase-like protochlorophyllide reductase from Rhodobacter capsulatus in Escherichia coli. *Photochem Photobiol. Sci* **7,** 1238-1242.

Yamazaki, S.; Nomata, J.; Fujita, Y. (2006). Differential operation of dual protochlorophyllide reductases for chlorophyll biosynthesis in response to environmental oxygen levels in the cyanobacterium *Leptolyngbya boryana*. *Plant Physiol* **142,** 911-922.

Zhang, D. P.; Wu, Z. Y.; Li, X. Y.; Zhao, Z. X. (2002). Purification and identification of a 42-kilodalton abscisic acid-specific-binding protein from epidermis of broad bean leaves. *Plant Physiol* **128,** 714-725.

Zhou, S.; Sawicki, A.; Willows, R. D.; Luo, M. (2012). C-terminal residues of oryza sativa GUN4 are required for the activation of the ChlH subunit of magnesium chelatase in chlorophyll synthesis. *FEBS Lett* **586,** 205-210.

Zouni, A.; Witt, H. T.; Kern, J.; Fromme, P.; Krauss, N.; Saenger, W.; Orth, P. (2001). Crystal structure of photosystem II from *Synechococcus* elongatus at 3.8 A resolution. *Nature* **409,** 739-743.